uOttawa

L'Université canadienne
Canada's university

FACULTÉ DES ÉTUDES SUPÉRIEURES ET POSTOCTORALES

uOttawa

L'Université canadienne
Canada's university

FACULTY OF GRADUATE AND POSDOCTORAL STUDIES

Anna Francina Jackson
AUTEUR DE LA THÈSE / AUTHOR OF THESIS

M.Sc. (Cellular and Molecular Medicine)
GRADE / DEGREE

Department of Cellular and Molecular Medicine
FACULTÉ, ÉCOLE, DÉPARTEMENT / FACULTY, SCHOOL, DEPARTMENT

The Functional Characterization of Wdr68 Regulation of Pax7 Activity in Myogenesis

TITRE DE LA THÈSE / TITLE OF THESIS

M. Rudnicki
DIRECTEUR (DIRECTRICE) DE LA THÈSE / THESIS SUPERVISOR

CO-DIRECTEUR (CO-DIRECTRICE) DE LA THÈSE / THESIS CO-SUPERVISOR

N. Wiper-Bergeron

R. Screaton

Gary W. Slater
Le Doyen de la Faculté des études supérieures et postdoctorales / Dean of the Faculty of Graduate and Postdoctoral Studies

The Functional Characterization of Wdr68 Regulation of Pax7 Activity in Myogenesis

Anna Francina Jackson

This thesis is submitted to the Faculty of Graduate and Postdoctoral Studies in partial fulfillment of the requirements for a Master of Science degree in Cellular and Molecular Medicine.

Department of Cellular and Molecular Medicine
Faculty of Medicine
University of Ottawa
May 14, 2010

Your file Votre référence
ISBN: 978-0-494-74221-1
Our file Notre référence
ISBN: 978-0-494-74221-1

Abstract

In response to tissue trauma, quiescent satellite cells in adult skeletal muscle undergo proliferative activation and migrate to the site of injury where they differentiate and fuse to mend and replace damaged myofibers. The tightly synchronized expression of myogenic regulatory factors plays a critical role in orchestrating the regenerative process. In recent studies, we identified the transcription factor Pax7 as able to recruit the Wdr5-Ash2L-MLL2 histone methyltransferase complex to the -57.5kb *Myf5* enhancer and to activate *Myf5* transcription. We also identified Wdr68 as a putative Pax7 binding protein. Wdr68 is a scaffold protein thought to integrate Shh signaling but about which very little is known. Therefore, we set out to characterize a role for Wdr68 with Pax7 in early myogenesis. The interaction of endogenous Pax7 and exogenous Wdr68 was validated by reciprocal co-immunoprecipitation and western blot analysis. Manipulation of Wdr68 levels in primary myoblasts followed by real-time PCR analysis of Pax7 target genes suggests that Wdr68 acts as a negative regulator of Pax7. It has been determined by ChIP experiments that Wdr68 does not bind chromatin at some known genomic Pax7 binding sites. In addition, Wdr68 appears not to function by regulating Pax7 nuclear localization. These experiments provide new insights into the molecular control of Pax7 function during regenerative myogenesis and emphasize its complexity.

Table of Contents

List of Tables

List of Figures

List of Abbreviations

ANOVA	Analysis of Variance
bFGF	Basic fibroblast growth factor
BPB	Bromophenol blue
BSA	Bovine Serum Albumin
CD34	Cluster of differentiation protein 34
ChIP	Chromatin immunoprecipitation
c-met	c-met receptor tyrosin kinase
COS	CV-1 in Origin, SV40 genome
C-terminal	Carboxy terminal
Cul4	Cullin containing ubiquitin E3 ligase-4
CXCR4	CXC chemokine Receptor, aka fusin
Dcaf7	DDB1- and Cul4- associated factor 7 (Wdr68)
DDB1	UV-damaged DNA binding protein-1
ddH_2O	Double distilled water
DMSO	Dimethyl sulfoxide
DTT	Dithiothreitol
EED	Embryonic ectoderm development protein
EGF	Epidermal growth factor
FACS	Fluorescence activated cell sorting
FBS	Fetal bovine serum
Fzd7	Frizzled-7 Wnt receptor
H3K4-2me	Histone 3, lysine 4, di-methylation
H3K4-3me	Histone 3, lysine 4, tri-methylation
HDAC	Histone deacetylase
HEK	Human embryonic kidney
HGF	Hepatocyte growth factor
HMT	Histone methyltransferase
HRP	Horseradish peroxidase
HS	Horse serum
IB	Immunoblot
ICC	Immunocytochemistry
IGF	Insulin-like growth factor 1
IP	Immunoprecipitation
LB-broth	Luria-Bertani broth
MAPK	Mitogen activated protein kinase
MEF2	Myocyte-specific enhancer factor 2
MITR	MEF2-interacting transcriptional repressor
MRF	Myogenic regulatory factor
MyHC	Myosin heavy chain
NLS	Nuclear localization sequence
NaCl	Sodium Chloride
N-terminal	Amino terminal
Pax7	Paired-box transcription factor 7

PE	Phycoerythrin fluorescent dye
PEI	Polyethylenimine
PCR	Polymerase chain reaction
PFA	Paraformaldehyde
PBS	Phosphate Buffer Saline
RhoA	Ras homolog gene family, member A
RT-PCR	Reverse transcriptase PCR
qPCR	Quantitative (Real time) PCR
SC	Satellite cell
SDS	Sodium dodecyl sulfate
SDS-PAGE	SDS-polyacrylamide gel electrophoresis
SEM	Standard error of the mean
Shh	Sonic hedgehog
TAP/MS	Tandem affinity purification, mass spectrometry
Vangl2	Vang-like 2
Vcam1	Vascular cell adhesion molecule-1
WB	Western blot
WCE	Whole cell extract
Wdr68	Aspartic Acid, Tryptophan repeat protein 68 (Dcaf7)
Wnt	Wingless and Int protein

Acknowledgements

I would like to begin by thanking my supervisor Michael Rudnicki for allowing me the opportunity to spend an intense two years in his laboratory. Thanks to Julia who joined the lab after I began and has offered me unlimited and indispensable guidance since then. In a couple of years you will have a lab full of extremely fortunate students. To Vahab, all I can say is that Aaran is going to have his hands full with you; thank you so much for your mentorship and please quit smoking. Feo, you have an astounding work ethic and an extremely cool disposition. Thank you for helping me troubleshoot and for some great chats. Sue and Mel, you are the glue that holds this place together, thank you for your limitless patience and unshakable positivity. Vanessa, you were a lifeline in my first year. Thanks for all of the help and best of luck in PEI with your beautiful son Conor. To the girls on the floor, Patricia, Becca, Ale and Dominique, you are all bright, persistent and incredible people and I can't wait to see what the future holds for you (or more aptly, what you hold for the future). To the rest of the Rudnicki lab members, you have all contributed to this and I am grateful for all of your input and ideas. Finally, to my good friends and family outside of the lab, your enduring friendship and support have been fundamental to this process; I am lucky to be surrounded by so many bright and exceptional people.

Thank you all,

Anna Francina Jackson

May 14, 2010

CHAPTER 1

Introduction

1.1 The Satellite Cell Niche

Skeletal muscle is responsible for mammalian locomotion and is controlled voluntarily by the somatic division of the peripheral nervous system. Skeletal muscle is composed of large bundles of muscle fibers which are characterized by their elongated morphology, multinucleation, and striated appearance. Muscle fiber contractility occurs by the sliding filament model in which sarcomeric units are shortened as myosin heads beat and form cross-bridges with adjacent actin filaments thereby pulling Z-disks together. Individual muscle fibers are wrapped in a layer of connective tissue called the endomysium, groups of 10-100 fibers are bundled by the perimysium, and these are then ensheathed by the epimysium to encompass the organ in its entirety.

Directly adjacent to the plasma membrane of the muscle fiber (the sarcolemma) sits an extracellular matrix called the basal lamina which is composed of collagen, laminin and glycoproteins. Satellite cells reside between the basal lamina and the sarcolemma. Satellite cells are a population of normally quiescent, mononucleated cells that are responsible for the maintenance and repair of skeletal muscle. Satellite cells were initially characterized by this niche and their low complement of cytoplasm (Mauro, 1961). More recently a host of molecular markers for satellite cells have been identified. Pax7 is considered the most reliable molecular marker as it is expressed uniformly in both quiescent and activated satellite stem cell populations and is exclusive to muscle (Kuang and Rudnicki, 2008; Seale et al., 2000). Other molecular markers include c-met,

CXCR4, CD34, α7 and β1 integrins, m-cadherin, syndecans 3 and 4, and Vcam1 (Burkin and Kaufman, 1999; Charge and Rudnicki, 2004; Cornelison et al., 2004; Rosen et al., 1992; Seale et al., 2004; Vasyutina et al., 2005).

The role of the satellite stem cell niche extends beyond its existence as a passive location. The niche plays an active role in directing satellite cell physiology through a combination of signals from the adjacent muscle fiber, capillaries and basal lamina. Satellite cells will remain quiescent unless muscle trauma occurs, at which point they will become activated. Signals indicating trauma may be received from nearby capillaries as a result of the inflammatory response or the host muscle fiber itself (Kuang et al., 2008). For instance, stretch trauma results in host fiber release of hepatocyte growth factor (HGF) which binds the satellite cell c-met receptor and causes satellite cell activation (Tatsumi et al., 2006).

Upon activation, satellite stem cells undergo a period of extensive proliferation. The niche provides apical-basal polarity to the satellite cell which plays a crucial role in directing the orientation and outcome satellite stem cell division. Specifically, the apical side of the satellite cell, docked to the muscle fiber via m-cadherin, receives molecular signals from the adjacent muscle fiber. The basal side of the satellite cell, which interacts with the basal lamina via integrins α7 and β1, obtains its molecular cues from the basal lamina. During a planar cellular division (where the plane of division is perpendicular to the muscle fiber) the two daughter cells receive molecular cues from both the apical and basal surfaces.

Conversely, during an apical-basal cellular division (where the plane of division is parallel to the muscle fiber) only the apical daughter cell will receive molecular cues from the host muscle fiber and, likewise, only the basal cell will receive signals from the basal lamina (Figure 1.1A) (Kuang et al., 2008).

The characterization of symmetric and asymmetric divisions has been a very important contribution in terms of understanding how satellite cells are able to both maintain the pool of quiescent cells and regenerate damaged muscle. A keystone observation in *Myf5*$^{+/Cre}$/*Rosa*$^{+/YFP}$ mice is that the satellite cell population is heterogenous, comprising ~10% Pax7^{+}/Myf5^{-} stem cells and ~90% Pax7^{+}/Myf5^{+} committed cells. A symmetric division, usually planar, indicates that the two daughter cells are identical with respect to Myf5 expression, whereas an asymmetric cell division, usually apical-basal, implies that one daughter expresses Myf5 and the other does not. Pax7^{+}/Myf5^{-} satellite stem cells have never expressed Myf5 but may undergo an asymmetric, apical-basal division in which the basal cell remains Pax7^{+}/Myf5^{-} and repopulates the stem cell niche, while the apical cell becomes Pax7^{+}/Myf5^{+} and proceeds through myogenic differentiation (Figure 1.1B) (Kuang et al., 2007).

While the signaling pathways that underlie symmetric and asymmetric cell division are still being actively explored, there is evidence to suggest that Notch signaling is responsible for directing apical-basal divisions, whereas Wnt signaling favors planar divisions (Kuang et al., 2007; Le Grand et al., 2009). Two

cells must come into contact for Notch signaling to proceed. The binding of Notch ligand Delta1 (expressed on the surface of one cell) with Notch (expressed on the surface of the second cell) results in the cleavage of the Notch intracellular domain which is translocated to the nucleus where it modulates Notch target gene expression. In satellite cells the $Pax7^{+}/Myf5^{+}$ express Delta1 and the $Pax7^{+}/Myf5^{-}$ express Notch3; thus indicating that Notch3 plays a role in the *maintenance of quiescence* (Figure 1.1B) (Kuang et al., 2007).

Wnt signaling can proceed by canonical and non-canonical pathways. In satellite cells, secreted Wnt7a binds the Fzd7 receptor and activates the non-canonical, planar cell polarity pathway resulting in an increase of planar, symmetric cell division. Fzd7 receptors are preferentially expressed in quiescent $Pax7^{+}/Myf5^{-}$ satellite stem cells and are upregulated upon activation of proliferation. In addition, proliferative activation results in an increase of Wnt7a expression by satellite cells. Activated $Pax7^{+}/Myf5^{-}$ satellite stem cells also express elevated levels of Vangl2, an essential regulator of the planar cell polarity pathway that is found at opposite poles of polarization in each daughter cell. Taken together, it appears that in binding Fzd7, Wnt7a causes the polarization of Vangl2 and α7-integrin causing each daughter cell to maintain adherence with the basal lamina and to thus remain in their niche and maintain the satellite stem cell population. The silencing of Wnt7a, Fzd7, or Vangl2 results in a bias toward apical-basal cell division (Figure 1.1B) (Le Grand et al., 2009).

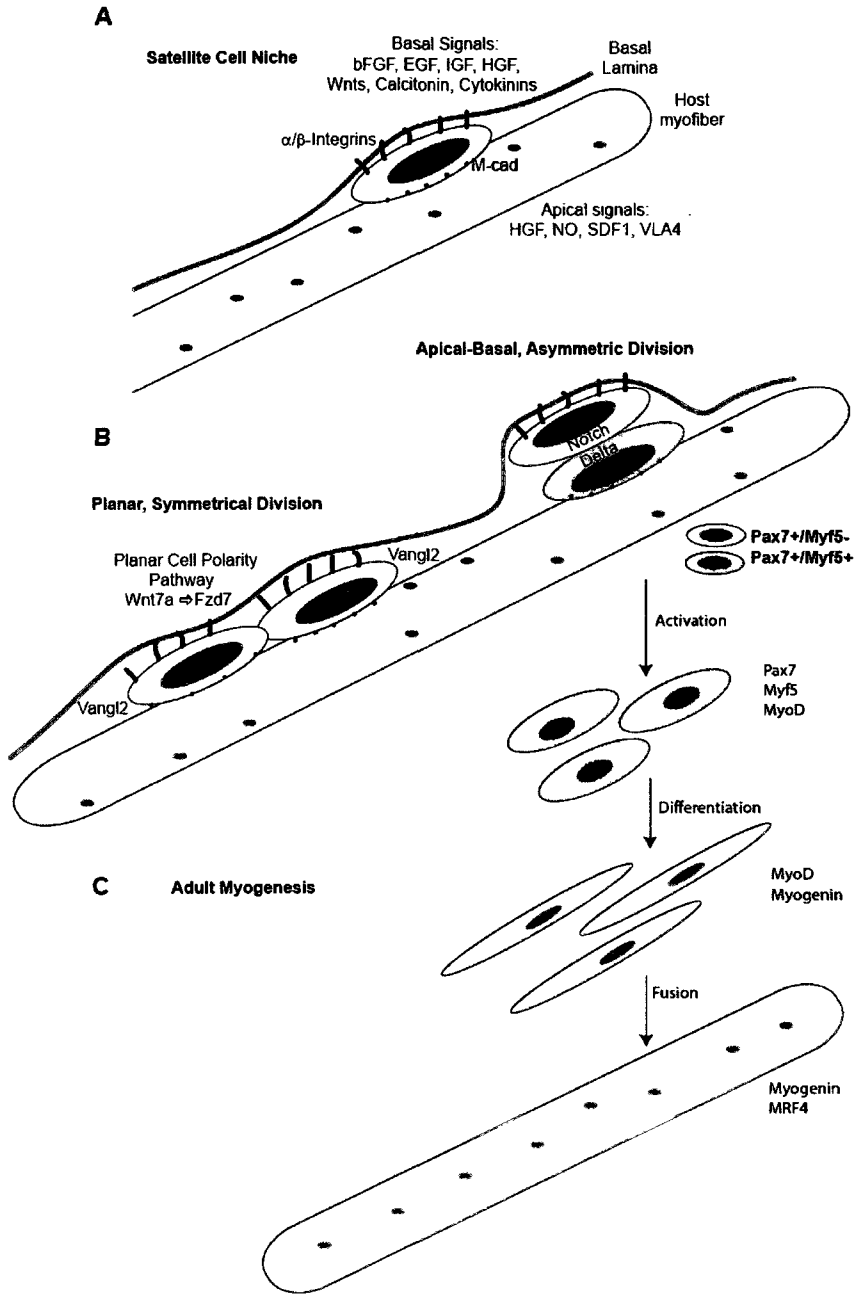

Figure 1.1: Adult myogenesis. (A) The satellite cell niche: SCs are normally quiescent and are primarily characterized by their niche, low amount of cytoplasm and Pax7 expression. The niche provides SCs with polarity such that they have an apical and a basal surface. **(B) Satellite cell division**: SCs usually divide in one of two ways (1) planar/symmetrical division which is regulated by Wnt signaling, or (2) apical-basal/asymmetric division which is regulated by Notch signaling. **(C) Myogenesis**: SCs expressing Myf5 proceed through the myogenic program and fuse with each other or existing myofibers to repair damaged muscle.

1.2 Myogenesis in Skeletal Muscle

Adult myogenesis occurs when muscles experience stress such as trauma, intensive exercise or degenerative disease, and require repair. Adult myogenesis is comprised of satellite cell activation, proliferation and differentiation, and proceeds based on the tightly synchronized expression of Pax7 and the myogenic regulatory factors (MRFs) Myf5, MyoD, Myogenin, MRF4 (Figure 1.1C) (Le Grand and Rudnicki, 2007).

No single 'activation trigger' has been identified for satellite cell activation and it is likely that multiple triggers exist in response to distinct stressors. For instance mechanical stretch of the muscle results in the production of nitric oxide. Nitric oxide induces folistatin which antagonizes myostatin allowing satellite cells to exit quiescence (Pisconti et al., 2006). Nitric oxide is also thought to induce HGF (Wozniak and Anderson, 2007). Fibroblast growth factor (FGF) obtained from the basal lamina is also involved in the induction of proliferation. FGF activates the p38α/β mitogen activated protein kinases (MAPK) which are required for satellite cell activation (Jones et al., 2005; Le Grand and Rudnicki, 2007).

Quiescent satellite cells are characterized by the expression of Pax7, a paired box transcription factor required for the postnatal maintenance, specification and self-renewal of satellite cells (Seale et al., 2000). Following activation, satellite cells become cycling myoblasts which are characterized by Pax7, Myf5 and MyoD expression. These myoblasts are highly proliferative and migratory and will translocate to the site of injury. Myf5 and MyoD are basic helix-loop-helix (bHLH)

transcription factors. Myf5 is required for the regulation of proliferation rate and homeostasis, while MyoD for entry into the differentiation program. Upon differentiation myoblasts become elongated and eventually fuse with each other forming new myofibers or with existing myofibers. Differentiation is accompanied by an up-regulation of bHLH transcription factors myogenin and MRF4 which are both required for the formation of myotubes and fibers (Le Grand and Rudnicki, 2007).

MRF expression is governed by a complex web of interactions that have yet to be fully elucidated. Pax7 is known to delay myoblast differentiation (Zammit et al., 2004) and can directly activate Myf5 transcription (McKinnell et al., 2008). Pax7 also appears to down-regulate MyoD expression (Olguin et al., 2007). In addition, Pax7 has been argued to prevent myogenin induction, and, moreover, that their expression is mutually exclusive (Le Grand and Rudnicki, 2007; Olguin et al., 2007).

1.3 Myogenic regulatory factors

1.3.1 Paired box transcription factor 7

Pax7 belongs to a highly conserved family of nine transcription factors defined by their 128-amino acid DNA binding, paired domain. The paired domain is a helix-turn-helix motif that is comprised of two adjacent homeodomains linked together (Noll, 1993). In addition to the paired domain, Pax7 also has a single 60-amino

acid homeodomain which is composed of three helices, the third of which interacts with the DNA major groove (Chi and Epstein, 2002). Understanding how Pax7 regulates genes has proved complicated due to its multiple DNA binding motifs. The paired domain will produce varied transcriptional outcomes based on whether the amino- or carboxy-terminus of the domain dominates the interaction (Czerny et al., 1993; Epstein et al., 1994; Xu et al., 1999). In addition, homedomains allow Pax protein dimerization over the 5`-TAAT$(N)_{2-3}$ATTA-3` palindrome (Wilson et al., 1993). The final Pax7 domain is the octapeptide domain which has been shown to play a repressive role in Pax5 (Chi and Epstein, 2002; Eberhard et al., 2000).

Pax7 is homologous to Pax3 (Chi and Epstein, 2002). These two transcription factors have similar, but distinct roles to play in skeletal myogenesis. Pax3 is required for skeletal muscle development during embryonic myogenesis. Pax3-null mice die *in utero* and have no limb skeletal muscle (Tajbakhsh et al., 1997). In the embryo, myogenic progenitor cells for the limb muscle are derived from the hypaxial dermomyotome of the somite and migrate to the limb bud. Cell migration to the limb bud occurs chemotactically through the interaction between c-met and HGF. Pax3 is responsible for c-met expression in myogenic precursor cells (Buckingham et al., 2003). In addition, upon arrival to the limb bud, Pax3 has been shown to directly activate *Myf5* expression which is required for myogenic determination of the progenitor cells (Bajard et al., 2006; Buchberger et al., 2007).

Pax7 is required for the specification and maintenance of adult satellite stem cells. Pax7 germline mutant mice are severely runted at birth, have decreased skeletal muscle mass, impaired growth, and succumb after ~2 weeks (Seale et al., 2000). In wild type mice, satellite cells account for ~30% of muscle nuclei at birth. Following an intense, 2-month phase of postnatal skeletal muscle growth and satellite cell fusion, satellite cells are reduced to less then 5% of myonuclei (Gibson and Schultz, 1983). Pax7-null mice are born without functional satellite cells thus accounting for their austere phenotype (Seale et al., 2000). Recent work conducted in a tamoxifen-inducible Cre-ER^T/$Pax7^{f/f}$ mouse model suggests that Pax7 plays a critical role perinatally, but is no longer required for muscle regeneration in the mature adult. It appears that if Pax7 is inactivated at P21 (3-weeks after birth) or anytime thereafter, satellite cells are not compromised in their ability to support sustained regeneration of skeletal muscle. To exclude the possibility that Pax3 might bolster regeneration by compensating for Pax7, a tamoxifen-inducible double knock-out for Pax3 and Pax7 was also created; regeneration was observed to proceed unaffected. This study indicates that Pax7 plays a key role in directing perinatal skeletal muscle growth followed by satellite cell transition into quiescence, but puts for the argument that Pax7 may not be a key player in adult muscle regeneration (Lepper et al., 2009).

Pax7 is a weak transcriptional activator due to *cis*-repression (Bennicelli et al., 1999). Affymetrix GeneChip microarray analysis of Pax7-CTAP over-expressing

C2C12 cells produced 43 up-regulated candidates for regulation by Pax7 including *Myf5*, *Zac1* (*PlagL1*), *Cipar1* (*Parm1*), *Lix1*, *Mest* and *Trim54*. Notably, this affect could not be recapitulated with Pax3-CTAP over-expression, underscoring the non-redundancy of these two transcription factors (McKinnell et al., 2008). Direct regulation of *Myf5* by Pax7 provides a solid molecular link between Pax7 and myogenic commitment. Ash2L-containing histone methyltransferase complexes have been previously described in muscle with respect to Mef2d (Rampalli et al., 2007). Pax7 was found to activate Myf5 expression by recruiting the Wdr5-Ash2L-MLL2 histone methyltransferase complex the -57.5kb *Myf5* region resulting in downstream histone3-lysine4 tri-methylation and transcriptional activation (McKinnell et al., 2008).

1.3.2 Myf5/MyoD

The MyoD family of basis helix-loop-helix (bHLH) transcription factors comprises Myf5, MyoD, myogenin and MRF4. The bHLH is a highly conserved, 68-amino acid domain is comprised of two alpha-helices attached by a linker region. Typically one helix is larger then the other and binds the DNA major groove. The smaller helix is involved in dimerization with another bHLH protein. Dimerization facilitates binding to palindromic E-box DNA sequences: CACGTG, or more generally CANNTG (Massari and Murre, 2000; Murre et al., 1994). Recent work from our lab indicates that the percent-GC content of the two central nucleotides dictates transcription factors binding affinity to these E-box sites (V. Soleimani, in review),

The first explorations of Myf5 and MyoD function surmised that the two factors were somehow interchangeable and that each could compensate for the loss of the other. *Myf5*- or *MyoD*-null were born with skeletal defects, but apparently normal skeletal muscle. *MyoD*-null mice showed a 3.5-fold increase in *Myf5* expression and an increased propensity for myoblast proliferation (Rudnicki et al., 1992; Rudnicki et al., 1993). Conversely, *Myf5*/*MyoD* double mutant mice were born without skeletal muscle (Braun et al., 1992; Rudnicki et al., 1992; Rudnicki et al., 1993). More recently their roles have been teased apart to some extent. Myf5 has been associated with maintaining myoblast proliferative state since *Myf5*-null myoblasts proliferate poorly and differentiate precociously (Montarras et al., 2000). MyoD is associated with facilitating the progression from proliferation to differentiation given that *MyoD*-null myoblasts displayed impaired capacity to differentiate, *MyoD*-null mice do not efficiently repair damaged muscle, and *MyoD*-null mice crossed with *mdx* mice exhibit increased myopathic severity (Megeney et al., 1996; Montarras et al., 2000; Sabourin et al., 1999).

1.3.3 Myogenin/MRF4

Myogenin-null mice die at birth due skeletal muscle deficiency; they demonstrate an increase in number of myoblasts but myoblast fusion does not occur (Hasty et al., 1993). When myogenin is knocked-out in the adult the mice are viable but exhibit a 30% reduction in size (Knapp et al., 2006). *MRF4* is present at the same

genomic locus as *Myf5*. MRF4-null mice are viable and have increased myogenin expression suggesting that it might be compensatory (Zhang et al., 1995).

The myogenin/MRF4, MyoD/MRF4, Myf5/Myogenin and MyoD/Myogenin double knockouts, are lethal at birth and, like the myogenin knockout, exhibit an increase in number of myoblasts and an absence of myoblast fusion (Rawls et al., 1998). The Myf5/MRF4 double mutant is viable but displays defects in myoblast proliferation (Rawls et al., 1995). The Myf5/MyoD/Myogenin and MyoD/myogenin/MRF4 triple knockouts are both lethal at birth. In the former this is due to the complete absence of myoblasts and muscle fibers, whereas in the latter it is due to the absence of myofibers (Kassar-Duchossoy et al., 2004; Valdez et al., 2000).

These knockout combinations support the idea of a MRF hierarchy. Myf5 is required for myoblast proliferation but on its own is unable to induce differentiation. MyoD is able to induce differentiation, but will do so precociously in the absence of Myf5 (Rudnicki et al., 1992; Rudnicki et al., 1993). Myogenin is required later in the differentiation program for myoblast fusion. A specific function for MRF4 has yet to be clarified however, based on the double-knockout experiments, it appears to act later in differentiation. There undoubtably remains a lot to disentangle, and the complexity of these regulatory networks ought not to be underestimated.

1.4 The WD40 repeat proteins

The WD40, or GH-WD, repeat domain is composed of a core of approximately 40 amino acid residues usually bracketed by a glycine-histidine (GH) dipeptide at its N-terminus and a tryptophan-aspartic acid (WD) dipeptide at its C-terminus; the repeat is preceded by a an ~11-24 residue variable region (Neer et al., 1994; Smith et al., 1999). The secondary protein structure of the WD40-repeat is a four stranded, antiparallel beta-pleated sheet. Each blade in a WD40 protein 'propeller' is composed of the last strand of the previous WD40 motif and the first three strands from the next. This arrangement infers protein stability and allows barrel formation because the first three strands of the N-terminal repeat interact with the last strand of the C-terminal repeat causing the polypeptide to circularize. The number of WD40 repeats comprising a single propeller varies, but is thought not to exceed 8. The global structure of the propeller is barrel-like with a large surface area for staging protein-protein interactions. Proteins may assemble on the bottom, top and around the circumference of the barrel; the interior 'tunnel' is thought to be too small to support this function (Figure S1.1) (Smith et al., 1999).

WD40-repeat proteins have been widely accepted as adaptor proteins well suited for staging reversible macromolecular assemblies. This function suggests that they have the potential to be involved in a broad variety of cellular processes and that their variable regions would specify the nature of the proteins which they assemble (Neer et al., 1994; Smith et al., 1999). The WD40-repeat was first described in the GTP-binding protein β-subunit (Gβ) (Fong et al., 1986); for this

reason it has also been referred to as the β-transducin repeat, however this name falsely implies functional similarity between WD40-repeat proteins where only structural similarity is present (Duronio et al., 1992). Crystal structure analysis of Gβ revealed that the seven WD40 repeats are circularly arranged around a central axis forming a sevenfold β-propeller. In addition, the conserved core motifs are inwardly directed, while the variable linker regions are externally directed (Wall et al., 1995). The predominating assumption is that all WD40-repeat containing proteins adopt a similar barrel-like structure (Smith et al., 1999).

WD40-repeat proteins are non-catalytic and have been associated with a plethora of cellular processes including signal transduction, RNA processing, gene regulation, chromatin assembly, vesicular traffic, regulation of cytoskeletal assembly and regulation of cell cycle (Table 1.1). No Wd40-repeat proteins have been identified in prokaryotes, however their abundance, omnipresence and variety in eukaryotes suggests that they appeared shortly after the evolutionary split between prokaryotes and eukaryotes and then diversified quickly (Smith et al., 1999).

Table 1.1: Examples of WD40-repeat containing proteins with diverse functions.

	WD40-repeat protein
Signal transduction	
	GTP-binding protein, β-subunit
	Receoptor for activated C-kinase (RACK1)
RNA synthesis and processing	
	TATA box-binding protein (TBP)
	Cleavage stimulation factor (CstF)
Gene regulation	
	Histone methyltransferase complex members: Wdr5 (H3K4), EED (H3K9/K27)
	Transcriptional repressor: Groucho
Chromatin assembly	
	Chromatin assembly factor 1 (CAF1)
Vesicular traffic	
	Some α/β clathrin order proteins (α/β–COPs)
Regulation of cytoskeletal assembly	
	Microtubule-associated protein (MAP)
	Actin-related proteins: Arp2, Arp3
Cell cycle	
	Cell division control proteins: CDC4, CDC20, CDC40, p55
	Spindle checkpoint protein: Mad2

*Reviewed in (Li and Roberts, 2001)

1.5 WD40-repeat protein 68 (Wdr68)

Wdr68 (also known as Dcaf1 and Han11) is the human homologue of the AN11 protein, first identified in the petunia (de Vetten et al., 1997). AN11 is thought to play a role in the cytoplasmic post-translational modification of AN2. AN2 is a bHLH transcriptional activator that controls the transcription of genes involved in anthocyanin biosynthesis (de Vetten et al., 1997). Although AN11 is involved in the production of anthocyanins in plants, it is highly conserved across a wide range of species, from yeasts to mammals, that do not produce plant pigments

(See multiple[1] and pair-wise[2] alignment scores). NCBI HomoloGene predicts 56% and 100% protein sequence homology between *H. sapiens* Wdr68 (NP_005819.3) and *A. thaliana* AN11 (NP_189298.1) or *M. musculus* Wdr68 (NP_0822221), respectively.[3]

The five WD40-repeat AN11 sequence deviates from the WD40 motif consensus but is classified as a WD40-repeat protein based on the criteria for WD40-repeat proteins put forth by Neer *et al.* (1994). This criterion stipulates that the protein have at least one WD40 motif with no greater than one amino acid deviation from the consensus sequence and at least one WD40 motif with no greater than three deviations. Accordingly, repeat 3 has one mismatch, repeats 2 and 5 have two mismatches, and repeats 1 and 4 have greater than five mismatches (Figure S1.2).

The alternative name for Wdr68 is Dcaf7 [DDB1- (UV-damaged DNA binding protein-1) and Cul4- (cullin containing ubiquitin E3 ligase-4) associated factor 7], is not based on experimental findings that apply directly to Wdr68, but rather is derived 'by similarity'[4] to the greater than 20 other WD40 proteins which have been assigned this function (Higa et al., 2006). This association is based on the hypothesis that a primary role for WD40-repeat proteins might be to act as substrate-specific adaptor proteins for CUL4-DDB1 ubiquitin ligase through an

[1] http://www.ncbi.nlm.nih.gov/sites/entrez?cmd=Retrieve&db=homologene&dopt=MultipleAlignment&list_uids=55930
[2] http://www.ncbi.nlm.nih.gov/sites/entrez?cmd=Retrieve&db=homologene&dopt=AlignmentScores&list_uids=55930
[3] NCBI BLAST analysis
[4] http://www.uniprot.org/uniprot/P61963

interaction between the WD40 motif and DDB1 (Higa et al., 2006). Substrate polyubiquitination commonly results in substrate degradation by the proteosome, while monoubiquitination usually results in altered cellular distribution or functionality.

It is postulated that the CUL4-DDB1 ubiquitin E3 ligase could be the missing link between WD40-repeat proteins and their involvement in such a broad complement of biological processes. For example, in the instance of histone methylation, DDB1 and Cul4 were found to associate with Wdr5 at di- and tri-methylated H3K4 and EED (WD40repeat-containing, embryonic ectoderm development protein) at tri-methylated H3K9 and H3K27. This was observed by immunoprecipitation of di- and tri-methylated mononucleosomes from human H1299 or HeLa cell lysates, followed by western blotting for DDB1, Cul4, Wdr5 and EED (Higa et al., 2006).

1.6 Wdr68 functionality

Wdr68 was identified as a candidate Pax7-binding protein in the same TAP-MS experiment that identified the Wdr5/Pax7 interaction ((McKinnell et al., 2008); McKinnell, unpublished data). Wdr68 is a WD40-repeat protein about which very little has been documented; however, developing zebrafish treated with morpholinos directed against Wdr68 showed impaired jaw (Nissen et al., 2006), cardiac and central nervous system development (Mazmanian et al.). In addition Wdr68 has been shown to modulate the actions of another transcription factor,

Gli1. Dyrk1a kinase works synergistically with Gli1 to promote cellular proliferation in SZ95 sebocytes and 293T cells. Wdr68 has been shown to interact with and inhibit the Dyrk1a kinase. In this instance, over-expression of Wdr68 increased cytoplasmic Gli1 resulting in decreased expression of Gli1 target genes and decreased cellular proliferation (Morita et al., 2006).

Gli1 is controlled by sonic hedgehog (Shh) signaling. Shh is a secreted protein that binds to the Patched receptor causing it to relinquish its inhibition of another membrane bound protein called Smoothened. The intracellular signaling cascade that ensues culminates at Gli which acts to mediate changes in Shh-target gene expression. During embryonic muscle development the *Myf5* epaxial somite enhancer is Shh-dependent and directly regulated by Gli (Gustafsson et al., 2002). Of interest is whether this characteristically embryonic signaling pathway is recapitulated post-natally during muscle regeneration. Shh is strongly upregulated in regenerating mouse skeletal muscle and has been demonstrated to act in an angiogenic capacity (Pola et al., 2003; Straface et al., 2008). In addition, Shh inhibition in regenerating muscle prevents the induction of Myf5 and MyoD and impairs SC migration (Straface et al., 2008). Finally, it has been demonstrated that Shh promotes cellular division, prevents differentiation and acts as a survival factor by inhibiting caspase-3 induction in C2C12 and satellite cells (Koleva et al., 2005). Consequently, an interaction between Wdr68 and Pax7 and the implied link of Shh signaling to myogenesis is quite interesting.

Wdr68 has also been shown to interact with Dyrk1b, the skeletal muscle-specific form of Dyrk. Dyrk1b is a serine/threonine kinase that is required for myotube differentiation (Nissen et al., 2006). Dyrk1b levels increase as cycling myoblasts transition to differentiation (Deng et al., 2003). Dyrk1b facilitates cellular differentiation by controlling myogenin expression via phosphorylation of class II HDACs such as the Mef2-interacting transcriptional repressor (MITR). This phosphorylation event relieves MITR inhibition of myocyte-specific enhancer factor 2 (MEF2) allowing it to enhance transcription of the myogenin gene (Deng et al., 2005; Mercer and Friedman, 2006). Dyrk1b has also been shown to mediate cell survival via an anti-apoptotic effect during C2C12 myoblast differentiation (Mercer et al., 2005) and to substantially enhance Gli1-dependant gene transcription (Mao et al., 2002).

Recent bioinformatic analyses of normal versus tumoral tissues has identified Wdr68 among one of the top seven genes identified as putative prostate cancer biomarkers (Fujita et al., 2008).

1.7 Hypothesis

Hypothesis:

Wdr68 plays an important role in myogenesis by interacting with Pax7 and modulating its ability to transcriptionally activate genes

Goals:

- Demonstrate an interaction between Pax7 and Wdr68 in primary myoblasts
- Observe a change in Pax7-target gene expression upon modulation of Wdr68 expression
- Determine if Wdr68 modulates Pax7 activity by (1) binding chromatin at known Pax7 binding sites (similar to Wdr5 (McKinnell et al., 2008)), or (2) translocating Pax7 to the cytoplasm (similar to Gli1 (Morita et al., 2006))
- Characterization of any phenotype produced by alteration of Wdr68 expression levels in primary myoblasts

CHAPTER 2

Materials

2 .1 Animal handling and primary myoblast cell isolation

PBS, pH 7.4	137mM NaCl 2.7mM KCl 10mM Na_2HPO_4 1.8mM KH_2PO_4
HAM's complete growth media	20% FBS 1%penicillin/streptomycin 2.5ng/ml basic fibroblast growth factor (in HAM's F-10 media growth media, Multicell)
Primary isolation media	10mM Hepes 2% FBS (in DMEM growth media)
FACS media	10% FBS 0.5M EDTA (in PBS)

FACS antibody	**Dilution factor**	**Company**	**Catalog number**
anti-alpha7-integrin	1/200	MBL International	K0046-3
anti-Sca-1 (PE-conjugated)	1/500	eBiosciences	12-5981
anti-CD45 (PE-conjugated)	1/500	eBiosciences	551968
anti-CD31 (PE-conjugated)	1/500	eBiosciences	12-0451
anti-CD11 (PE-conjugated)	1/500	eBiosciences	12-0112
anti-IgG1 mouse Alexa Fluor 647	1/200	Invitrogen	A-21236

2.2 Tissue culture of primary and immortalized cell lines

Trypsin	0.25% trypsin 0.2mM EDTA (in PBS)
DMEM complete growth media	10% FBS 1% penicillin/streptomycin (in DMEM media growth media, Multicell)
Differentiation media	5% HS (in DMEM media growth media, Multicell)

Freeze media	50% Regular growth media 40% FBS 10% DMSO

2.3 Plasmid DNA preparation

Solution I	50mM glucose 25mM Tris HCl pH8.0 10mM EDTA pH 8.0
Solution II	0.2N NaOH 1%SDS
Solution III	3M potassium acetate 11.5% acetic acid
TE buffer, pH 8.0	10mM Tris-HCl, pH8.0 1mM EDTA, pH8.0

2.4 Transient transfection of plasmid DNA

NH Buffer (A)	50mM HEPES 280mM NaCl
Phosphate buffer (B)	70mM Sodium phosphate
NHP Buffer	40:1, A:B

2.5 Transient transfection of siRNA

Ambion siRNA ID#	**Sequence 5`→3`**
S90133	CGGUUGCUAGGCUAAACAAtt
S90134	GCAGCUUCGUGGAAGAGUAtt
S90135	GGAACGAGGUGGAUCCUUAtt

2.6 RNA extraction and cDNA synthesis

Reverse transcriptase PCR master mix (one reaction)	5μg RNA in 10μl 3μl 5X first strand buffer 6μl 25mM $MgCl_2$ 1μl random primers (1.8μg/μl) 0.5μl SuperScript II 14μl RNase-free water

2.7 Real-time polymerase chain reaction

Table 2.1: Expression and ChIP primers for real-time PCR

Gene	Expression primers	ChIP primers
Pax7	L: GCTACCAGTACAGCCAGTATG R: GTCACTAAGCATGGGTAGATG	
Wdr68	L: TATCCAGACCTCCTGGCAAC R: ATGGTGCACGTTGTGTCAAT	
Myf5	L: ACAGCAGCTTTGACAGCATC R: AAGCAATCCAAGCTGGACAC	-15kb (L): TATGCACCCATTCCAAACAA -15kb (R): CCTCATGTTCATGGAGAAGT -57.5kb (L): TGTGGCTCTCTCTCCGTATG -57.5kb (R): AATACAGACATGCAGGCTTCAC -111kb (L): CATCCCACATAATCCAATCAC -111kb (R): ACACAGATGGATGGGAAAGA
MyoD	L: CGCTCCAACTGCTCTGATG R: TAGTAGGCGGTGTCGTAGCC	
Myogenin	L: GAAAGTGAATGAGGCCTTCG R: ACGATGGACGTAAGGGAGTG	
MRF4	L: TAGAGCCCCTGTCCTAAGCA R: AGGAAAACCAAAGCAGCAGA	
MyHC	L: TGTCTGCCCTGT TCAGAGAGA R: CATTGGGGATGATACACCTCA	
Zac1	L: CCACTACCACAGCCACAGAT R: TGCTGCTGAGGTTGCAGT	-25kb (L): CTGGCTCAGCCTAAACTTGG -25kb (R): TCAGGTTTCTTCTCGCTTCC +11kb (L): CCACTACCACAGCCACAGAT +11kb (R): TGCTGCTGAGGTTGCAGT
Cipar1	L: TTGGTCAGACCCAGGAAACT R: CAATGGGACTGTTGGTGAAC	-15kb (L): AACTGTGGTGGCCTGAGTTT -15kb (R): GTGCGTGCATCTGTGTATCC
Lix1	L: GCAGCAGAAAGCCACCTT R: GGGTCATCCGCATCATCT	Prom. (L): GGGATTGCTTGCTACTGCTC Prom. (R): ATTACAAGGGGAAGGCTTGG
Mest	L: GCAACCTGGTCATCGACA R: TGATGGCCAGGACCTCTT	-15kb (L): AACAGTCCTCTGCTCCCTCA -15kb (R): ATTAGGCGCAGAAAATCCAA
Trim54	L: AGCGGAACCTGCTAGTGG R: TCTGTCTGCGGCTGTTGT	
Syne1	L: ACCCGGGTCAGCTCTTTT R: GCCAACAGCTCAACCAGA	
GAPDH	L: TGTCCGTCGTGGATCTGAC R: GGTCCTCAGTGTAGCCCAAG	+3kb (L): TCCAGTGAGGACGGTATGAT +3kb (R): CATAAAGATGGGGCAAAATG

2.8 Protein extraction

RIPA buffer
20mM Tris-HCl pH 7.6
300mM NaCl
5mM EDTA pH8.0
1% triton-X
0.1% SDS
0.2% DOC

2.9 Protein immunoprecipitation

0.5% Triton buffer
50mM Tris-HCl pH 7.6
150mM NaCl
0.5% Triton X-100

2X Sample buffer
In 40ml water:
5mL 2M Tris-HCl, pH6.8
20mL Glycerol
4g SDS
200mg BPB
3.1 g DTT

2.10 SDS-polyacrylamide gel electrophoresis and western blot

5% SDS-polyacrylamide stacking gel
125mM Tris-HCl pH 6.8
5% acrylamide
0.1% SDS
0.1% ammonium persulfate
0.05% TEMED

10% SDS-polyacrylamide resolving gel
375mM Tris-HCl pH 8.8
10% acrylamide
0.1% SDS
0.1% ammonium persulfate
0.05% TEMED

10X Running buffer
In 4L water:
Tris base 121g
Glycine 577g
SDS 40g

10X Transfer buffer
In 4L water:
Tris base 121g
Glycine 577g

Blocking buffer	5% skim milk powder 0.05% Tween-20 (in PBS)
Washing Buffer	0.05% Tween-20 (in PBS)
Stripping buffer	62.5mM Tris-HCl pH6.7 2% SDS 0.07% β-mercaptoethanol

Table 2.2: Antibodies used for immuno-analysis

Antibody (Company)	Animal origin	Application (Dilution)
Anti-Flag (M2, Sigma, F3165)	Mouse, monoclonal	IP (5ug), IB (10ug/ml), ChIP (50ul M2-conjugated beads)
Anti-His (Cell signaling technologies, 2366)	Mouse, monoclonal	IP (1/200), IB (1/1000)
Anti-HA (Sigma, 12CA5)	Mouse	IP (5ug), IB (1/1000), ICC (1/1000)
Anti-GFP (Invitrogen, A11122)	Rabbit	ICC (1/500)
Anti-MyHC (Santa Cruz, sc53091)	Mouse, monoclonal	ICC (1/100)
Anti-Ki67 (Abcam, ab15580)	Rabbit	ICC (1/200)
Anti-Pax7 (produced in lab from hybridoma cells)	Mouse, monoclonal	IP (1/3), IB (1/10)
Anti-Mouse, HRP, light-chain specific (Jackson 115-035-174)	Goat	IB (1/5000)
Anti-Rabbit, HRP, light-chain specific (Jackson, 211-032-171)	Mouse, monoclonal	IB (1/5000)
Anti-Mouse, Alexa-546 (Invitrogen, A21143)	Goat	ICC (1/1000)
Anti-Rabbit, Alexa-488 (Invitrogen, A21206)	Donkey	ICC (1/1000)

IP=Immunoprecipitation; IB=immunoblot; ChIP=chromatin immunoprecipitation; ICC=immunocytochemistry

2.11 Chromatin immunoprecipitation

Fixation buffer	11% Formaldehyde 50mM Hepes, pH8.0 1mM EDTA 0.5mM EGTA 100mM NaCl
Glycine quenching buffer	1M Glycine (in PBS)
PBS wash buffer	1X PBS 1μg/ml protease inhibitors (pepstatin A, PMSF, leupeptin and aprotinin)
ChIP lysis buffer	40mM Tris-HCl, pH8.0 1% Triton-X 4mM EDTA 300mM NaCl 1μg/ml protease inhibitors (pepstatin A, PMSF, leupeptin and aprotinin)
ChIP dilution buffer	40mM Tris-HCl, pH8.0 4mM EDTA 1μg/ml protease inhibitors (pepstatin A, PMSF, leupeptin and aprotinin)
Low salt ChIP wash buffer	150mM NaCl 0.1% SDS 1% Triton-X 2mM EDTA 20mM Tris-HCl, pH8.0
High salt ChIP wash buffer	500mM NaCl 0.1% SDS 1% Triton-X 2mM EDTA 20mM Tris-HCl, pH8.0
LiCl salt ChIP wash buffer	0.25M LiCl 1% Nonidet-P40 1% sodium deoxychlorate 1mM EDTA 10mM Tris-HCl, pH8.0

ChIP elution buffer	0.1M $NaHCO_3$ 1% SDS

2.12 Immunocytochemistry

ICC Fixation Buffer	2% PFA in PBS
ICC Permeabilization solution	0.5% Triton-X in PBS
ICC Quenching solution	100mM glycine in PBS
ICC Blocking Buffer	5% HS 1% BSA (in PBS)

CHAPTER 3

Methods

3 .1 Animal handling and primary myoblast cell isolation

All animal handling was done in accordance with the Canadian Council on Animal Care's '*Guide to the Care and Use of Experimental Animals*' Vol. 1, 2nd edn., 1993, and the Province of Ontario's '*Animals for Research Act.*' This research carried out under the approval of the University of Ottawa Animal Care protocol: OGHRI28.

Primary myoblasts were isolated from Balb/C mice of approximately 4 weeks of age by FACS or pre-plating techniques. Work surfaces and tools were sterilized with 70% ethanol. Total muscle from hind-limbs was dissected out using dissecting scissors and washed in PBS. Tissue placed in collagenase/dispase solution for chemical digestion and mechanically digested using dissection scissors. Collagenase/dispase solution was inhibited with primary isolation media. The slurry was passed through a 50μm filter and cells were pelleted (5min; 1500rpm).

FACS – Cell pellets were resuspended in FACS media and incubated with anti-α7-integrin; PE-conjugated anti-Sca-1, anti-CD45, anti-CD31, anti-CD11; anti-IgG1 mouse AlexaFluor647; and Hoechst for 15min on ice. Final cell wash and resuspension were carried out in FACS media. α7-integrin-positive, Hoechst-positive, PE-negative cells were plated on a 6cm collagen-coated plate and passaged to a maximum of 12 times.

Pre-plating – Cell pellets were resuspended in HAM's complete growth media and plated on a 10cm plate for 30min at 37°C. Supernatant was transferred to a 10cm collagen-coated plate and incubated overnight at 37°C.

Preplating was repeated until a pure population of myoblasts was obtained. This technique makes use of the higher affinity of primary myoblasts to collagen-coated plates versus fibroblasts to uncoated plastic and the higher proliferative capacity of primary myoblasts in comparison to aging fibroblasts.

3.2 Tissue culture of primary and immortalized cell lines

Primary myoblasts were plated on collagen-coated plates in sterile, HAM's complete growth media. Plates were coated with rat tail tendon collagen (Roche) resuspended in 0.02% acetic acid for a final concentration of 2mg/ml, for one hour at room temperature and dried overnight. Primary cells were passaged by tryspinization to a maximum of 12 times.

293T immortalized-human embryonic kidney cells, C2C12 immortalized-myoblasts, 10T½ fibroblasts and Phoenix-eco viral packaging cells were cultured in non-coated plates in sterile DMEM growth media. Cells were passaged indefinitely.

Differentiation of primary and C2C12 myoblasts into myotubes was carried out using sterile differentiation media over a time course of 5-7 days.

Long-term cell-stocks were stored at -80°C in freezing media.

3.3 Plasmid DNA preparation

Cloning – The Gateway system (Invitrogen) was used to make pDEST-Wdr68-Flag-HA. attb1-Wdr68-attb2 cDNA PCR was amplified from a gateway compatible plasmid vector, pBRIT-Wdr68-CTAP (obtained from V.- Soleimani). Step-down PCR program: 1-cycle of 5min/94°C (initial denaturation); 6-cycles of 30sec/94°C (denaturation), 30sec/58°C* (annealing), 90sec/72°C (extension);

24-cycles of 30sec/94°C (denaturation), 30sec/53.5°C* (annealing), 90sec/72°C (extension); 1-cycle of 7min/72°C (final extension); hold at 4°C (*step-down annealing temperature by 0.5°C each cycle). cDNA separated from pDNA on a 1%-agarose gel (90V, 1.5hr), visualized with ethidium bromide, and gel extracted with the QIAquick Gel Extraction kit (as per manufacturers microcentrifuge protocol; Qiagen). Purified attb1-Wdr68-attb2 cDNA cloned into a pDONR(zeo) vector (from V. Soleimani) by BP reaction (as per Gateway protocol). pDONR(zeo)-Wdr68 vector was transformed into OmniMax *E. coli* and amplified (amplification protocol below). The cDNA was then cloned by LR reaction into pBRIT-GW-Dst2-FLAG-HA (from V. Soleimani) and the vector was transformed into OmniMax *E. coli*, amplified, purified and sequenced (T3 primers).

Transformation – 50-100ul OmniMAX chemically competent *E. coli* (Invitrogen) were transformed with 150-300ng of plasmid DNA. Transformation scheme: 30min incubation on ice, 30sec heat shock at 42°C, 2min incubation on ice, addition of 250ul SOC media, 60min incubation shaking at 37°C, plating 50-100ul on 10cm LB-agar plates (Invitrogen) with appropriate antibiotic for selection (Ampicillin 50ug/ml, Zeomycin 25ug/ml).

Amplification – Single bacterial colonies were amplified overnight shaking at 37°C. Small and large scale colony amplifications were carried out in 5-10ml and 400-500ml LB-broth with appropriate antibiotic for selection, respectively.

Plasmid purification – Small scale plasmid purification was achieved using the MiniPrep plasmid purification kit (as per the manufacturer's protocol; Invitrogen). Large scale plasmid purifications were done by Cesium Chloride

gradient ultracentrifugation, protocol as follows: 500ml of overnight bacterial culture was pelleted (10min, 4000rpm), resuspended in 8ml of sterile, cold solution I, lysed for 5min in 16ml freshly made solution II, and pH restored and pDNA re-solublized by addition of 12ml of solution III. The solution was then spun down (15min at 4000rpm) and passed through a gauze filter. Precipitated protein was discarded. Nucleic acids were precipitated from the liquid phase with 12ml isopropanol for 15min at room temperature and then pelleted (15min at 4000rpm). Cell pellets were dried and then resuspended in 7.4ml TE buffer, pH 8.0. 8.0g cesium chloride was added to the TE-DNA solution, mixed, and incubated at 37°C for 30min. 250µl of ethidium bromide was added for a final concentration of 10mg/ml, mixed, and incubated in the dark for 15min. Proteins were precipitated by centrifugation (10min, 4000rpm), supernatant was then loaded into ultracentrifugation tubes, and each tube was balanced within 0.01g of the others. Ultracentrifugation of CsCl-DNA samples occurred overnight (55000rpm, 20°C) to separate pDNA from genomic DNA in solution. The pDNA band was removed with an 18-gauge needle on a 10ml syringe. Ethidium bromide was extracted from the pDNA solution by mixing it with one volume of 2-butanol, allowing phase separation and discarding the upper (pink) phase; the extraction was repeated at least 3-times (until no pink colour was visible in the bottom phase). Two volumes of ddH_2O were added to the pDNA solution, followed by one volume of isopropanol. The solution was incubated for 15min and DNA pelleted (10min, 4000rpm). The DNA pellet was washed with 70%-ethanol to remove salts and re-pelleted (13000rpm, 5min). pDNA was

resuspended in TE buffer and allowed to dissolve overnight at 4°C. pDNA quality and concentration were assessed by NanoDrop photospectrometry (Thermo Scientific). Plasmid identity was verified by sequencing (StemCore laboratories, DNA sequencing facility).

3.4 Transient transfection of plasmid DNA

PEI – HEK293T cells were grown to 60% confluency in 10cm plates. Two hours before transfection, growth media was replaced with 6ml fresh antibiotic-free growth media. 20ug pDNA and 60ul 1.5M NaCl were incubated in 540ul of unsupplemented DMEM media for 5min. 60ul 1.5M NaCl and 220ul linear PEI (polyethylenimine) were combined in 320ul DMEM. The two solutions were combined, incubated at room temperature for 30min, added to the 10cm dish, and incubated overnight at 37°C. The transfection solution was replaced with growth media the following morning and the cells were collected 48-72hrs post-transfection.

Calcium Phosphate – Pheonix Eco cells were grown to 80% confluency in 10cm plates. 30min prior to transfection growth media was replaced with DMEM-complete growth media supplemented with chloroquine (1:1000). 20ug pDNA was combined with 250ul ddH_2O and 250ul 0.5M$CaCl_2$. This solution was added drop-wise to NHP buffer while vortexing and incubated at room temperature for 20min. The transfection solution was added to the 10cm dish, incubated overnight at 37°C and replaced with growth media the following morning. Retrovirus-containing supernatant and cells were collected 48-72hrs post-transfection.

3.5 Retroviral production and creation of stable cell lines

Based on the protocol developed by the Nolan Lab at Stanford University[5], Pheonix Eco viral packaging cells were transfected as described above. 72hrs post-transfection the cells were resuspended and pelleted (5min, 1500rpm). The retrovirus-containing supernatant was passed through a 0.45uM filter and stored in cryogenic tubes at -80°C. Cells were infected using a solution of 7ml growth media, 2ml retrovirus, and 18ug/ml polybrene. Infection solution was replaced with fresh growth media 8-12hrs post-infection. Selection media was applied 36-48hrs post infection (Puromycin selection: 2.5ug/ml for C2C12 myoblasts and 1.25ug/ml for primary myoblasts). Extent of protein over expression was assessed by real-time PCR.

3.6 Transient transfection of siRNA

Primary myoblasts were transfected with siRNA against Wdr68 (Ambion) using Lipofectamine RNAiMax transfection reagent (Invitrogen) as per the manufacturers protocol. Knockdown efficiency was assessed by real-time PCR.

3.7 RNA extraction and cDNA synthesis

Cells grown in 10cm plates were washed with PBS, trypsinized, resuspended in 5mL media and spun down for five minutes at 1900-rpm. RNA was extracted from pelleted cells using the Qiagen RNeasy Mini kit as per manufacturer's protocol. RNA concentration and integrity were assessed by spectrophotometry (NanoDrop, Thermo Scientific); with an expected concentration of approximately 400ng/ul and a minimum Absorbance260/Absorbance280 ratio of 2.00.

[5] http://www.stanford.edu/group/nolan/protocols/pro_helper_dep.html

RT-PCR was conducted using 5ug of RNA, 100U of SuperScript II (Invitrogen) in a total volume of 40ul. Samples were incubated at 25°C for 10min, 42°C for 60min, 95°C for 30sec and stored at -20°C.

3.8 Real-time polymerase chain reaction

cDNA was diluted 1 in 5 for analysis by qPCR. ChIP DNA was not diluted. PerfeCta SYBR Green SuperMix for iQ (Quanta Biosciences) was used as per the manufacturer's protocol. Reactions were carried out in an MxPro-Mx3000P Thermocycler (Stratagene) according to the following thermal profile: 1-cycle of 10min/95°C (initial denaturation); 40-cycles of 30sec/95°C (denaturation), 30sec/55*°C (annealing), 30sec/72°C (extension); 1-cycle of 30sec/95°C, 30sec/55*°C, 30sec/95°C (dissociation curve) (*annealing temperatures between 55-58°C). All experimental real-time PCR results were normalized to GAPDH expression. Results were analyzed using Excel (Microsoft). Expression primers were designed to span a large intron to avoid amplification of genomic DNA.

3.9 Protein extraction

Total protein extraction – Lysis of pelleted cells was achieved using RIPA buffer with protease inhibitors and mechanical disruption. Lysis was performed on ice for 20 minutes. Cellular debris was pelleted out during a 20min, 14000-rpm centrifugation at 4°C. Protein concentration was measured by Bradford assay and spectrophotometry (Ultrospec 2100 pro, GE Healthcare).

3.10 Protein co-immunoprecipitation

Cultured cells were trypsinized, resuspended in 5ml growth media, pelleted (2500rpm, 5min) and placed on ice. Cells were lysed and protein was extracted using 0.5% Triton Buffer and incubation on ice for 20min with occasional vortexing. Cellular debris were pelleted (30min, 13000rpm) and protein concentration of the supernatant was measured by the Bradford method. 30-50μg protein extract was set aside as input control and the remainder was precleared by rotating at 4°C with protein-A/G sepharose beads for one hour. Precleared protein supernatant was immunoprecipitated by rotation with primary antibody at 4°C overnight and captured using protein-A/G sepharose beads in the final 1-2 hours of rotation, or 2-4 hours rotation at 4°C with 50μl M2-agarose beads (Sigma). Beads were washed 5 times for 5min with 0.5% Triton buffer and protein was eluted and denatured using sample buffer followed by a 3-5min incubation at 100°C. Purified protein was analyzed by western blot.

3.11 SDS-polyacrylamide gel electrophoresis and western blot

Protein samples were separated by gel electrophoresis (90V) on a 10% SDS-polyacrylamide gel. Proteins were transferred to an Immobilon-P membrane (Bio-Rad) for one hour (90V) or overnight (20V). Membranes were blocked for 1-16hrs (room temperature/4°C) in blocking buffer. Primary antibodies were diluted in blocking buffer and membranes were incubated in primary antibody solution overnight at 4°C. HRP-conjugated secondary antibodies were diluted 1:5000 in blocking buffer. Membranes were washed three times for at least 10 minutes with 1% Tween-20 in PBS before and after incubation with secondary antibodies. Membranes were visualized with Enhanced Chemiluminescence plus (GE

Healthcare) or SuperSignal (Pierce Protein Research Products, Thermo Scientific) HRP substrates. The signal was detected on MR film (Kodak). To reprobe for a loading control, membranes were stripped in stripping buffer for 45min at 55°C.

3.12 Chromatin immunoprecipitation

Primary myoblasts stably over expressing CTAP, Wdr68-CTAP, or Pax-CTAP by retroviral infection were expanded to ~16x10cm plates. Fixation was achieved by adding 1mL fixation buffer to 9mL growth media and rocking the plates at low speed for 10min. Formaldehyde was quenched by adding glycine to a final concentration of 125mM and rocking at low speed for 5min. Cells were washed twice for 5min with PBS wash buffer. Cells were scraped in 1mL PBS wash buffer and pelleted by centrifugation at 4°C for 5min at 2500rpm. Cell pellets were lysed for 10min on ice using the equivalent of 100μl ChIP lysis buffer per 10cm plate and occasional vortexing. DNA was fragmented to 300-500bp in length in a 4°C water-bath sonicator for 14 cycles: 30sec of high sonication/1min off. Sonicated samples were spun at 13000rpm for 10min at 4°C and the protein concentration of the supernatant was measured by the Bradford method. 20ul of protein lysate for each sample was taken and diluted to 100ul in ChIP dilution buffer to be used as input DNA. The remaining protein lysates were diluted in ChIP dilution buffer to a final concentration of 1mg/ml, immunoprecipitations were carried out using 1.5mg. 1.5mg of protein was precleared using 60μl of salmon sperm DNA/protein A agarose slurry by rotating for 1 hour at 4°C. Beads were pelleted by light centrifugation (1min, 1500rpm, 4°C) and the supernatant was

immunoprecipitated using 50μl of α–flag M2-agarose beads (Sigma) by rotating for 2-5 hours at 4°C. M2-agarose beads were washed once each with low salt ChIP wash buffer, high salt ChIP wash buffer, LiCl ChIP wash buffer, and twice with TE. Elution was repeated twice by using 250μl of ChIP elution buffer and rotating at room temperature for at least 15min. Reversal of formaldehyde cross-links was accomplished by adding sodium chloride to a final concentration of 0.2M and incubating for 12 hours at 65°C. Protein was degraded by incubating samples for one hour at 42°C with 20μg/ml Proteinase K. DNA fragments were purified by phenol/chloroform purification and analyzed by real-time PCR.

Phenol/chloroform DNA purification – Upon Proteinase K treatment, one volume of phenol/chloroform/isoamylalcohol (25:24:1) was added to each ChIP sample. Samples were shaken vigorously, transferred to phase lock columns and spun (5min, 13000rpm). The top phase was transferred to a new tube and combined with 0.1 volume of 3M sodium acetate, 1 ul glycoblue and 2.5 volumes of ice-cold 100% ethanol. Ethanol precipitation was carried out for at least one hour at -80°C. DNA was spun (15min, 13000rpm, 4°C) and the supernatant was discarded. The pellet was washed with 70% ethanol and spun down (5min, 13000rpm, 4°C). DNA pellets were dried using a SpeedVac on medium for 5-10min and resuspended in 50μl TE with 10μg/ml RNaseA. 2ul of purified DNA was used for each real-time PCR reaction.

3.13 Immunocytochemistry

Primary myoblasts were grown on collagen coated chamber slides or 12-well plates. Cells were washed with PBS and fixed with 2% PFA in PBS for

20min, permeabilized with 0.5% Triton-X in PBS for 10min, and quenched with 100mM glycine in PBS for 10min (with 5min PBS washes in between each of these steps). Fixed cells were blocked with ICC blocking buffer for one hour at room temperature or overnight at 4°C followed by a 5min wash in PBS. Primary antibodies were diluted in blocking buffer and incubated on the cells for 2 hours at room temperature or overnight at 4°C, followed 3x5min washes in PBS. Secondary antibody was diluted in blocking buffer and the cells were incubated in the dark at room temperature for one hour, followed by 3x5min washes in PBS. Nuclei were stained with Hoechst (diluted 1/1000 in PBS) for 10min in the dark at room temperature, followed by 3x5min washes in PBS. Slides were mounted using 2-3 drops of fluorescence mounting media (Dako), dried at room temperature, sealed using clear nail polish, and stored in the dark at 4°C.

All slides were visualized using an inverted fluorescent microscope (Zeiss, LSM510), with the exception of the visualization of Pax7 localization in primary nuclei which was done using a confocal microscope (Zeiss, LSM501-meta).

3.14 Tunel Assay

Primary myoblasts were grown in 4-chamber slides and transiently transfected in triplicate with siRNA against Wdr68 or scrambled siRNA or Wdr68-CTAP pDNA or an empty vector control. Tunel assay was carried out using the In Situ Cell Death Detection Kit (Roche-Boehringer) as per the manufacturers protocol.

3.15 ChIP-seq

High throughput Solexa ChIP-seq analysis of primary myoblasts expressing exogenous Pax7-CTAP was previously conducted (V. Punch and V. Soleimani). Analysis of Pax7 enrichment peaks was conducted using the UCSC genome browser and identification of genomic Pax7 binding sites within these peaks was accomplished using the IRC genome browser.

3.16 Statistical Analysis

Pair-wise comparisons were made by single factor ANOVA in Excel 2003 (Microsoft).

CHAPTER 4

Results

4.1 Wdr68 decreases primary myoblast proliferative capacity but does not affect primary myoblast viability.

Wdr68 was over-expressed by 350-fold or knocked-down by 77% by transient transfection of pBRIT-Wdr68-CTAP or Wdr68 siRNA, respectively. Wdr68 levels were assessed by real-time PCR at 48-hours post-transfection (Figure 4.1). Immunocytochemical analysis using an antibody directed against the proliferation marker Ki67 was conducted to ascertain whether alterations in Wdr68 expression levels would perturb myoblast proliferative capacity. While no significant difference in proliferative capacity was seen in cells transfected with scrambled or Wdr68 siRNA, over-expression of Wdr68 significantly decreased the number of Ki67-positive cells from 37% to 27% of total cells (Figure 4.2). A Tunel assay was performed to exclude the possibility that modulations of Wdr68 levels were causing cell death (Figure 4.3). Immunocytochemical or western blot analyses of Wdr68 expression levels were not possible due to the lack of a reliable primary antibody against Wdr68, therefore we used real-time PCR.

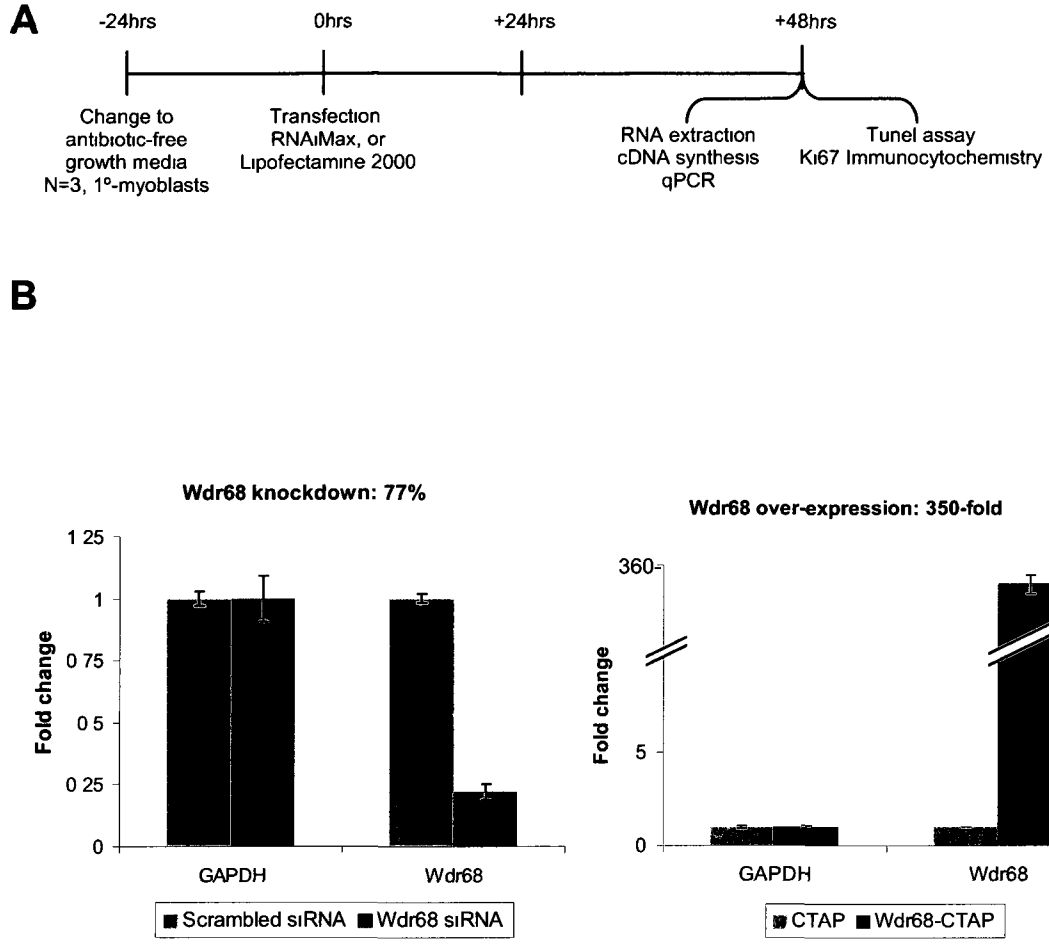

Figure 4.1: Knockdown and over-expression of Wdr68 in primary myoblasts. (A) Wdr68 over-expression and knockdown strategies in primary myoblasts. (B) Gene expression levels in Wdr68 over-expressing (red) and 48-hour knockdown (blue) primary myoblasts measured by real-time PCR. Error bars are SEM.

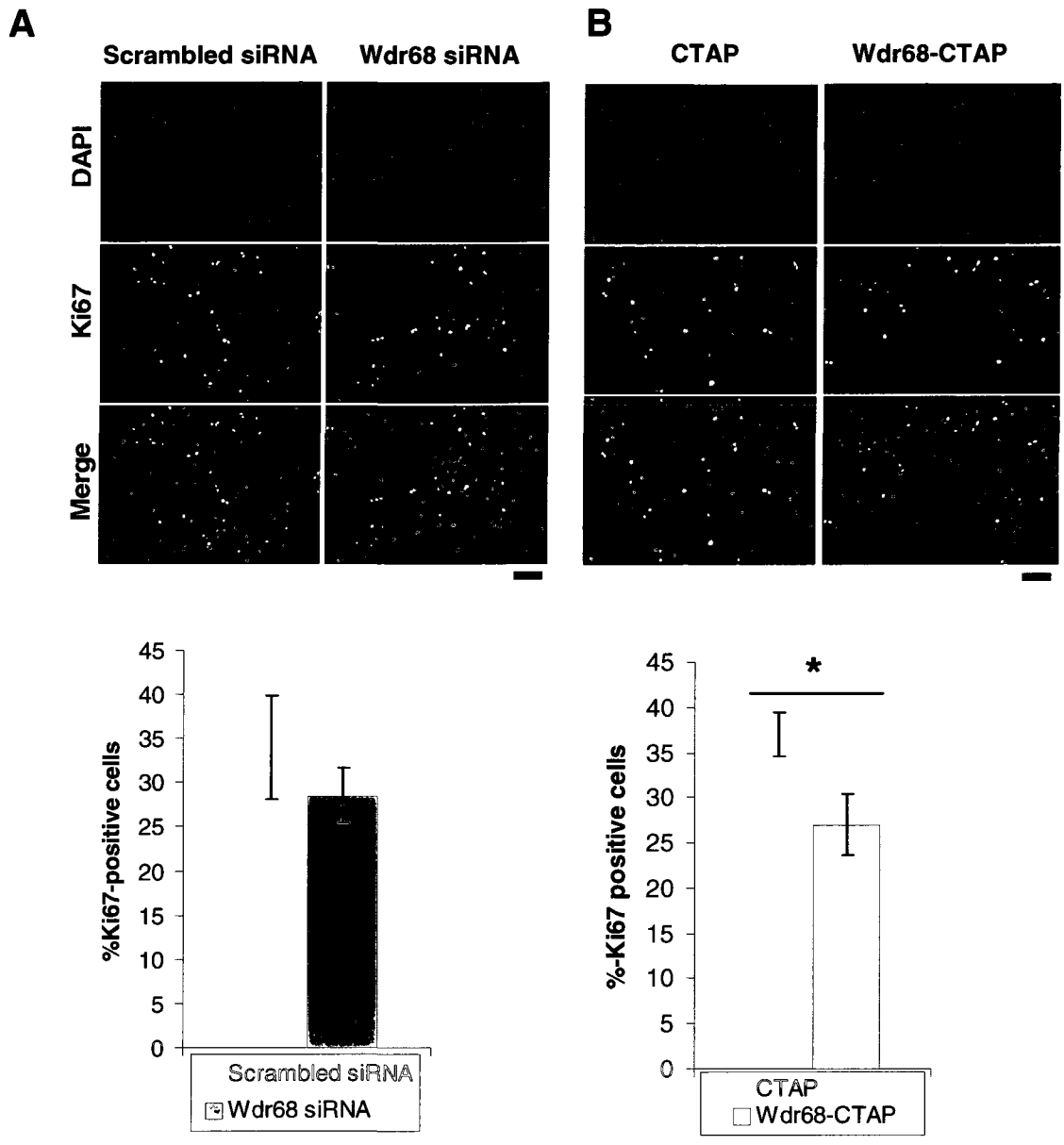

Figure 4.2: Over-expression of Wdr68 does decreases primary myoblast proliferative capacity. Ki67 immunocytochemistry for cell proliferative capacity in Wdr68-knockdown (A) and Wdr68 over-expressing (B) primary myoblasts. Scale bar is 75uM; $p<0.01$ by single factor ANOVA, n=3, error bars are SEM.

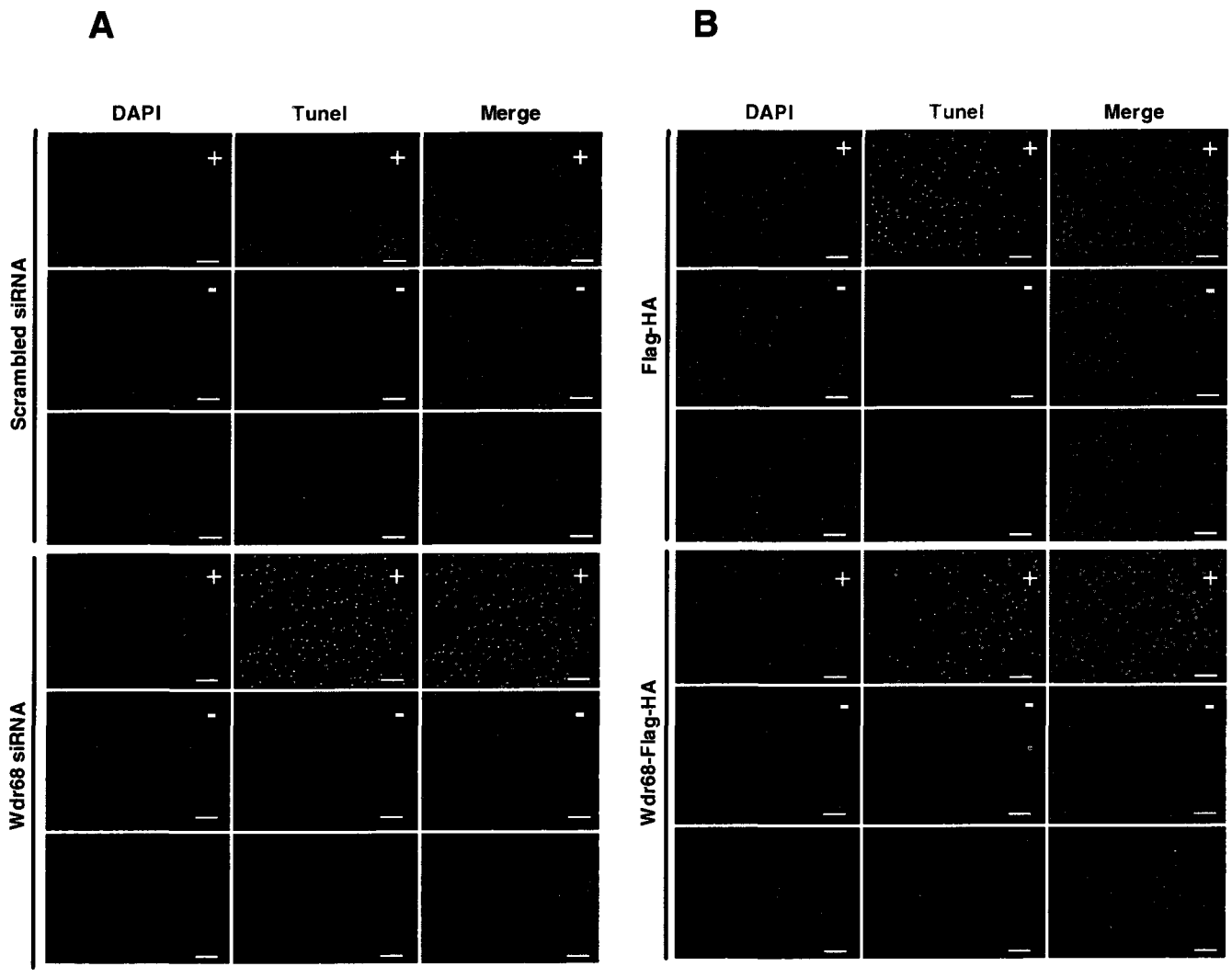

Figure 4.3: Over-expression or knockdown of Wdr68 does not affect primary myoblast viability. Tunel assay for cell viability in Wdr68-knockdown (A) and Wdr68 over-expressing (B) primary myoblasts. Scale bar is 50uM. "+" denotes DNase treated positive control; "-" denotes negative control; n=3.

4.2 Wdr68 binds Pax7 in C2C12 and primary myoblasts

Tandem affinity purification followed by MALDI-TOF mass spectrometry conducted previously in C2C12 myoblasts over-expressing Pax7-CTAP identified various candidate Pax7-binding proteins (McKinnell *et al.* 2008). Among these was the scaffold protein Wdr68. This interaction was validated between endogenous Pax7 and exogenous Wdr68-CTAP in primary myoblasts isolated from mouse hind limb. Validation was achieved by generating primary myoblasts that stably over-expressed Wdr68-CTAP using a Wdr68-CTAP retrovirus (Figure 4.4A). Reciprocal immunoprecipitation/western blot was achieved using antibodies against Pax7 and the Flag-tag (Figure 4.4B).

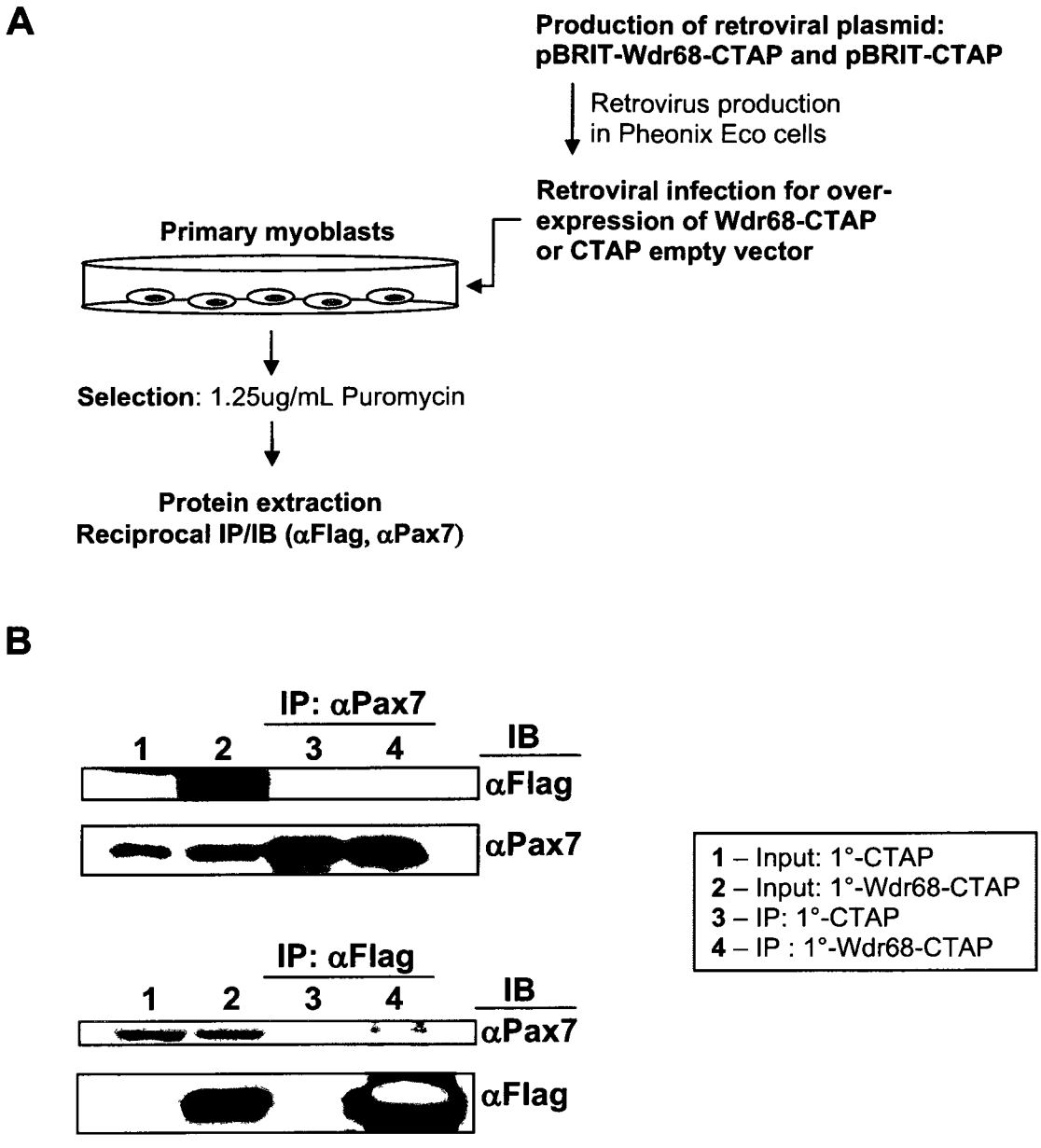

Figure 4.4: **Wdr68 binds Pax7 in primary myoblasts**. (A) Wdr68-CTAP stable over-expression by retroviral infection of primary myoblasts. (B) Reciprocal co-immunoprecipitation of endogenous Pax7 and exogenous Wdr68-CTAP in primary myoblasts.

4.3 Wdr68 does not bind Pax7 in HEK293T cells

To ascertain with which domain of Pax7 Wdr68 was interacting, Pax7-CTAP and Wdr68-Flag-HA constructs were transfected into HEK293T cells. Full length Pax7-CTAP as well as mutant Pax7-CTAP deletion constructs were previously generated (McKinnell *et al.* 2008). Gateway cloning was employed to vary the Wdr68 tag to Flag-HA (from CTAP) (Figure 4.5A). HEK293T cells were transiently transfected with pHIT-GFP to verify transfection; a high transfection efficiency of 80-90% was achieved (Figure 4.5B). Reciprocal immunoprecipitation and western blotting was achieved using antibodies directed to the His-tag for Pax7 and the HA-tag for Wdr68. In HEK293T cells (and COS cells, not shown) no interaction between full length Wdr68-Flag-HA and Pax7-CTAP was observed. Likewise, no interaction between full-length Wdr68 and the three Pax7-CTAP deletion constructs (deletion of Pax7 C-terminal, paired-domain, or homeodomain) was seen (Figure 4.5C).

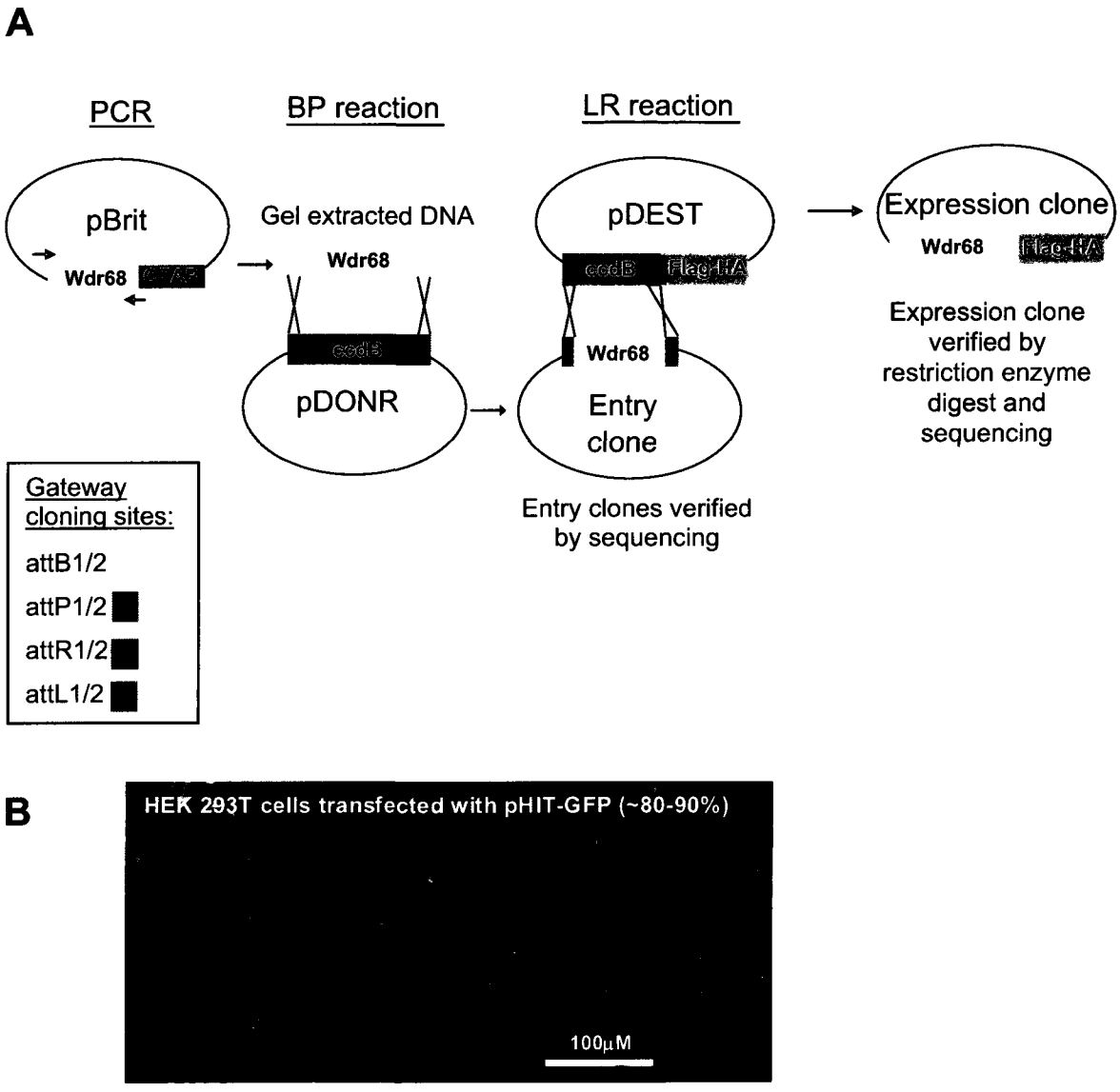

Figure 4.5: Wdr68 does not bind Pax7 in HEK293T cells. (A) Gateway cloning strategy for production of pBRIT-Wdr68-Flag-HA. (B) HEK 293T cell transfection efficiency. (C) Reciprocal co-immunoprecipitation of exogenous full-length Wdr68-Flag-HA and mutated Pax7-(mut)-CTAP transiently transfected into HEK293T cells.

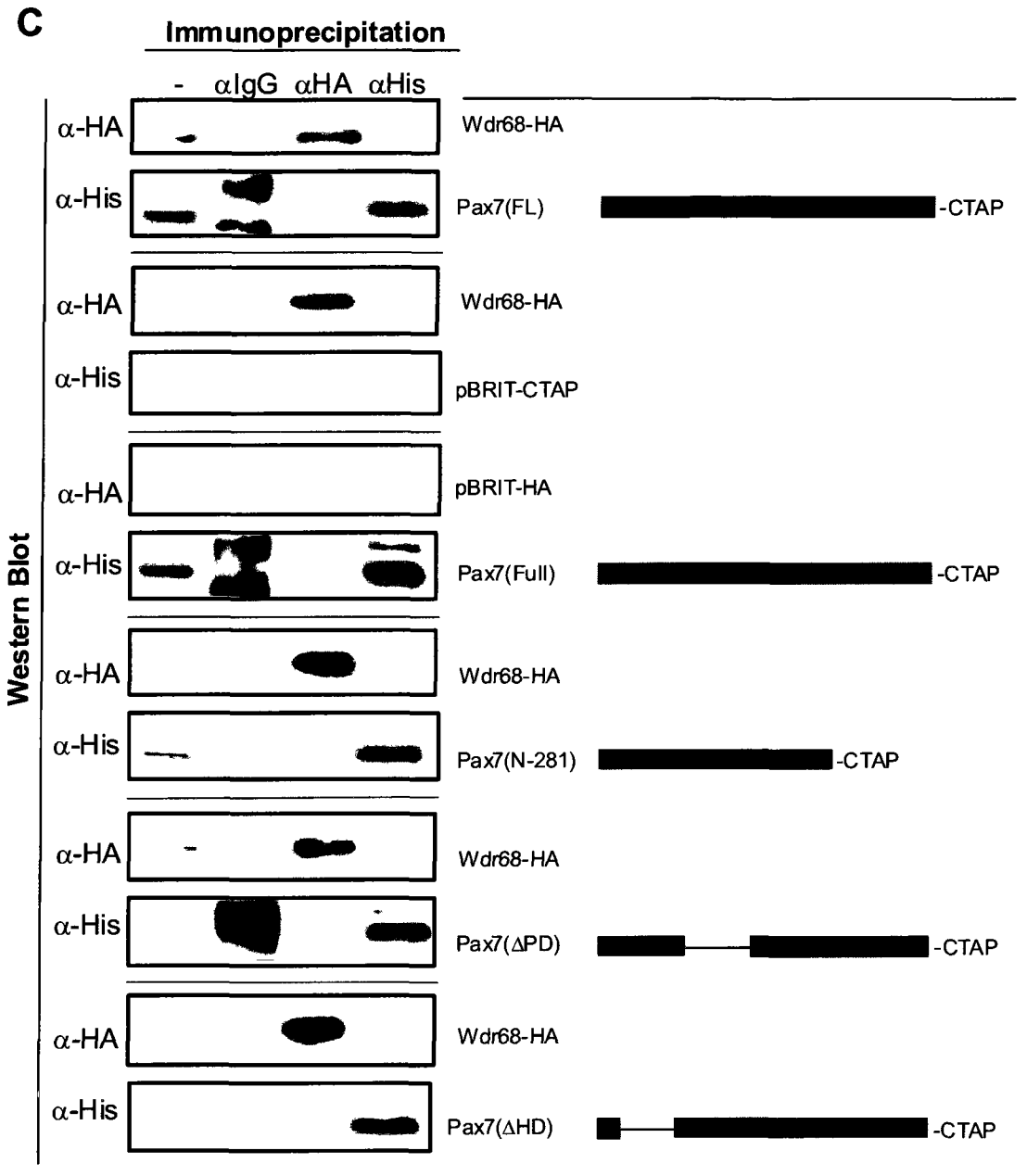

Figure 4.5: Wdr68 does not bind Pax7 in HEK293T cells. (A) Gateway cloning strategy for production of pBRIT-Wdr68-Flag-HA. (B) HEK 293T cell transfection efficiency. (C) Reciprocal co-immunoprecipitation of exogenous full length Wdr68-Flag-HA and mutated Pax7-(mut)-CTAP transiently transfected into HEK 293T cells.

4.4 Wdr68 modulates the gene expression levels of Pax7-target gene and myogenic regulatory factors

Primary myoblasts in growth conditions were transiently transfected with Wdr68 siRNA for 48- or 72-hours, or pBRIT-Wdr68-CTAP for 48-hours. Pax7 expression was observed not to change, while GAPDH expression fluctuated significantly. As such, Pax7 was chosen for normalization (Appendix II).

Putative Pax7 target genes: Zac1, Myf5, Cipar1, Lix1, Mest, Trim54 and Syne1, were identified previously by McKinnell *et al.* (2008). At 48-hours post-transfection, Wdr68 gene expression was reduced by 78%; in addition, expression of Zac1 and Lix1 were significantly increased. MRF expression levels were not seen to fluctuate significantly (Figure 4.6A). At 72-hours post-transfection with Wdr68 siRNA Wdr68 expression was reduced by 64%. The expression of Zac1 was significantly elevated. Interestingly, the gene expression of Myf5, Cipar1, Lix1 and Trim54 were slightly, but significantly, reduced. Additionally, MyoD expression was seen to decrease slightly but significantly (Figure 4.7B).

A 21.7-fold over-expression of Wdr68 resulted in a striking decrease in gene expression of Cipar1, Lix1, Mest and Trim54. Conversely, Zac1 and Syne1 expression increased significantly. MyoD expression was seen to increase slightly, while the expression levels of myogenin and MRF4 showed a striking decrease (Figure 4.7C).

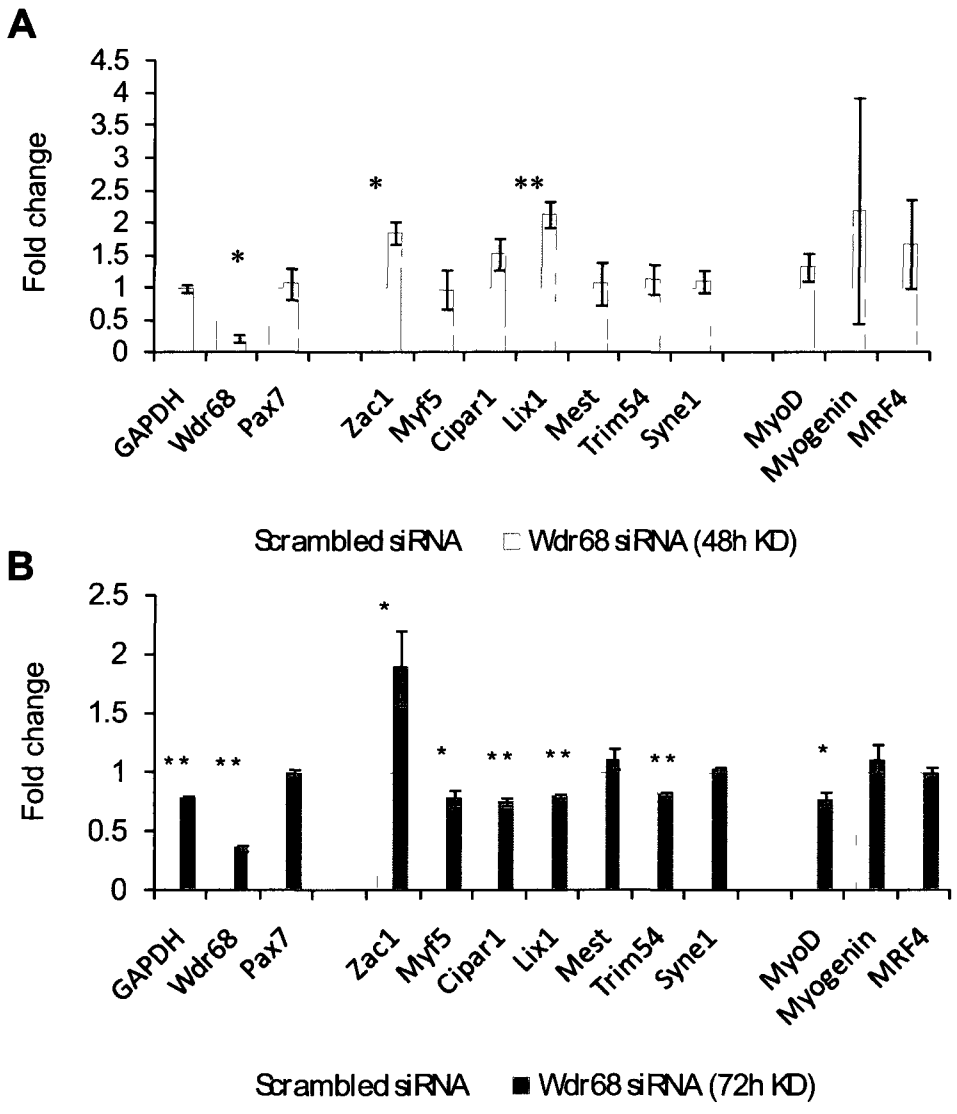

Figure 4.6: **Wdr68 is a putative negative regulator of Pax7 transcriptional activity**. Pax7 target gene expression measured by real-time PCR for Wdr68 knockdown after (A) 48 hours or (B) 72 hours, and (C) Wdr68-CTAP over-expressing primary myoblasts. N=3; *=$p<0.05$, **=$p<0.01$ by single factor ANOVA; error bars are SEM.

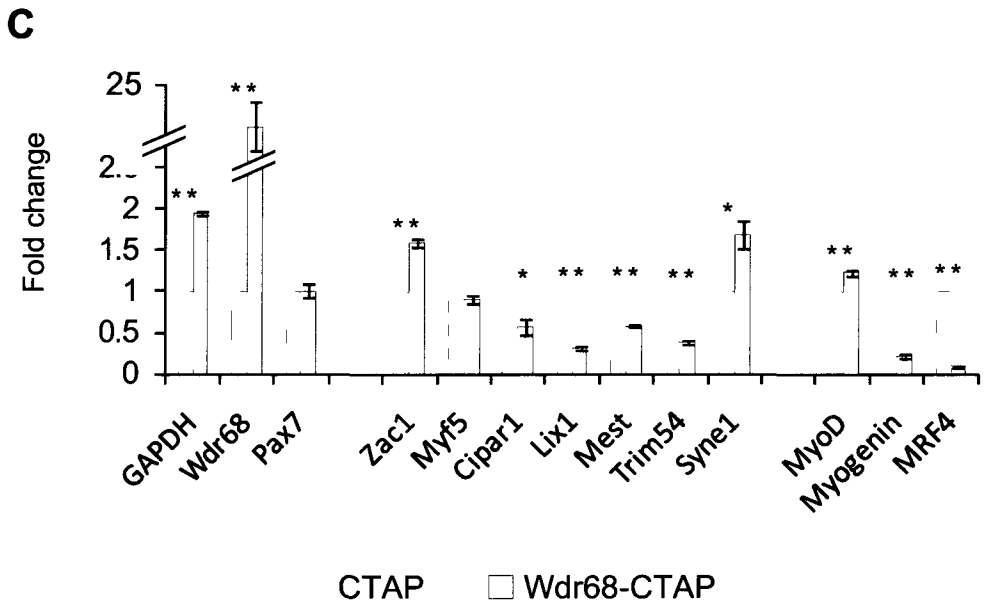

Figure 4.6: **Wdr68 is a putative negative regulator of Pax7 transcriptional activity**. Pax7 target gene expression measured by real-time PCR for Wdr68 knockdown after (A) 48 hours or (B) 72 hours, and (C) Wdr68-CTAP over-expressing primary myoblasts. N=3; *=$p<0.05$, **=$p<0.01$ by single factor ANOVA; error bars are SEM.

4.5 Pax7 modulates gene expression by binding specific sequences in the genome

A genome wide ChIP-seq analysis using Pax7-CTAP over-expressing primary myoblasts was conducted to identify Pax7-enriched genomic regions. Further bioinformatic analysis was conducted to first identify and then screen for Pax7 binding-motifs (V. Punch, unpublished). To test the hypothesis that Wdr68 modulates Pax7 target gene expression by binding chromatin at known Pax7 binding domains, it was first necessary to identify whether Pax7 enrichment peaks were present near the Pax7 target genes listed above; this was accomplished using the UCSC genome browser. If a candidate peak was identified, the sequence below it was scanned for a Pax7 binding motif manually or using the IRC genome browser. Pax7 binding motifs have been characterized for the homeodomain, paired domain, and a combination of the two (V. Punch, unpublished). Finally, real-time PCR primers were designed against the region below the peak.

The genomic region upstream of the *Myf5* coding region has three strong Pax7 enrichment peaks at -15kb, -57.5kb, and -111kb (Figure 4.8A). The latter two each have a paired binding domain (Figure 4.8B,C), while the former, yet to be characterized, has a manually identified, putative homeodomain binding motif (Figure 4.8D). All peaks are largely conserved across species, particularly under their Pax7 binding motifs.

The genomic region surrounding *Zac1* contains two zones of Pax7 enrichment (Figure 4.9A). The first is at +11kb downstream from the transcriptional start site and was previously characterized (V. Seale, MSc thesis). There are many conserved regions under the peak, however there are no identifiable Pax7-binding motifs. The novel Pax7 binding motif identified by V. Seale by DNA foot-printing is adjacent to the site of Pax7 enrichment and not well conserved across species (Figure 4.9B). The second peak is -25kb upstream from the *Zac1* transcriptional start site. While impressive, this peak is also poorly conserved across species. The -25kb homeodomain binding motif (identified using the IRC genome browser) does not fall in the highly conserved region under the peak, but is well situated directly under the center of the peak.

There is one Pax7 enrichment peak -15kb from the *Mest* transcriptional start site (Figure 4.10A). It contains a putative homeodomain binding motif, identified manually, in a non-conserved region near the peak's edge (Figure 4.10B).

Pax7 is enriched -15kb upstream from the *Cipar (Parm1)* transcriptional start site (Figure 4.11A). The peak contains two Pax7-binding domains, the first is a homeodomain binding motif located in the center of the peak, the second is a paired domain binding motif located in a very well conserved region at the periphery of the peak (Figure 4.11B). Each of these Pax7 binding motifs were identified on the –strand using the IRC genome browser.

Two large areas of Pax7 enrichment were identified adjacent to the *Lix1* transcriptional start site (Figure 4.12A). The decision was made to investigate the slightly upstream peak due to the homeodomain binding motif identified using the IRC genome browser located auspiciously at the center of the peak (Figure 4.12B).

No Pax7 enrichment was observed in the genomic region surrounding *Trim54* or *Syne1*.

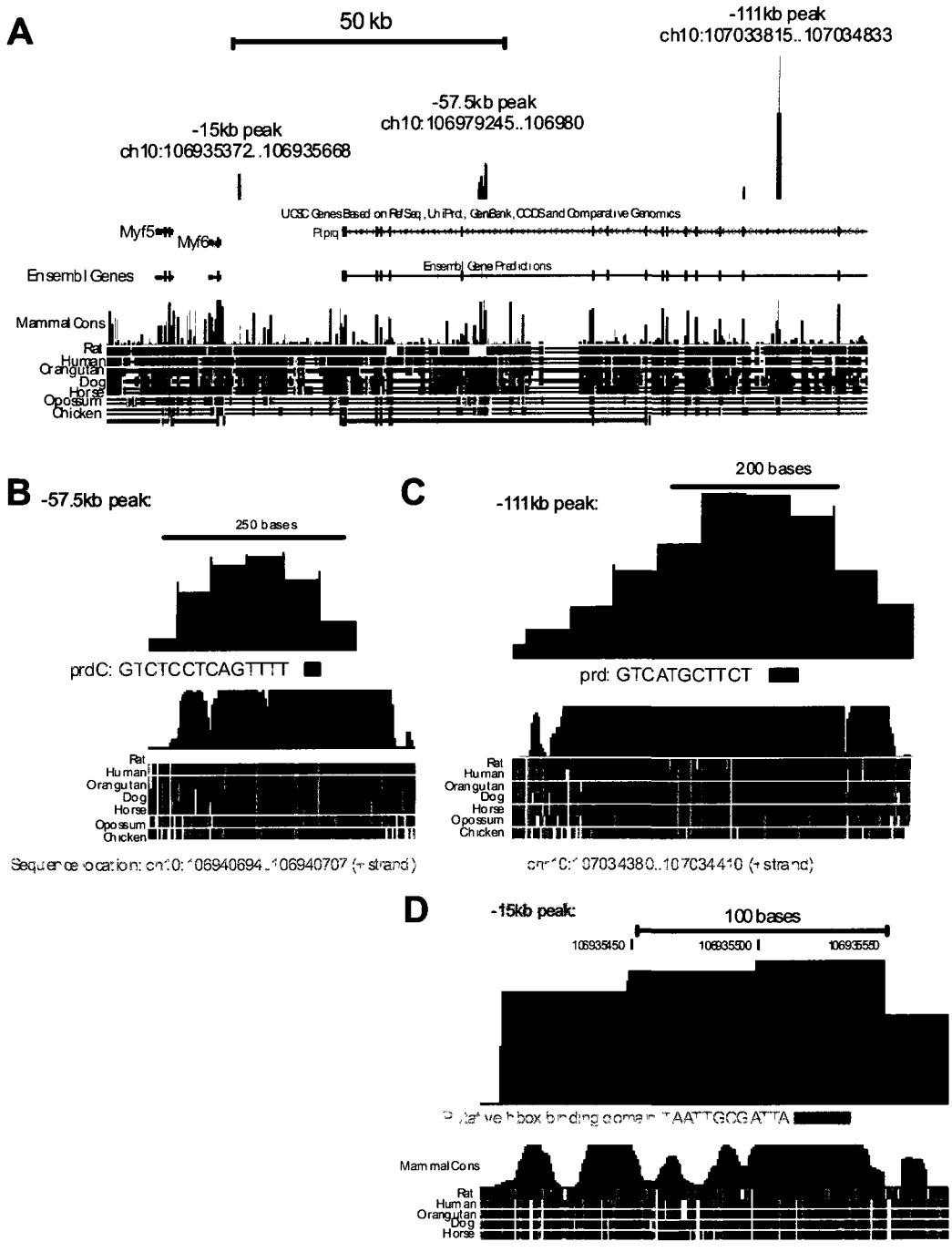

Figure 4.8: **Pax7 enrichment peaks upstream from the *Myf5* locus identified by ChIP-seq.** (A) Entire *Myf5* locus. Zoomed-in views of the (B) -57.5kb, (C) -111kb, and (D) -15kb Pax7-binding peaks with Pax7-binding motifs indicated in red.

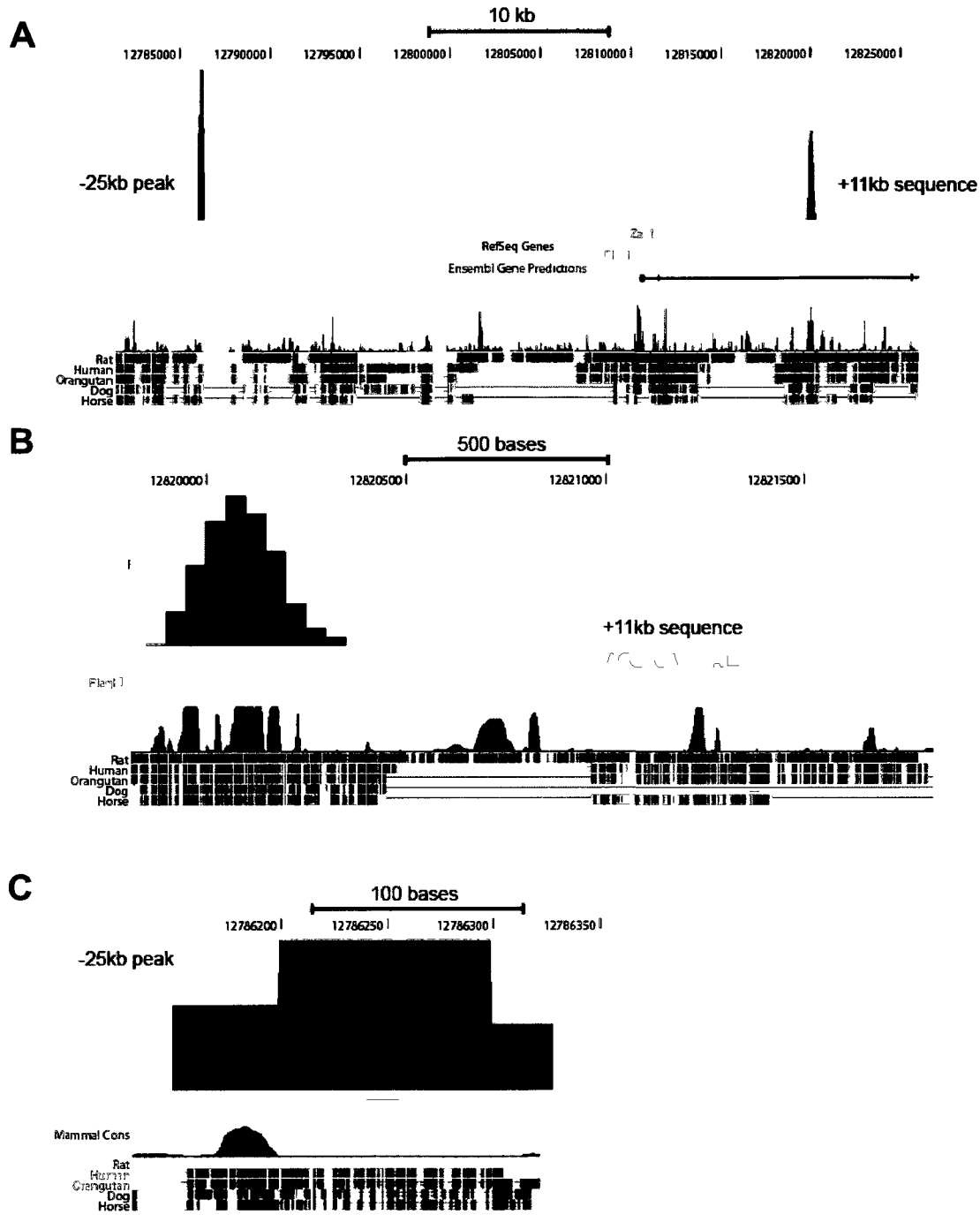

Figure 4.9: **Pax7 enrichment peaks at the *Zac1* locus identified by ChIP-seq.** (A) Entire *Zac1* locus. Zoomed-in views of the (B) +11kb and (C) -25kb Pax7-binding peaks with Pax7-binding motifs indicated in red.

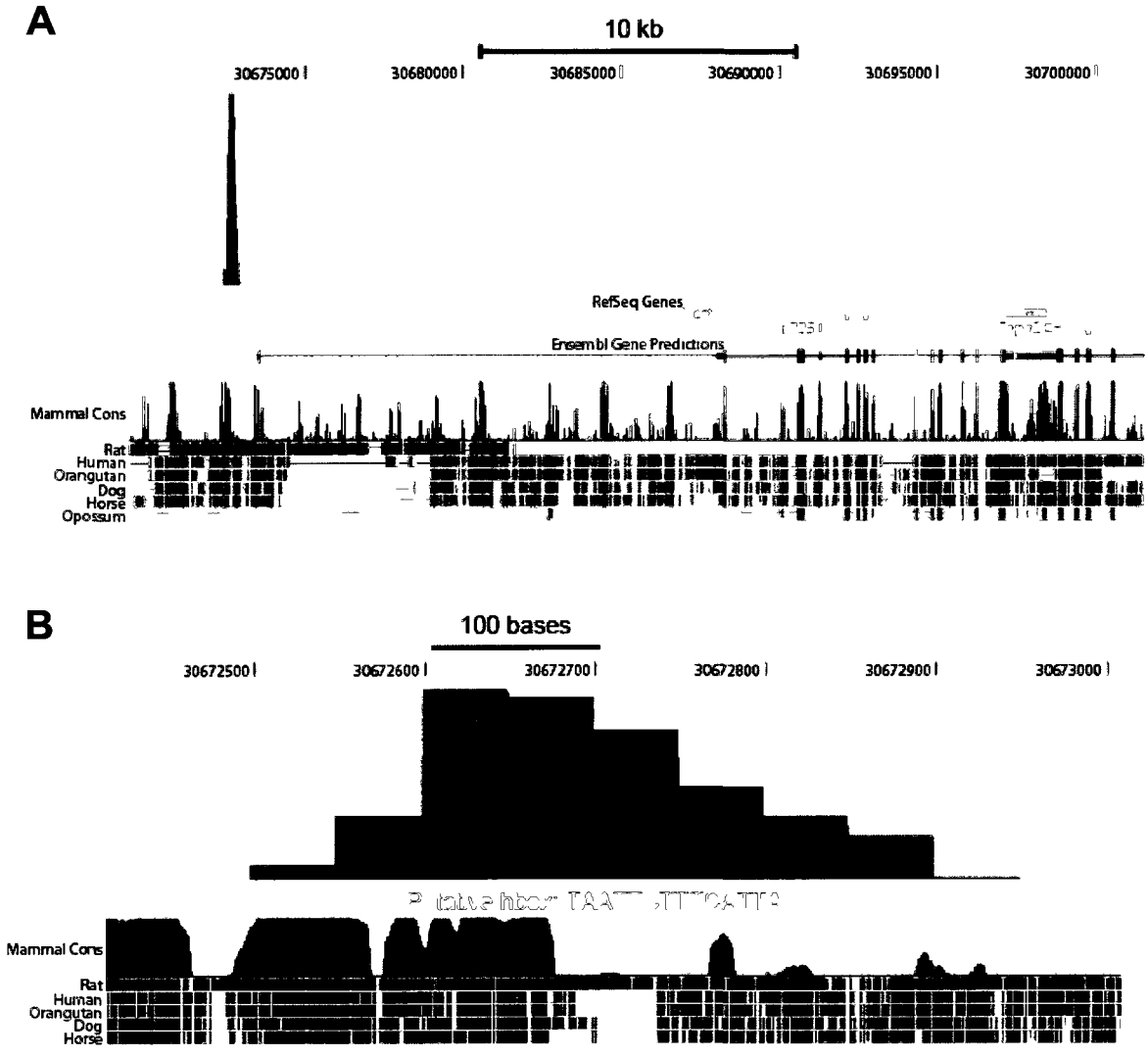

Figure 4.10: Pax7 enrichment peaks at the *Mest* locus identified by ChIP-seq. (A) Entire *Mest* locus. (B) Zoomed-in views of the -15kb Pax7-binding peak with a Pax7-binding motif indicated in red.

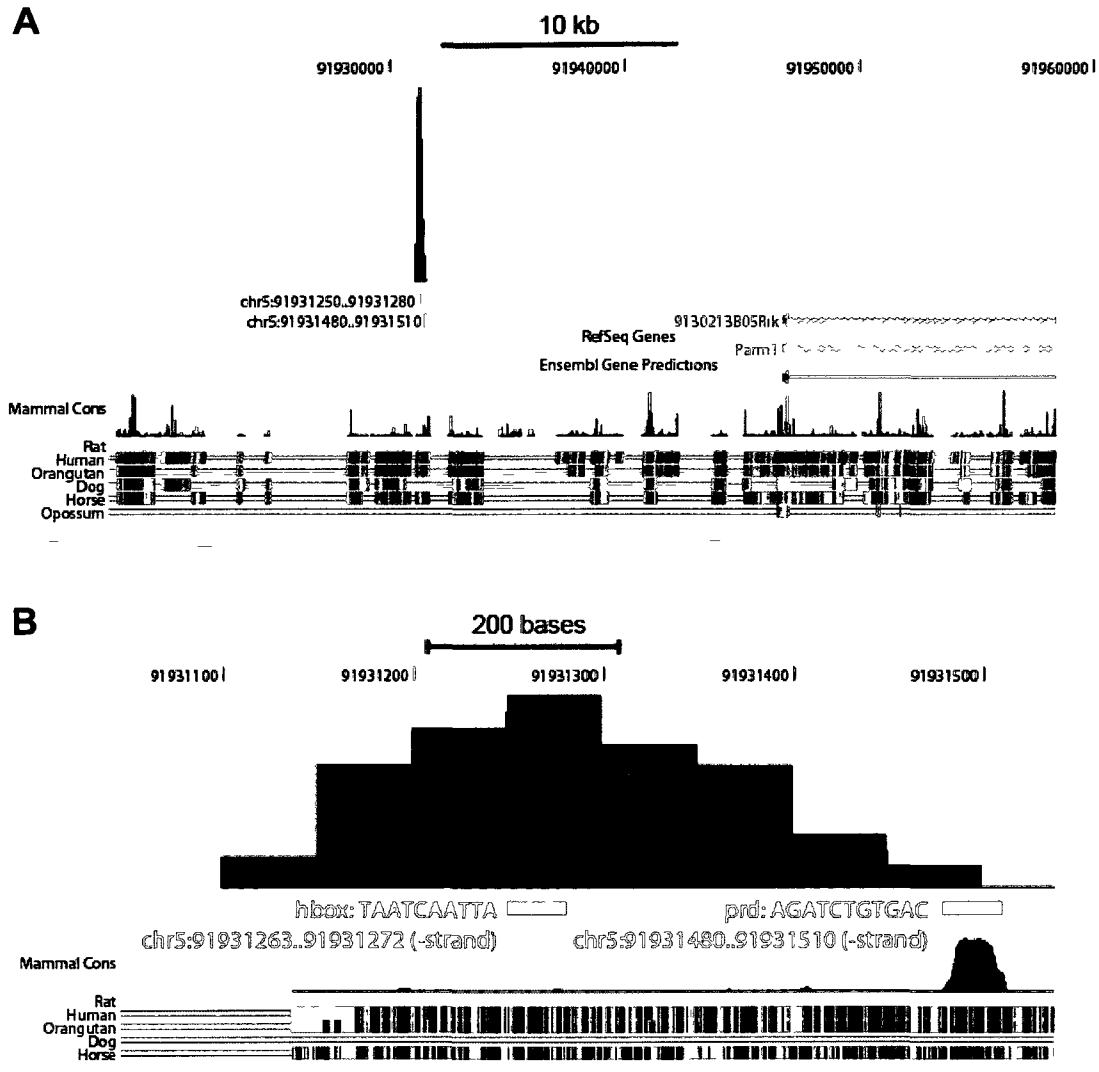

Figure 4.11: Pax7 enrichment peaks at the *Cipar1 (Parm1)* locus identified by ChIP-seq. (A) Entire *Cipar1* locus. (B) Zoomed-in views of the -15kb Pax7-binding peak with Pax7-binding motifs indicated in red.

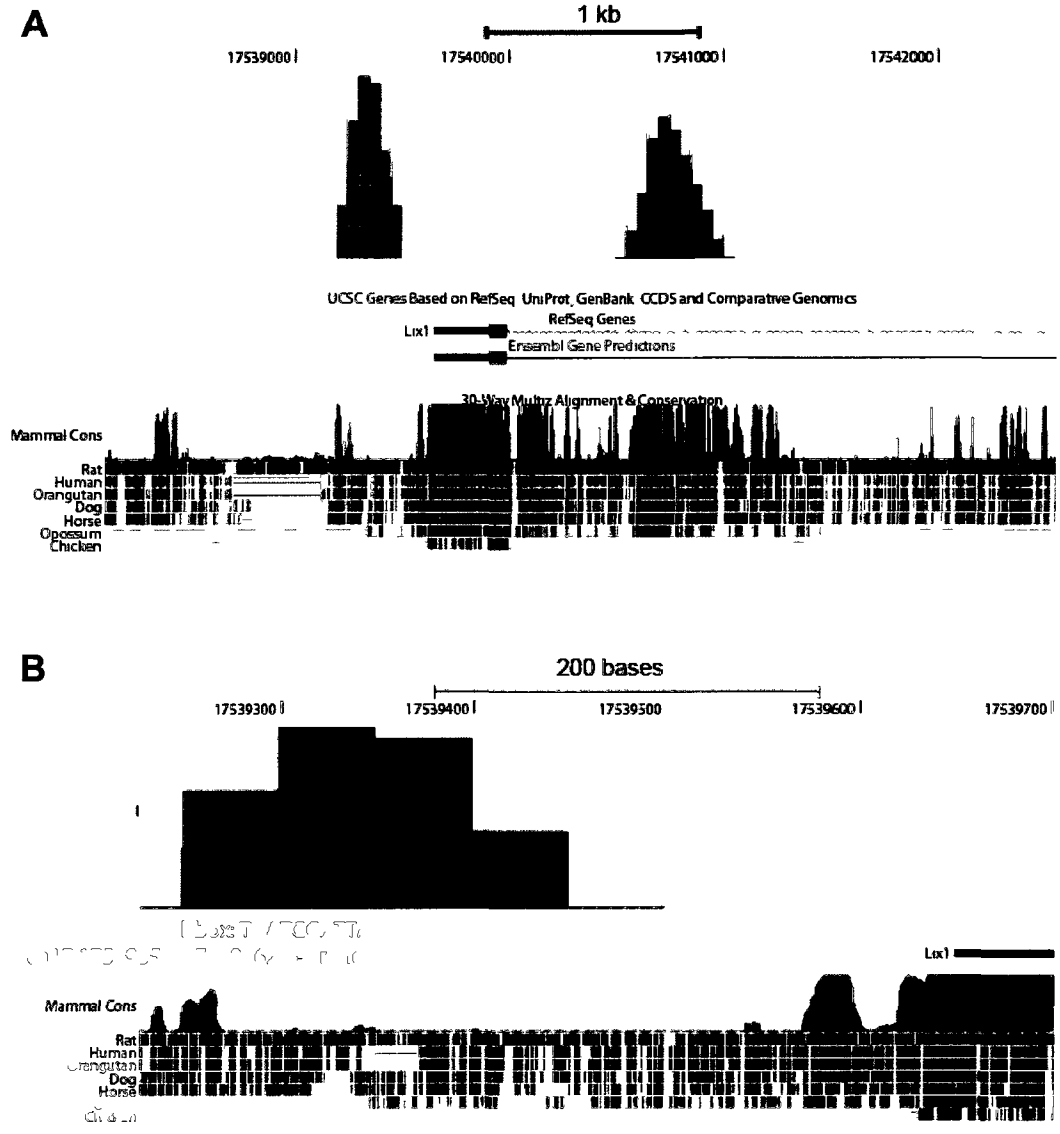

Figure 4.12: Pax7 enrichment peaks at the *Lix1* locus identified by ChIP-seq. (A) Entire *Lix1* locus. (B) Zoomed-in views of the *Lix1*-promoter Pax7-binding peak with a Pax7-binding motif indicated in red.

4.6 Wdr68 does not bind genomic DNA at known Pax7 binding sites

Chromatin immunoprecipitation was conducted from primary myoblasts stably over-expressing CTAP, Pax7-CTAP and Wdr68-CTAP to determine if Wdr68 is enriched at the same genomic locations as Pax7. Pax7-CTAP over expression was verified by western blot (Figure 4.13A) and Wdr68-CTAP over expression was verified by real-time PCR (Figure 4.13B). Pax7-CTAP enrichment was validated at each of the genomic regions identified by ChIP-seq (Ct= ~27), but not at the +11kb Zac1 site previous identified by DNA foot-printing (Ct= ~32). Wdr68 was not enriched at any of the genomic Pax7 binding sites (Figure 4.13C).

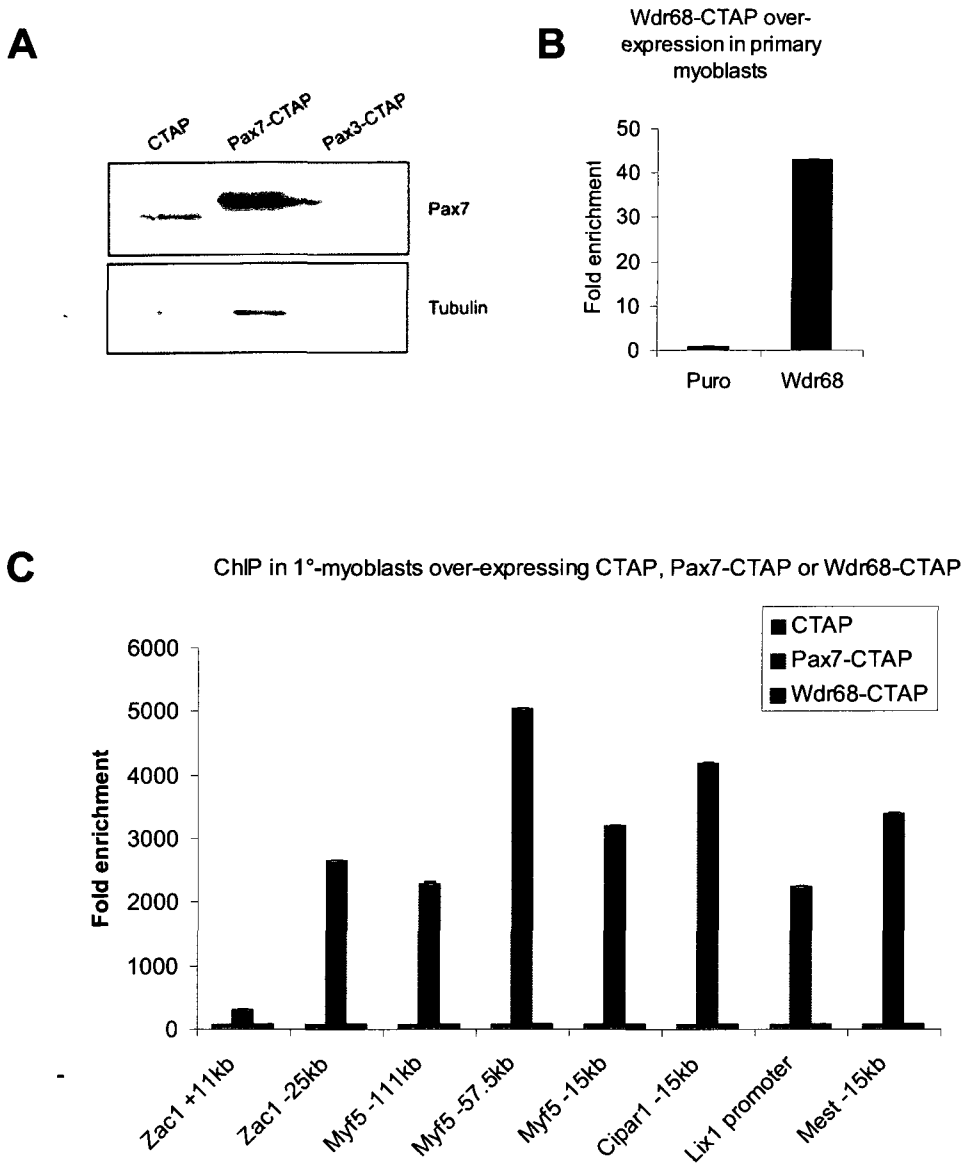

Figure 4.13: Wdr68 does not bind chromatin at known Pax7 binding sites. Demonstration of over-expression of (A) Pax7-CTAP by western blot analysis and (B) Wdr68-CTAP by real-time PCR in primary myoblasts. (C) Chromatin immunoprecipitation conducted from primary myoblasts stably over-expression CTAP, Pax7-CTAP, or Wdr68-CTAP ("no Ct" values seen for CTAP and Wdr68-CTAP were assigned a Ct of 40 cycles in order to calculate Pax7-CTAP fold enrichment). Error bars are SEM.

4.7 Wdr68 does not repress Pax7 transcriptional activity by removing Pax7 from the nucleus

Previous studies regarding the function of Wdr68 demonstrated that it is responsible for repressing Gli1 by removing Gli1 from the nucleus (Morita et al., 2006). To determine whether Wdr68 might exert the same function on Pax7 primary myoblasts were transiently transfected with Pax7-GFP (from Y. Kawabe) and Wdr68-Flag-HA for 48hours (Figure 4.14A). Immunocytochemical analysis and confocal microscopy of the myoblast nuclear region demonstrate that, in the absence of exogenous Wdr68, Pax7 is localized to the nucleus (Figure 4.14B). Upon introduction of exogenous Wdr68, both Pax7 and Wdr68 remain in the nucleus suggesting that Wdr68 is not achieving the repression of Pax7 target genes by translocating Pax7 to the cytoplasm (Figure 4.14C).

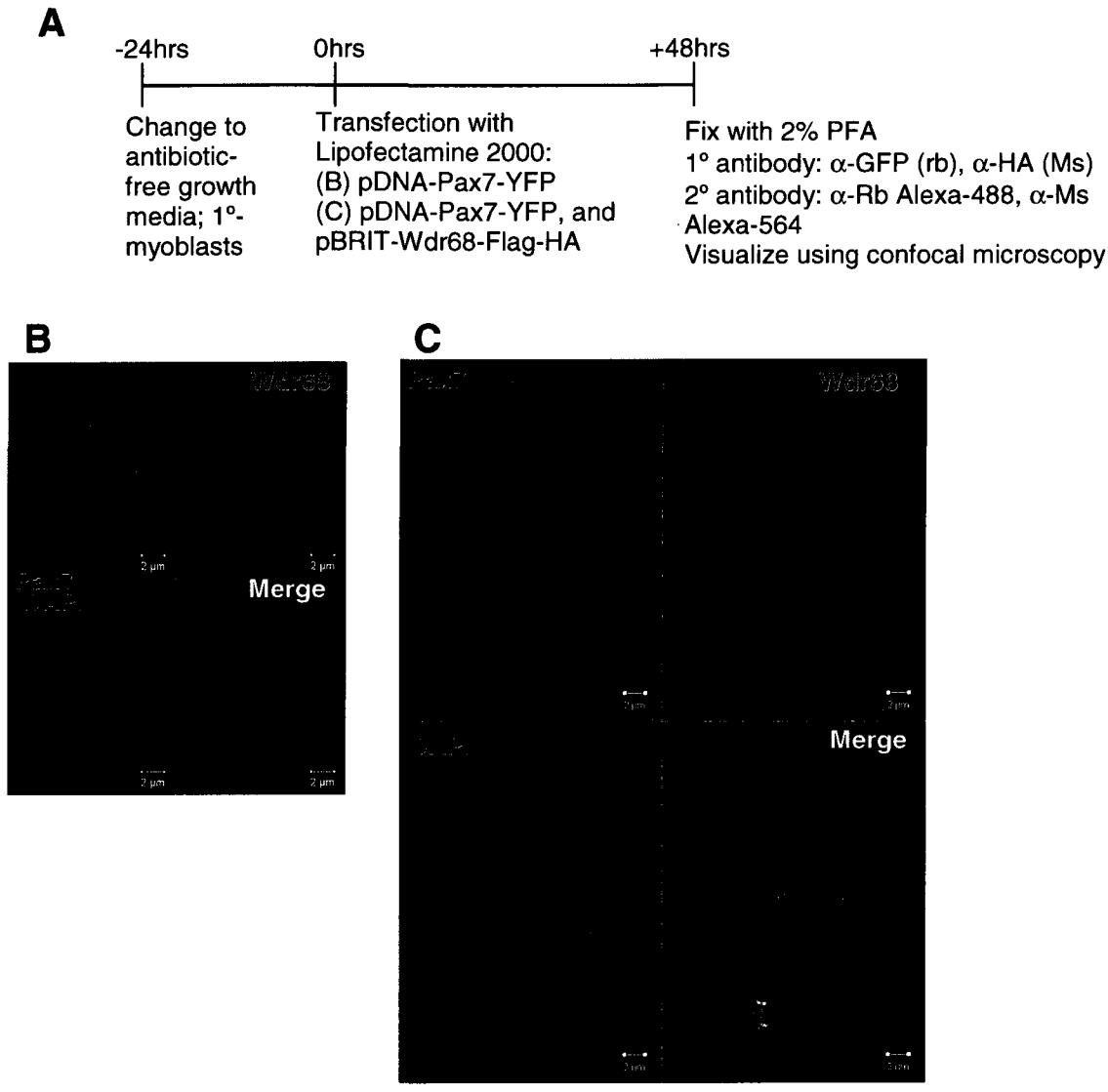

Figure 4.14: Wdr68 does not modulate Pax7 transcriptional activity by translocating Pax7 to the cytoplasm. (A) Schematic of experimental design. (B) Confocal micrograph of immunocytochemical analysis of Pax7 subcellular localization in the absence (B) and presence (C) of exogenous Wdr68. Scale bar is 2μm.

4.8 Wdr68 expression is not altered during myoblast differentiation

Wdr68 expression levels during adult myogenesis in wild type satellite cells were investigated. Wdr68 expression levels were not seen to fluctuate significantly over 7-days of differentiation by microarray analysis (E233 StemBase, MA Rudnicki, 2006) or over 5-days of differentiation by real-time PCR (Figure 4.15). MRF expression levels (Figure 4.15A) and Pax7 expression levels (Figure 4.15B) are also shown as positive controls for the differentiation program.

A

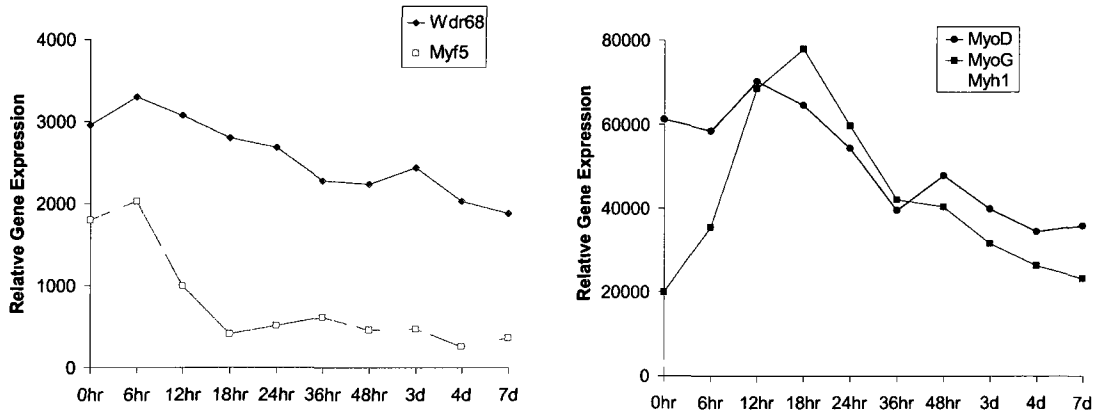

B

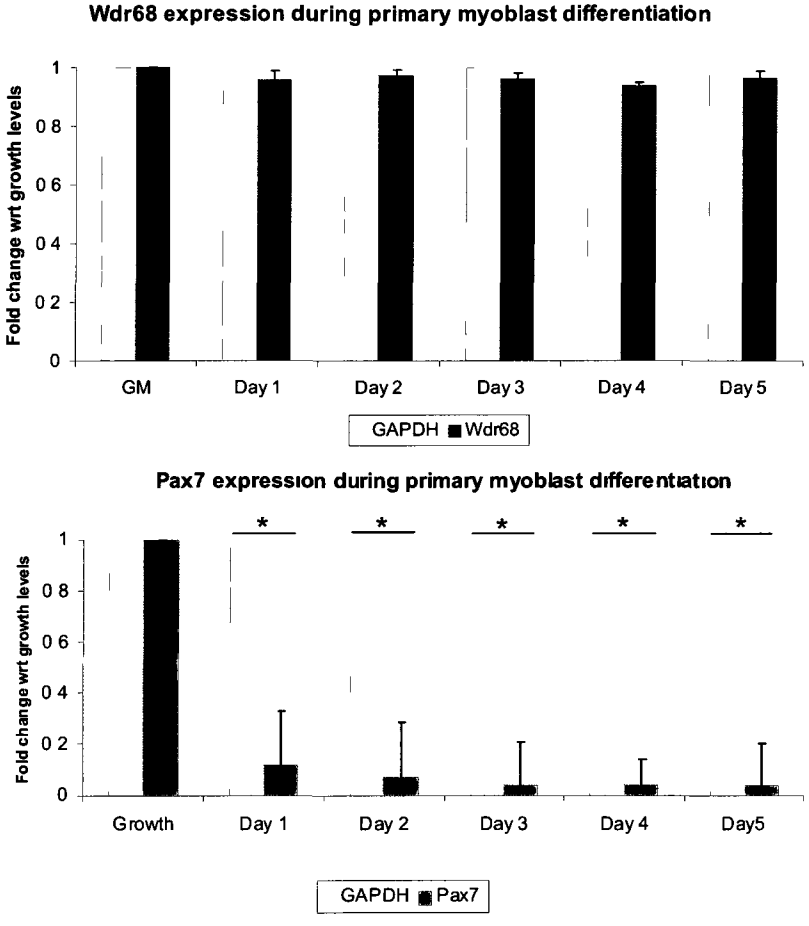

Figure 4.15: **Wdr68 expression levels do not change during wild type primary myoblast differentiation**. (A) Wdr68 and MRF expression profiles measured by microarray (E233 StemBase, MA Rudnicki, 2006). (B) Wdr68 (purple) and Pax7 (green) expression profiles measured by real-time PCR; N=3, $p<0.01$ by single factor ANOVA.

4.9 Wdr68 does not affect myoblast capacity to differentiate

Wdr68 was transiently knocked-down or over-expressed over 4.5 days of differentiation. Cells were transfected twice: once in growth conditions and once more after 60-hours of differentiation. Real-time PCR analysis confirmed that Wdr68 knockdown levels remained between -72% and -85%. Over-expression levels remained between 126- and 415-fold (Figure 4.16A). Despite these severe modulations of Wdr68 expression levels, myoblast fusion indices remained unchanged with respect to control (Figure 4.16B, C).

A

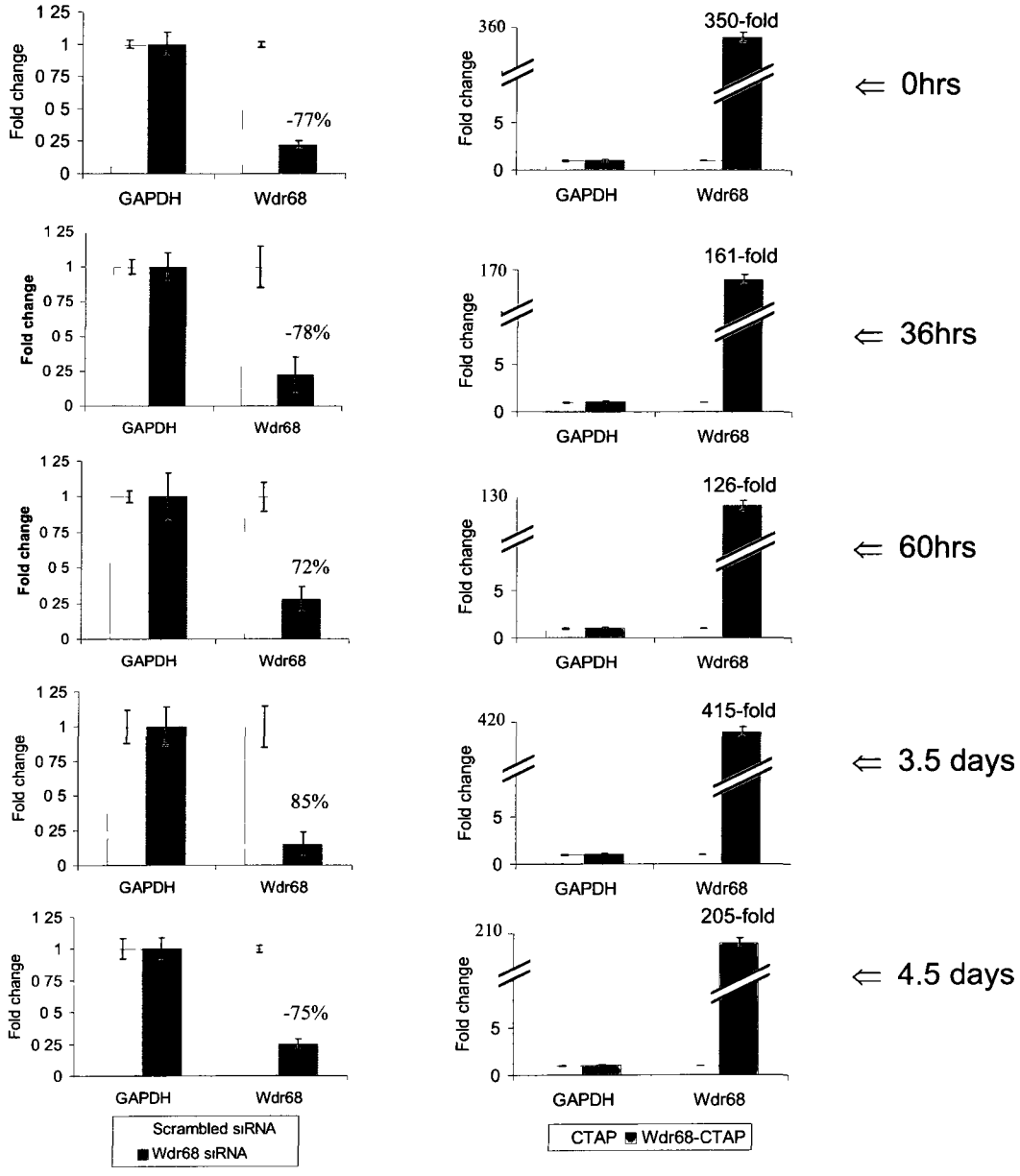

Figure 4.16: **Wdr68 does not affect myoblast capacity to differentiate**. Wdr68 was transiently knocked-down (blue) or over-expressed (red) in primary myoblasts over a 4.5-day differentiation time course. (A) Gene expression of Wdr68 measured by real-time PCR. (B) Cells were stained for myosin heavy chain and (C) fusion index was calculated. N=3, error bars are SEM.

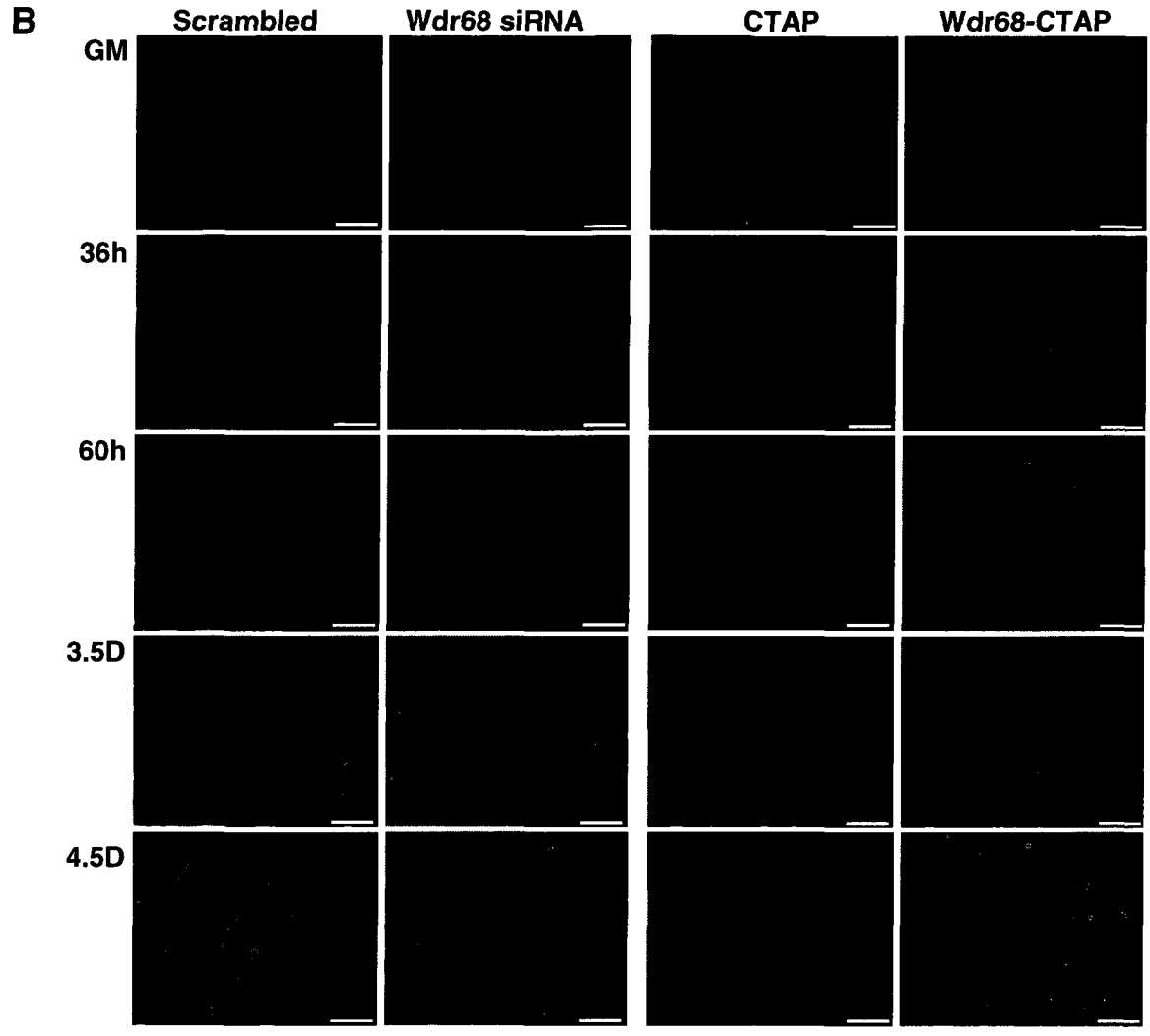

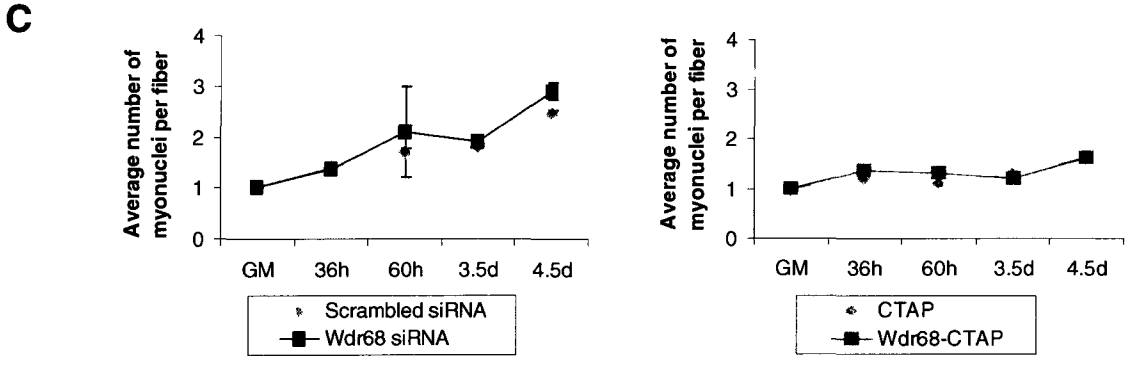

Figure 4.16: **Wdr68 does not affect myoblast capacity to differentiate**. Wdr68 was transiently knocked-down (blue) or over-expressed (red) in primary myoblasts over a 4.5-day differentiation time course. (A) Gene expression of Wdr68 measured by real-time PCR. (B) Immunocytochemical analysis was conducted using antibodies directed against myosin heavy chain and (C) fusion index (or, average number of nuclei per fiber) was calculated. N=3, error bars are SEM.

4.10 MyoD and MyoG are enriched near the Wdr68 promoter region upon 48-hrs differentiation, but not in growth

A genome wide ChIP-seq analysis was conducted in primary myoblasts to identify MRF-enriched genomic regions (V. Soleimani and V. Punch, unpublished). Using the UCSC genome browser we observed that after 48-hours of primary myoblast differentiation, both MyoD and myogenin were enriched at the *Wdr68* locus near the transcriptional start site (Figure 4.18).

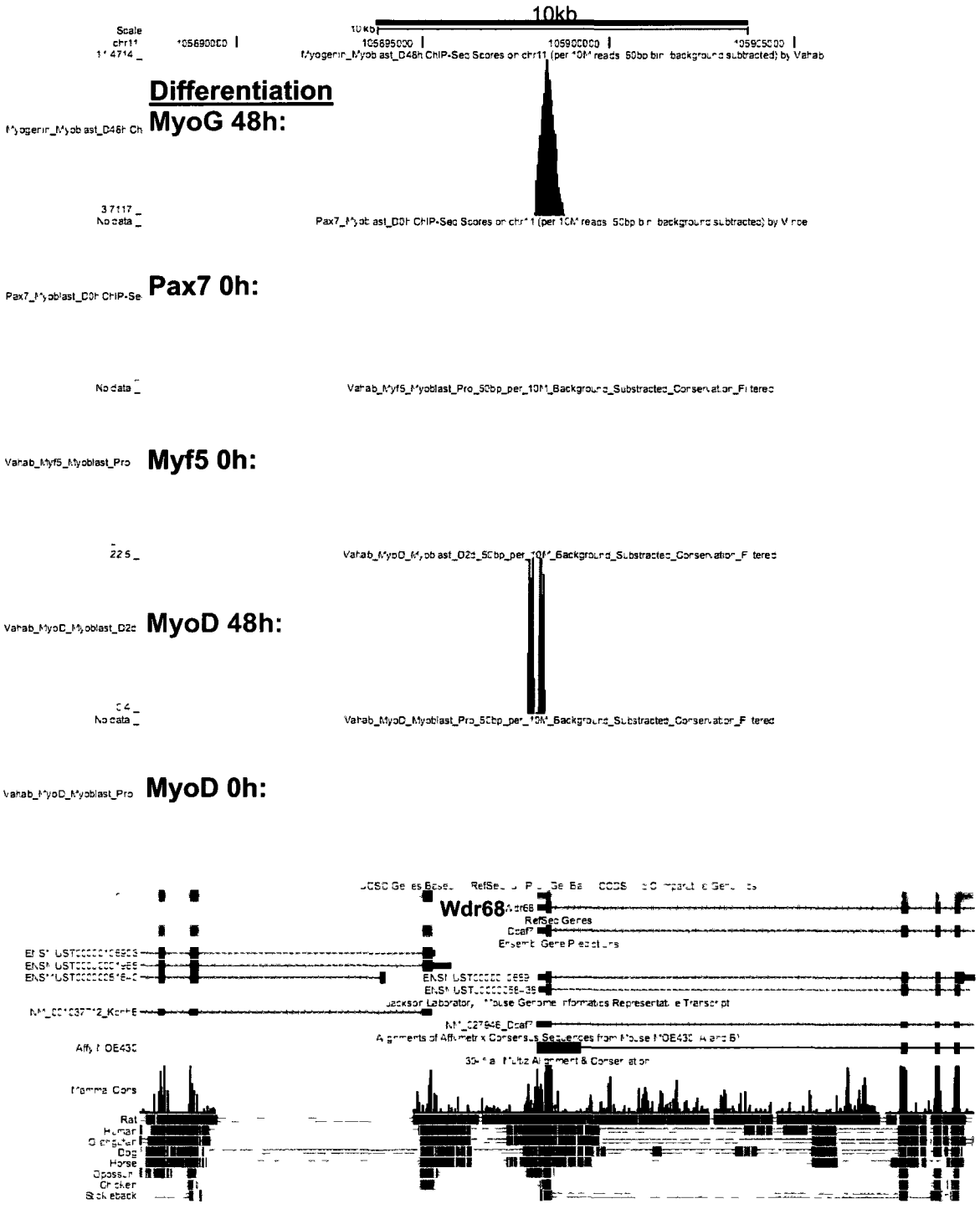

Figure 4.17: The Wdr68 promoter is bound by MyoD and Myogenin after 48hrs of primary myoblast differentiation.

CHAPTER 5

Discussion

5.1 Discussion

Healthy adult skeletal muscle has a remarkable capacity to grow and regenerate. This capacity is largely due to the heterogeneous population of satellite cells present beneath the basal lamina and adjacent to the muscle fiber. Regenerative ability is lost in aging and myopathic muscle. The molecular mechanisms that underlie the natural regenerative program are under active investigation with the expectation that gaining an understanding of these will open avenues for treatment of those who suffer from myopathy due to impaired regenerative capacity. The power in understanding the adult muscle stem cell lies in its putative capacity to regenerate any afflicted muscle, regardless of the specific myopathy. Quiescent and activated muscle satellite cells are best characterized by their expression of the paired-box transcription factor Pax7. Pax7 is required for the specification, maintenance and survival of satellite cells (Seale et al., 2000). In addition Pax7 is the first myogenic regulatory factor expressed in the tightly regulated and highly conserved myogenic program. For these reasons Pax7 is both an attractive and powerful candidate for those interested in investigating adult myogenesis.

Recent insight into the Pax7 molecular mechanism of action revealed that Pax7 can activate target gene expression by recruitment of the Wdr5-Ash2L-MLL2 histone methyltransferase (HMT) complex which modifies chromatin to a transcriptionally active conformation via tri-methylation of the fourth lysine of histone three (H3K4-3me) (McKinnell et al., 2008). In this study Pax7 target

genes were identified by microarray comparison of Pax7-CTAP over-expressing C2C12 myoblasts against wild type C2C12 myoblasts. One exciting candidate for Pax7 activation was the Myf5 basic helix-loop-helix transcription factor which showed a 2.2-fold upregulation by microarray analysis and a 3-fold upregulation by real-time PCR. Myf5 is required for the proliferative phase of adult myogenesis (Montarras et al., 2000). It was demonstrated by chromatin immunoprecipitation experiments that Pax7 binds an enhancer region located 57.5kb upstream from the *Myf5* transcriptional start site. In addition, tandem affinity purification of Pax7-CTAP, followed by MALDI-TOF mass spectrometric analysis, identified the Wdr5-Ash2L-MLL HMT complex as interacting with Pax7. This interaction was validated by co-immunoprecipitation and demonstrated to activate *Myf5* gene expression via H3K4 tri-methylation of the *Myf5* locus using H3K4-2me and -3me specific antibodies. It was proposed that Pax7 is able to transcriptionally activate other targets in the same manner (McKinnell et al., 2008).

Wdr68 was identified by the same TAP/MS analysis of Pax7-CTAP over-expressing C2C12 cells and deemed interesting based on its implied structural similarity to Wdr5. Because a comprehensive understanding of Pax7's molecular mechanism of action remains incomplete and is likely not fully accounted for by the Wdr5-Ash2L-MLL HMT complex, we postulated that Wdr68 might act in a similar fashion to Wdr5 by assembling regulatory proteins at Pax7-responsive genomic regions. The inference that Pax7 transcriptional complex variation is

mediated by different WD40-repeat proteins is probable given that these proteins are defined both by (1) their structural similarity which allows for their conserved ability to stage the assembly of protein complexes, and (2) the high sequence variability of their variable regions which allows for high complex specificity within a WD40-repeat protein and high complex variability across distinct WD40-repeat proteins. Similar suggestions have been put forth including the postulation that distinct WD40-repeat proteins are the substrate-specific adaptor proteins of the CUL4-DDB1 ubiqutin ligase which has been previously observed at the level of histone 3 methylation (Higa et al., 2006). Investigation of Wdr68 with respect to Pax7 presented us with a unique and intriguing opportunity to pursue a novel protein candidate about which very little has been documented generally and nothing as been documented with respect to skeletal muscle.

Given that Wdr68 is a protein about which very little has been published there existed no established functional paradigm which could be applied to this investigation. The primary goal of this project was to pursue Wdr68's putative interaction with Pax7 and consequent perturbation of Pax7-mediated gene regulation. In particular, we hypothesized that Wdr68 plays an important role in myogenesis by interacting with Pax7 and modulating its ability to transcriptionally activate genes. The specific aims were to (1) demonstrate an interaction between Pax7 and Wdr68 in primary myoblasts, (2) observe a change in Pax7-target gene expression upon modulation of Wdr68 expression, (3) functionally elicit how

Wdr68 is able to modulate Pax7 activity, and (4) describe any phenotype produced by alteration of Wdr68 expression levels in primary myoblasts.

5.1.1 Demonstrate an interaction between Pax7 and Wdr68 in primary myoblasts

The first step toward understanding the role for Wdr68 in adult mogenesis was to validate the Wdr68/Pax7 interaction in primary myoblasts. Since the current commercially available anti-Wdr68 antibodies are not suitable for immuno-analysis, we produced a Wdr68-CTAP tagged version of the protein and successfully co-immunoprecipitated exogenous Wdr68-CTAP with endogenous Pax7 in primary myoblasts (Figure 4.4). It was important to validate this interaction in primary myoblasts because, unlike C2C12 myoblasts, they endogenously express Pax7 and therefore represent an earlier and more physiologically-relevant system.

The apparently weak interaction between Pax7 and Wdr68 was first attributed to complex squelching due to the substantial over-expression of Wdr68-CTAP. To gain insight into the interaction between Pax7 and Wdr68 we were interested to determine with which domain of Pax7 Wdr68 interacted. We produced another tagged version of Wdr68 (Wdr68-Flag-HA) which was co-transfected into HEK293T cells (as well as COS cells, not shown) with various Pax7-CTAP deletion constructs. No interaction between Wdr68-Flag-HA and Pax7-CTAP was observed in these two non-myogenic cell populations thus indicating that the weakness of the interaction observed in primary myoblasts by co-immunoprecipitation and western blot analysis was more likely a reflection of an

indirect interaction between these two proteins (Figure 4.5). The fact that the interaction between Pax7 and Wdr68 has also been observed in C2C12 myoblasts suggests that components unique to the myogenic cellular environment are required for this interaction to occur. As such, it would be useful to repeat this experiment in myogenic cells. This result is unlike the Wdr5/Pax7 interaction which is a direct one between Wdr5 and the Pax7 paired domain (McKinnell et al., 2008).

5.1.2 Observe a change in Pax7-target gene expression upon modulation of Wdr68 expression

To establish a role for Wdr68 with respect to Pax7, we over-expressed or knocked-down Wdr68 in primary myoblasts and then quantified Pax7 target gene expression by real-time PCR (Figure 4.6). These two conditions led to an unexpected and significant change in GAPDH expression levels, a gene which is typically categorized as a house-keeping gene due to its canonically stable expression profile and therefore often used for gene expression normalization in real-time PCR. Pax7 gene expression remained largely stable and was therefore considered a more appropriate contender and used for normalization of gene expression. The concordant stability of Myf5 expression, a gene whose fluctuations in expression usually mirror those of Pax7, was used as support that Pax7 expression levels were indeed remaining unchanged. This finding signifies two important points regarding Wdr68. The first is that Wdr68 does not play a role in *Pax7* gene regulation. The second is that Wdr68 cannot override Pax7 to interfere with *Myf5* gene expression levels. This offers cadence to the notion that different genes respond to Pax7 via different mechanisms.

We tested the expression level of other Pax7 target genes in order to assess Wdr68 penetrance of Pax7 transcriptional control (Figure 4.6). The genes chosen were previously identified to respond positively to Pax7 transcriptional control and demonstrated the following sensitivity to Pax7-CTAP over-expression in C2C12 cells by microarray/real-time PCR analysis: Zac1 (385/136-fold), Lix1 (12.3/3.8 fold), Syne2 (11.3/2.2 fold), Cipar1 (8.1/166.6 fold), Trim54 (7.2/4.1 fold), and Mest (5.0/17.9 fold) (McKinnell et al., 2008). Strikingly, real-time PCR analysis of gene expression in Wdr68 over-expressing primary myoblasts led to a large and significant decrease in the expression of *Cipar1, Lix1, Mest* and *Trim54*. In addition, 48- and 72-hours of Wdr68 knockdown led to a significant increase in the expression of Lix1 (48h only) and Zac1, the two Pax7 target genes that demonstrated the overall highest sensitivity to Pax7 by microarray analysis. From this we put forth the hypothesis that Wdr68 might assemble a complex that negatively regulates Pax7. This complex would represent the first known complex identified to do so.

While the trend of Pax7 negative regulation by Wdr68 is the strongest and most striking in this set of data, there inevitably exist some outliers that oppose this trend and must be accounted for. The most apparent aberration is seen after 72-hours of Wdr68 knockdown when *Myf5*, *Cipar1*, *Lix1* and *Trim54* gene expression levels were observed to decrease slightly. It is first important to highlight that these decreases in expression levels gain their mathematical

significance not from the magnitude of their drop, but from their consistency across replications; and, that these modest decreases might not be sufficient in size to dramatically perturb cellular activity. What is likely more significant is the fact that Wdr68 expression has risen 14% from 78%-knockdown at 48-hours to 64%-knockdown after 72-hours. This suggests the induction of some compensatory mechanism after 72-hours of knockdown reflecting the myoblast's efforts to regain homeostasis. This homeostatic kickback is likely also reflected in the decrease in expression of this collection of Pax7 target genes. Another possibility is that there is a dose difference in Wdr68 function. And finally, one cannot exclude the possibility that, in addition to assembling repressive complexes, Wdr68 might also be able to provide scaffolding for activating complexes depending upon the cellular environment.

Another anomaly is present in Zac1. Interestingly, while Zac1 appears to be most sensitive to Wdr68 perturbation, its response is paradoxically a consistent increase in expression. At this point it is important to clarify that an interaction between Wdr68 and Pax7 only implies a functional relationship; and, while the flux observed by Pax7-target gene expression upon modulation of Wdr68 expression supports this hypothesis, on its own it cannot conclude causality. In addition, flux in the expression of genes thought not to respond directly to Pax7 such as GAPDH, MyoD, Myogenin and MRF4 in response to changing Wdr68 expression levels suggests that an indirect, potentially Pax7-independent and certainly more complicated mechanism might be in effect. A Pax7-independent

Wdr68 transcriptional mechanism of action does not preclude the existence of a Pax7-dependent mechanism, and is in fact supported by co-localization schematics generated by confocal microscopy which revealed that Wdr68 and Pax7 are often, but not always, co-localized in the nucleus (not shown). This supposition is also supported by the fact that Wdr68 expression persists far beyond the point of Pax7 down-regulation as myoblast differentiation progresses. Recent work from our group surmised that although Zac1 is a Pax7-target gene, it might not be under the control of the Wdr5-Ash2L-MLL HMT complex (V. Seale, MSc thesis). Wdr68 represents an interesting alternative for consideration when studying regulation of *Zac1*.

It is noteworthy that Wdr68 has been shown to be required for the transcriptional expression of the *endothelin-1* gene which mediates the *end1* signaling pathway required for lower jaw formation in embryonic zebrafish (Nissen 2006). In addition, Wdr68 over-expression has been shown to decrease Gli1-mediated gene transcription in SZ95 sebocytes (Morita 2006). Therefore there exist precedents for Wdr68-mediated gene regulation which bolsters the argument that Wdr68 might play some yet uncharacterized role in the control of gene expression during myogenesis.

5.1.3 Functionally elicit how Wdr68 is able to modulate Pax7 activity

Based on the few precedents in the literature we put forth two hypotheses addressing how Wdr68 might functionally regulate Pax7: (1) Similar to Wdr5, Wdr68 might bind chromatin and mediate complex formation at Pax7-sensitive

loci, or (2) Wdr68 might translocate Pax7 to the cytoplasm, in the same way it has been shown to affect Gli localization.

To address the first hypothesis, we identified genomic sites of Pax7 enrichment from previously generated Pax7 ChIP-seq data (V. Punch, unpublished) using the UCSC genome browser. Genomic Pax7-binding motifs within these peaks were identified using the IRC genome browser (Figures 4.8-4.12). Primers were designed against the sequence under these peaks with an amplification product not exceeding 185bp. Next, chromatin immunoprecipitation of primary myoblasts expressing exogenous CTAP (negative control), Pax7-CTAP (positive control), or Wdr68-CTAP (experimental) were conducted and enrichment at these sites was quantified by real-time PCR (Figure 4.13). The Pax7 enrichment at these sites was validated however, surprisingly, Wdr68 was not observed to bind chromatin at any of these loci. This result does not preclude the possibility that Wdr68 binds elsewhere in the genome, nor does it exclude the possibility that binding elsewhere might affect Pax7 activity via an interaction made possible by chromatin looping.

Wdr5 has been shown to directly bind histone three (Couture et al., 2006; Han et al., 2006; Ruthenburg et al., 2006; Wysocka et al., 2005). To ascertain whether Wdr68 binds chromatin in general, it would be useful to attempt to co-immunoprecipitate it with histone three. Further, it would be interesting to extend this study by repeating the co-immunoprecipitation with antibodies directed

against epigenetic modifications of histone three known to represent open and closed chromatin. If Wdr68 is indeed causing negative regulation of Pax7-target genes via recruitment of factors that cause epigenetic modification of histones, one would expect it to co-immunoprecipitate with methylated H3K4 and H3K27, but not H3K4. Finally, upon validation of an interaction between Wdr68 and chromatin, it would be useful to conduct a TAP/MS analysis of Wdr68-CTAP expressing myoblasts and then identify putative complex components by cross-comparison with the list generated by the Pax7-CTAP TAP/MS experiment conduct previously (McKinnell et al., 2008).

Wdr68 over-expression in SZ95 sebocytes has been shown to decrease cell proliferation and increase cytoplasmic Gli1 (Morita et al., 2006). To address our second hypothesis, that Wdr68 negatively regulates Pax7 by removing from the nucleus, primary myoblasts expressing only Pax7-GFP or both Pax7-GFP and Wdr68-Flag-HA were analyzed by immunocytochemistry (Figure 4.14). Translocation of Pax7 from the nucleus in response to exogenous Wdr68 was not observed. This result was quite conclusive and underscores how reliant the non-catalytic WD40-repeat proteins are on the other proteins present in their cellular environment to dictate their functionality. This result suggests that proteins able to bind Wdr68 and mediate transcription factor translocation in SZ95 sebocytes are likely not present in primary myoblasts.

5.1.4 Describe any phenotype produced by alteration of Wdr68 expression levels in primary myoblasts

Wdr68 expression does not fluctuate significantly in wild type primary myoblasts over seven days of differentiation indicating that it has an expression profile that is distinct to that of Pax7 (Figure 4.15). This implies that Wdr68 likely supports other functions in the cell beyond mediating Pax7 activity that extend to later time-points in differentiation. Wdr68 is thought to act upstream of the bHLH transcription factor AN2 by mediating its post-translational modification in petunia (de Vetten et al., 1997). It is therefore not implausible to foresee a role for Wdr68 later during the myogenic program in which it might mediate the modification of members of the MyoD basic helix-loop-helix family of transcription factors. In an interesting twist, it appears that this putative regulation might be reciprocated by MyoD and myogenin, both of which are enriched near the Wdr68 promoter upon 48-hours of primary myoblast differentiation (figure 4.17).

In growth conditions, over-expression or knock-down of Wdr68 were not observed to have an effect on myoblast viability by Tunel assay Figure 4.3). This suggests that Wdr68 doesn't play a role in programmed cell death in cultured primary myoblasts. This is consistent with Wdr68 involvement in cell survival implied both by its interaction with Dyrk1b which promotes survival of rhabdomyosarcomas (Mercer et al., 2006) and its putative role as a biomarker for prostate cancer (Fujita et al., 2008). Interestingly, Wdr68 over-expression significantly slowed myoblast rate of proliferation (as seen previously (Morita et al., 2006)). This was observed in practice while expanding Wdr68-CTAP

expressing cells and then quantified by Ki67 staining (Figure 4.2). At a molecular level this slow down in proliferation was accompanied by a slight but significant increase in MyoD expression which supports the idea of precocious cell cycle exit and differentiation (Figure 4.6). In addition, there is an accompanying and striking down-regulation of myogenin which has interesting implications (see the following section and Figure 5.1).

There is an indirect link between Wdr68 and myogenesis in the literature: the Dyrk1b kinase. Dyrk1b is a well described Serine/Threonine kinase that is enriched in skeletal muscle and has been highly implicated in the regulation of growth arrest and differentiation (Mercer and Friedman, 2006). Its expression is induced by the RhoA GTPase and as well as the transition from growth to differentiation (Deng et al., 2003). Dyrk1b is required for myoblast fusion due to its regulation of myogenin expression. Dyrk1b transcriptional control over *myogenin* was demonstrated in C2C12 myoblasts and occurs via Dyrk1b phosphorylation of the nuclear localization sequence of class II HDACs, including HDAC5 and MEF2-interacting transcriptional repressor (MITR), causing their accumulation in the cytoplasm and relieving their inhibition on MEF2C thereby allowing MEF2C to activate myogenin transcription (Deng et al., 2005). Dyrk1b has been shown to directly interact with Wdr68 in zebrafish; the significance of this interaction has yet to be satisfactorily explained but appears to be implicated in the regulation of the expression of a number of genes (Mazmanian et al.). In addition, Wdr68 was shown to bind Dyrk1a, a Dyrk1b paralog, in SZ95 sebocytes

and respond to RhoA by translocating to the cytoplasm (Morita et al., 2006). If one combines the information gleaned by these two studies to infer an explanation for the reduction in the expression of myogenin with Wdr68 over-expression one might suggest that: during the normal transition from growth to differentiation RhoA induces the increase in the transcription of Dyrk1b. Phosphorylation events catalyzed by Dyrk1b culminate in myogenin expression and are required for myoblast fusion. While active RhoA normally prevents Wdr68 interference by translocating it to the cytoplasm, over-expression of Wdr68 over-powers the endogenous RhoA signal thereby allowing Wdr68 to accumulate in the nucleus and prevent induction of myogenin expression by binding Dyrk1b and blocking its ability to phosphorylate MITR (Figure 5.1).

This supposition is supported by closer examination of the fusion index of Wdr68 over-expressing primary myoblasts (Figure 4.16). Wdr68 over-expressing primary myoblasts appear to show a fusion defect, however this is reciprocated in the CTAP control cells. Both Wdr68-CTAP and CTAP are under the control of the potent CMV promoter which ensures that each are expressed at a high level, potentially this high level of expression has hindered myoblast fusion by simply clogging the cell. Wdr68 over-expressing myoblasts are able to elongate into myocytes and upregulate myosin heavy chain, a late marker of myogenic differentiation; it would be useful to carry this differentiation time course with a lower extent of Wdr68 over-expression and through to later time points to ascertain whether this phenotype represents a delay or defect in myoblast fusion.

Based on the current data however, Wdr68 does not appear to be absolutely required for cultured myoblasts to proceed through the myogenic program, nor can Wdr68 cause its inhibition.

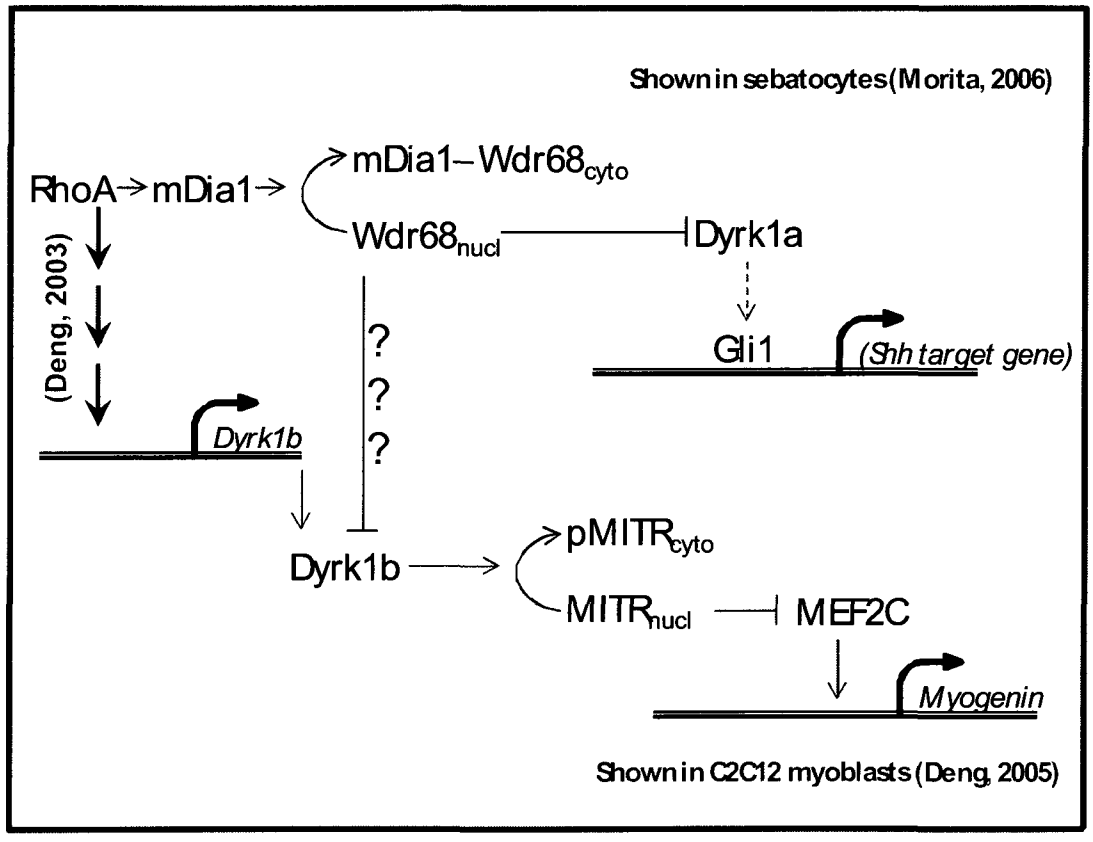

Figure 5.1: Hypothesis regarding how Wdr68 might antagonize Dyrk1b in myocytes (in the same way it antagonizes Dyrk1a in sebatocytes), thereby blocking myogenin gene expression.

5.2 Future Directions

In addition to the suggestions made above, there exist some other interesting avenues regarding investigation of the role of Wdr68 in adult myogenesis. Recently a kinome screen was conducted in order to identify kinases able to phosphorylate Pax7 (R. Screaton, unpublished). Dyrk1b was not among the candidates produced, however this was not unexpected given that it acts later in the promotion of myoblast differentiation. Because Wdr68 has been shown to be expressed throughout myogenesis, to interact with Dyrk1b in zebrafish, and postulated to mediate post-translational modification of bHLH transcription factors in plants, it would be interesting to screen the kinome against the MyoD bHLH family of transcription factors to ascertain whether Dyrk1b is among the kinases able to catalyze their phosphorylation. In addition, it would be valuable to follow up this study with co-immunoprecipitation analysis to determine whether Wdr68 is the adaptor protein responsible for mediating these putative phosphorylation events.

The implications of the recapitulation of the embryonic Shh pathway during adult myogenesis are under active investigation (Pola et al., 2003). Embryonically, Gli1 has been shown to bind the *Myf5* epaxial enhancer region thereby up-regulating *Myf5* expression (Gustafsson et al., 2002). Although Wdr68 has been shown to affect Gli1 subcellular localization in SZ95 sebocytes and 293T cells (Morita et al., 2006), perturbation of Wdr68 expression levels in primary myoblasts does not appear to manifest by altering *Myf5* expression levels as one would expect if

Wdr68 was involved the integration of Shh signaling at the level of Gli1. As such, while Shh signaling is certainly important for adult myogenesis, Wdr68 is likely not a key player.

Finally it has been hypothesized that a primary role for WD40-repeat proteins might be to act as substrate-specific adaptor proteins for CUL4-DDB1 ubiqutin ligase through an interaction between the WD40 motif and DDB1 (Higa et al., 2006). This has been observed for Wdr5 at tri-methylated histone 3 in human H1299 and HeLa cell lines (Higa et al., 2006). It would be interesting to determine whether 'Dcaf7' is an apt name for Wdr68 by conducting co-immunoprecipitation reactions to detect the putative interaction between it and the CUL4-DDB1 ubiqutin ligase in primary myoblasts. In addition, it would be interesting to screen key regulators of adult myogenesis to see if they undergo Wdr68/CUL4-DDB1 ubiqutin ligase-mediated mono- or poly-ubiqutination.

5.3 Overall Conclusions

Understanding the molecular mechanisms that underlie the natural regenerative program of adult skeletal muscle is being pursued based on its potential to uncover treatments for those who suffer from myopathy due to impaired regenerative capacity. Pax7 is an appealing candidate for study because it is required for satellite cell maintenance and specification and is the first myogenic regulatory factor expressed in the adult myogenic program. This study sought to elucidate the putative interaction between Wdr68 and Pax7. We were able to demonstrate an indirect interaction between Pax7 and Wdr68 in primary

myoblasts and observe a change in myogenic regulatory factor and Pax7-target gene expression upon modulation of Wdr68 expression. We excluded two ways that Wdr68 might be able to modulate Pax7 transcriptional activity and described the phenotype produced by alteration of Wdr68 expression levels in primary myoblasts.

Works Cited

Bajard, L., Relaix, F., Lagha, M., Rocancourt, D., Daubas, P., and Buckingham, M. E. (2006). A novel genetic hierarchy functions during hypaxial myogenesis: Pax3 directly activates Myf5 in muscle progenitor cells in the limb. Genes Dev *20*, 2450-2464.

Bennicelli, J. L., Advani, S., Schafer, B. W., and Barr, F. G. (1999). PAX3 and PAX7 exhibit conserved cis-acting transcription repression domains and utilize a common gain of function mechanism in alveolar rhabdomyosarcoma. Oncogene *18*, 4348-4356.

Braun, T., Rudnicki, M. A., Arnold, H. H., and Jaenisch, R. (1992). Targeted inactivation of the muscle regulatory gene Myf-5 results in abnormal rib development and perinatal death. Cell *71*, 369-382.

Buchberger, A., Freitag, D., and Arnold, H. H. (2007). A homeo-paired domain-binding motif directs Myf5 expression in progenitor cells of limb muscle. Development *134*, 1171-1180.

Buckingham, M., Bajard, L., Chang, T., Daubas, P., Hadchouel, J., Meilhac, S., Montarras, D., Rocancourt, D., and Relaix, F. (2003). The formation of skeletal muscle: from somite to limb. J Anat *202*, 59-68.

Burkin, D. J., and Kaufman, S. J. (1999). The alpha7beta1 integrin in muscle development and disease. Cell Tissue Res *296*, 183-190.

Charge, S. B., and Rudnicki, M. A. (2004). Cellular and molecular regulation of muscle regeneration. Physiol Rev *84*, 209-238.

Chi, N., and Epstein, J. A. (2002). Getting your Pax straight: Pax proteins in development and disease. Trends Genet *18*, 41-47.

Cornelison, D. D., Wilcox-Adelman, S. A., Goetinck, P. F., Rauvala, H., Rapraeger, A. C., and Olwin, B. B. (2004). Essential and separable roles for Syndecan-3 and Syndecan-4 in skeletal muscle development and regeneration. Genes Dev *18*, 2231-2236.

Couture, J. F., Collazo, E., and Trievel, R. C. (2006). Molecular recognition of histone H3 by the WD40 protein WDR5. Nat Struct Mol Biol *13*, 698-703.

Czerny, T., Schaffner, G., and Busslinger, M. (1993). DNA sequence recognition by Pax proteins: bipartite structure of the paired domain and its binding site. Genes Dev *7*, 2048-2061.

de Vetten, N., Quattrocchio, F., Mol, J., and Koes, R. (1997). The an11 locus controlling flower pigmentation in petunia encodes a novel WD-repeat protein conserved in yeast, plants, and animals. Genes Dev *11*, 1422-1434.

Deng, X., Ewton, D. Z., Mercer, S. E., and Friedman, E. (2005). Mirk/dyrk1B decreases the nuclear accumulation of class II histone deacetylases during skeletal muscle differentiation. J Biol Chem *280*, 4894-4905.

Deng, X., Ewton, D. Z., Pawlikowski, B., Maimone, M., and Friedman, E. (2003). Mirk/dyrk1B is a Rho-induced kinase active in skeletal muscle differentiation. J Biol Chem *278*, 41347-41354.

Duronio, R. J., Gordon, J. I., and Boguski, M. S. (1992). Comparative analysis of the beta transducin family with identification of several new members including PWP1, a nonessential gene of Saccharomyces cerevisiae that is divergently transcribed from NMT1. Proteins *13*, 41-56.

Eberhard, D., Jimenez, G., Heavey, B., and Busslinger, M. (2000). Transcriptional repression by Pax5 (BSAP) through interaction with corepressors of the Groucho family. Embo J *19*, 2292-2303.

Epstein, J., Cai, J., Glaser, T., Jepeal, L., and Maas, R. (1994). Identification of a Pax paired domain recognition sequence and evidence for DNA-dependent conformational changes. J Biol Chem *269*, 8355-8361.

Fong, H. K., Hurley, J. B., Hopkins, R. S., Miake-Lye, R., Johnson, M. S., Doolittle, R. F., and Simon, M. I. (1986). Repetitive segmental structure of the transducin beta subunit: homology with the CDC4 gene and identification of related mRNAs. Proc Natl Acad Sci U S A *83*, 2162-2166.

Fujita, A., Gomes, L. R., Sato, J. R., Yamaguchi, R., Thomaz, C. E., Sogayar, M. C., and Miyano, S. (2008). Multivariate gene expression analysis reveals functional connectivity changes between normal/tumoral prostates. BMC Syst Biol *2*, 106.

Gibson, M. C., and Schultz, E. (1983). Age-related differences in absolute numbers of skeletal muscle satellite cells. Muscle Nerve *6*, 574-580.

Gustafsson, M. K., Pan, H., Pinney, D. F., Liu, Y., Lewandowski, A., Epstein, D. J., and Emerson, C. P., Jr. (2002). Myf5 is a direct target of long-range Shh signaling and Gli regulation for muscle specification. Genes Dev *16*, 114-126.

Han, Z., Guo, L., Wang, H., Shen, Y., Deng, X. W., and Chai, J. (2006). Structural basis for the specific recognition of methylated histone H3 lysine 4 by the WD-40 protein WDR5. Mol Cell *22*, 137-144.

Hasty, P., Bradley, A., Morris, J. H., Edmondson, D. G., Venuti, J. M., Olson, E. N., and Klein, W. H. (1993). Muscle deficiency and neonatal death in mice with a targeted mutation in the myogenin gene. Nature *364*, 501-506.

Higa, L. A., Wu, M., Ye, T., Kobayashi, R., Sun, H., and Zhang, H. (2006). CUL4-DDB1 ubiquitin ligase interacts with multiple WD40-repeat proteins and regulates histone methylation. Nat Cell Biol *8*, 1277-1283.

Jones, N. C., Tyner, K. J., Nibarger, L., Stanley, H. M., Cornelison, D. D., Fedorov, Y. V., and Olwin, B. B. (2005). The p38alpha/beta MAPK functions as a molecular switch to activate the quiescent satellite cell. J Cell Biol *169*, 105-116.

Kassar-Duchossoy, L., Gayraud-Morel, B., Gomes, D., Rocancourt, D., Buckingham, M., Shinin, V., and Tajbakhsh, S. (2004). Mrf4 determines skeletal muscle identity in Myf5:Myod double-mutant mice. Nature *431*, 466-471.

Knapp, J. R., Davie, J. K., Myer, A., Meadows, E., Olson, E. N., and Klein, W. H. (2006). Loss of myogenin in postnatal life leads to normal skeletal muscle but reduced body size. Development *133*, 601-610.

Koleva, M., Kappler, R., Vogler, M., Herwig, A., Fulda, S., and Hahn, H. (2005). Pleiotropic effects of sonic hedgehog on muscle satellite cells. Cell Mol Life Sci *62*, 1863-1870.

Kuang, S., Gillespie, M. A., and Rudnicki, M. A. (2008). Niche regulation of muscle satellite cell self-renewal and differentiation. Cell Stem Cell *2*, 22-31.

Kuang, S., Kuroda, K., Le Grand, F., and Rudnicki, M. A. (2007). Asymmetric self-renewal and commitment of satellite stem cells in muscle. Cell *129*, 999-1010.

Kuang, S., and Rudnicki, M. A. (2008). The emerging biology of satellite cells and their therapeutic potential. Trends Mol Med *14*, 82-91.

Le Grand, F., Jones, A. E., Seale, V., Scime, A., and Rudnicki, M. A. (2009). Wnt7a activates the planar cell polarity pathway to drive the symmetric expansion of satellite stem cells. Cell Stem Cell *4*, 535-547.

Le Grand, F., and Rudnicki, M. A. (2007). Skeletal muscle satellite cells and adult myogenesis. Curr Opin Cell Biol *19*, 628-633.

Lepper, C., Conway, S. J., and Fan, C. M. (2009). Adult satellite cells and embryonic muscle progenitors have distinct genetic requirements. Nature *460*, 627-631.

Li, D., and Roberts, R. (2001). WD-repeat proteins: structure characteristics, biological function, and their involvement in human diseases. Cell Mol Life Sci *58*, 2085-2097.

Mao, J., Maye, P., Kogerman, P., Tejedor, F. J., Toftgard, R., Xie, W., Wu, G., and Wu, D. (2002). Regulation of Gli1 transcriptional activity in the nucleus by Dyrk1. J Biol Chem *277*, 35156-35161.

Massari, M. E., and Murre, C. (2000). Helix-loop-helix proteins: regulators of transcription in eucaryotic organisms. Mol Cell Biol *20*, 429-440.

Mauro, A. (1961). Satellite cell of skeletal muscle fibers. J Biophys Biochem Cytol *9*, 493-495.

Mazmanian, G., Kovshilovsky, M., Yen, D., Mohanty, A., Mohanty, S., Nee, A., and Nissen, R. M. The zebrafish dyrk1b gene is important for endoderm formation. Genesis *48*, 20-30.

McKinnell, I. W., Ishibashi, J., Le Grand, F., Punch, V. G., Addicks, G. C., Greenblatt, J. F., Dilworth, F. J., and Rudnicki, M. A. (2008). Pax7 activates myogenic genes by recruitment of a histone methyltransferase complex. Nat Cell Biol *10*, 77-84.

Megeney, L. A., Kablar, B., Garrett, K., Anderson, J. E., and Rudnicki, M. A. (1996). MyoD is required for myogenic stem cell function in adult skeletal muscle. Genes Dev *10*, 1173-1183.

Mercer, S. E., Ewton, D. Z., Deng, X., Lim, S., Mazur, T. R., and Friedman, E. (2005). Mirk/Dyrk1B mediates survival during the differentiation of C2C12 myoblasts. J Biol Chem *280*, 25788-25801.

Mercer, S. E., Ewton, D. Z., Shah, S., Naqvi, A., and Friedman, E. (2006). Mirk/Dyrk1b mediates cell survival in rhabdomyosarcomas. Cancer Res *66*, 5143-5150.

Mercer, S. E., and Friedman, E. (2006). Mirk/Dyrk1B: a multifunctional dual-specificity kinase involved in growth arrest, differentiation, and cell survival. Cell Biochem Biophys *45*, 303-315.

Montarras, D., Lindon, C., Pinset, C., and Domeyne, P. (2000). Cultured myf5 null and myoD null muscle precursor cells display distinct growth defects. Biol Cell *92*, 565-572.

Morita, K., Lo Celso, C., Spencer-Dene, B., Zouboulis, C. C., and Watt, F. M. (2006). HAN11 binds mDia1 and controls GLI1 transcriptional activity. J Dermatol Sci *44*, 11-20.

Murre, C., Bain, G., van Dijk, M. A., Engel, I., Furnari, B. A., Massari, M. E., Matthews, J. R., Quong, M. W., Rivera, R. R., and Stuiver, M. H. (1994). Structure and function of helix-loop-helix proteins. Biochim Biophys Acta *1218*, 129-135.

Neer, E. J., Schmidt, C. J., Nambudripad, R., and Smith, T. F. (1994). The ancient regulatory-protein family of WD-repeat proteins. Nature *371*, 297-300.

Nissen, R. M., Amsterdam, A., and Hopkins, N. (2006). A zebrafish screen for craniofacial mutants identifies wdr68 as a highly conserved gene required for endothelin-1 expression. BMC Dev Biol *6*, 28.

Noll, M. (1993). Evolution and role of Pax genes. Curr Opin Genet Dev *3*, 595-605.

Olguin, H. C., Yang, Z., Tapscott, S. J., and Olwin, B. B. (2007). Reciprocal inhibition between Pax7 and muscle regulatory factors modulates myogenic cell fate determination. J Cell Biol *177*, 769-779.

Pisconti, A., Brunelli, S., Di Padova, M., De Palma, C., Deponti, D., Baesso, S., Sartorelli, V., Cossu, G., and Clementi, E. (2006). Follistatin induction by nitric oxide through cyclic GMP: a tightly regulated signaling pathway that controls myoblast fusion. J Cell Biol *172*, 233-244.

Pola, R., Ling, L. E., Aprahamian, T. R., Barban, E., Bosch-Marce, M., Curry, C., Corbley, M., Kearney, M., Isner, J. M., and Losordo, D. W. (2003). Postnatal recapitulation of embryonic hedgehog pathway in response to skeletal muscle ischemia. Circulation *108*, 479-485.

Rampalli, S., Li, L., Mak, E., Ge, K., Brand, M., Tapscott, S. J., and Dilworth, F. J. (2007). p38 MAPK signaling regulates recruitment of Ash2L-containing methyltransferase complexes to specific genes during differentiation. Nat Struct Mol Biol *14*, 1150-1156.

Rawls, A., Morris, J. H., Rudnicki, M., Braun, T., Arnold, H. H., Klein, W. H.. and Olson, E. N. (1995). Myogenin's functions do not overlap with those of MyoD or Myf-5 during mouse embryogenesis. Dev Biol *172*, 37-50.

Rawls, A., Valdez, M. R., Zhang, W., Richardson, J., Klein, W. H., and Olson, E. N. (1998). Overlapping functions of the myogenic bHLH genes MRF4 and MyoD revealed in double mutant mice. Development *125*, 2349-2358.

Rosen, G. D., Sanes, J. R., LaChance, R., Cunningham, J. M., Roman, J., and Dean, D. C. (1992). Roles for the integrin VLA-4 and its counter receptor VCAM-1 in myogenesis. Cell *69*, 1107-1119.

Rudnicki, M. A., Braun, T., Hinuma, S., and Jaenisch, R. (1992). Inactivation of MyoD in mice leads to up-regulation of the myogenic HLH gene Myf-5 and results in apparently normal muscle development. Cell *71*, 383-390.

Rudnicki, M. A., Schnegelsberg, P. N., Stead, R. H., Braun, T., Arnold, H. H., and Jaenisch, R. (1993). MyoD or Myf-5 is required for the formation of skeletal muscle. Cell *75*, 1351-1359.

Ruthenburg, A. J., Wang, W., Graybosch, D. M., Li, H., Allis, C. D., Patel, D. J., and Verdine, G. L. (2006). Histone H3 recognition and presentation by the WDR5 module of the MLL1 complex. Nat Struct Mol Biol *13*, 704-712.

Sabourin, L. A., Girgis-Gabardo, A., Seale, P., Asakura, A., and Rudnicki, M. A. (1999). Reduced differentiation potential of primary MyoD-/- myogenic cells derived from adult skeletal muscle. J Cell Biol *144*, 631-643.

Seale, P., Ishibashi, J., Holterman, C., and Rudnicki, M. A. (2004). Muscle satellite cell-specific genes identified by genetic profiling of MyoD-deficient myogenic cell. Dev Biol *275*, 287-300.

Seale, P., Sabourin, L. A., Girgis-Gabardo, A., Mansouri, A., Gruss, P., and Rudnicki, M. A. (2000). Pax7 is required for the specification of myogenic satellite cells. Cell *102*, 777-786.

Smith, T. F., Gaitatzes, C., Saxena, K., and Neer, E. J. (1999). The WD repeat: a common architecture for diverse functions. Trends Biochem Sci *24*, 181-185.

Straface, G., Aprahamian, T., Flex, A., Gaetani, E., Biscetti, F., Smith, R. C., Pecorini, G., Pola, E., Angelini, F., Stigliano, E., *et al.* (2008). Sonic Hedgehog Regulates Angiogenesis and Myogenesis During Post-Natal Skeletal Muscle Regeneration. J Cell Mol Med.

Tajbakhsh, S., Rocancourt, D., Cossu, G., and Buckingham, M. (1997). Redefining the genetic hierarchies controlling skeletal myogenesis: Pax-3 and Myf-5 act upstream of MyoD. Cell *89*, 127-138.

Tatsumi, R., Liu, X., Pulido, A., Morales, M., Sakata, T., Dial, S., Hattori, A., Ikeuchi, Y., and Allen, R. E. (2006). Satellite cell activation in stretched skeletal muscle and the role of nitric oxide and hepatocyte growth factor. Am J Physiol Cell Physiol *290*, C1487-1494.

Valdez, M. R., Richardson, J. A., Klein, W. H., and Olson, E. N. (2000). Failure of Myf5 to support myogenic differentiation without myogenin, MyoD, and MRF4. Dev Biol *219*, 287-298.

Vasyutina, E., Stebler, J., Brand-Saberi, B., Schulz, S., Raz, E., and Birchmeier, C. (2005). CXCR4 and Gab1 cooperate to control the development of migrating muscle progenitor cells. Genes Dev *19*, 2187-2198.

Wall, M. A., Coleman, D. E., Lee, E., Iniguez-Lluhi, J. A., Posner, B. A., Gilman, A. G., and Sprang, S. R. (1995). The structure of the G protein heterotrimer Gi alpha 1 beta 1 gamma 2. Cell *83*, 1047-1058.

Wilson, D., Sheng, G., Lecuit, T., Dostatni, N., and Desplan, C. (1993). Cooperative dimerization of paired class homeo domains on DNA. Genes Dev *7*, 2120-2134.

Wozniak, A. C., and Anderson, J. E. (2007). Nitric oxide-dependence of satellite stem cell activation and quiescence on normal skeletal muscle fibers. Dev Dyn *236*, 240-250.

Wysocka, J., Swigut, T., Milne, T. A., Dou, Y., Zhang, X., Burlingame, A. L., Roeder, R. G., Brivanlou, A. H., and Allis, C. D. (2005). WDR5 associates with histone H3 methylated at K4 and is essential for H3 K4 methylation and vertebrate development. Cell *121*, 859-872.

Xu, H. E., Rould, M. A., Xu, W., Epstein, J. A., Maas, R. L., and Pabo, C. O. (1999). Crystal structure of the human Pax6 paired domain-DNA complex reveals specific roles for the linker region and carboxy-terminal subdomain in DNA binding. Genes Dev *13*, 1263-1275.

Zammit, P. S., Golding, J. P., Nagata, Y., Hudon, V., Partridge, T. A., and Beauchamp, J. R. (2004). Muscle satellite cells adopt divergent fates: a mechanism for self-renewal? J Cell Biol *166*, 347-357.

Zhang, W., Behringer, R. R., and Olson, E. N. (1995). Inactivation of the myogenic bHLH gene MRF4 results in up-regulation of myogenin and rib anomalies. Genes Dev *9*, 1388-1399.

APPENDIX I

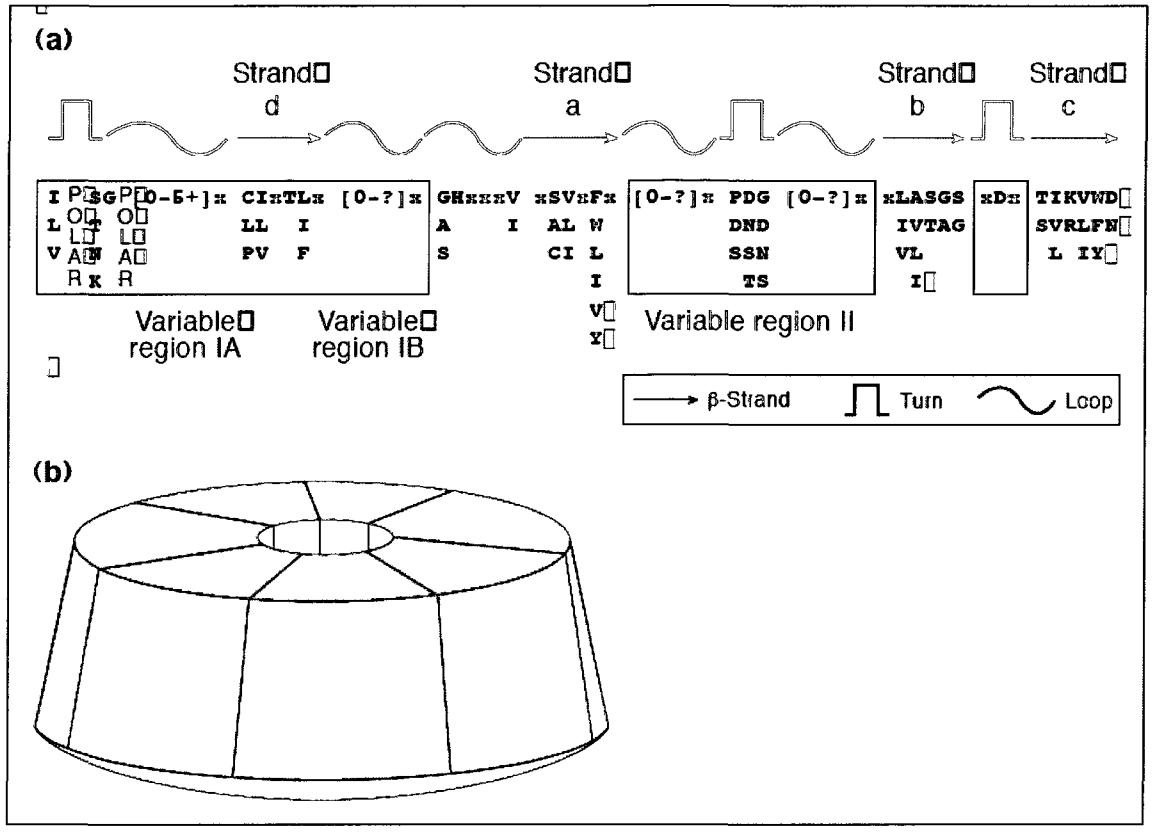

Figure 1

The WD repeat. **(a)** Schematic illustration of the structural elements within a single repeat. The alternative amino acids for each position are listed in approximate order of their frequency of occurrence. In the case of strand d, the listed alternative amino acids are only evident in about a third of the repeats. A surface-defining sequence pattern can be defined by replacing all the residues in strand a, strand b and strand c by 'x' (any residue). **(b)** Schematic representation of the positions of the elements shown in (a) in the three-dimensional structure of the fold. The predicted bottom or larger of the flat surface regions is shown in red; the top flat surface is shown in lighter blue. The circumference, which is composed primarily of the d β-strand residues, is shown in green. Polar, polar residue.

Figure S1.1: The WD40-repeat and barrel structure schematic (from (Smith et al., 1999)).

A

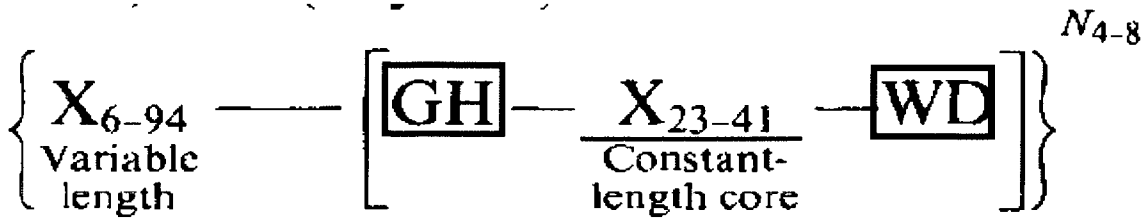

B

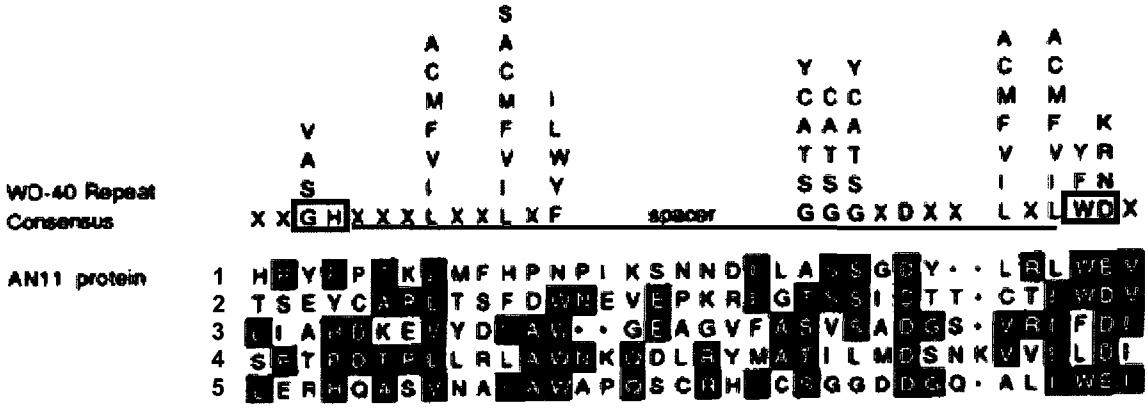

Figure 1.3: (A) Neer *et al.* Wd40 motif (adapted from (Neer et al., 1994)), and (B) the five AN11 WD40 repeats. (adapted from (de Vetten et al., 1997)).

APPENDIX II

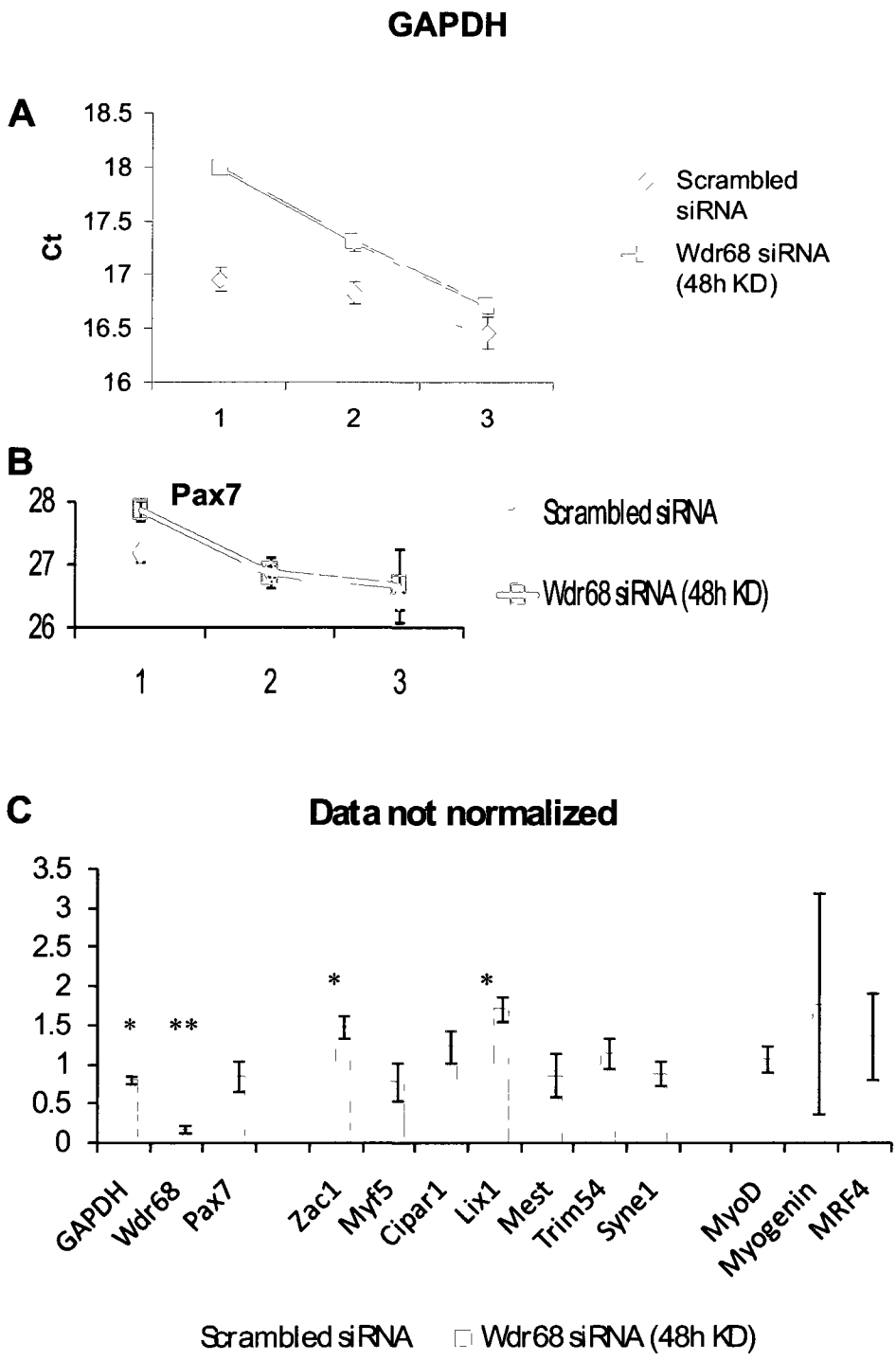

Figure S2.1: Pax7 expression is unaffected by Wdr68 knockdown (48h). Ct plot of the average values of three technical replicates for three biological replicates of (A) GAPDH, and (B) Pax7. (C) Non-normalized real-time PCR data. Error bars are SEM; *=p<0.05; **=p<0.01; n=3.

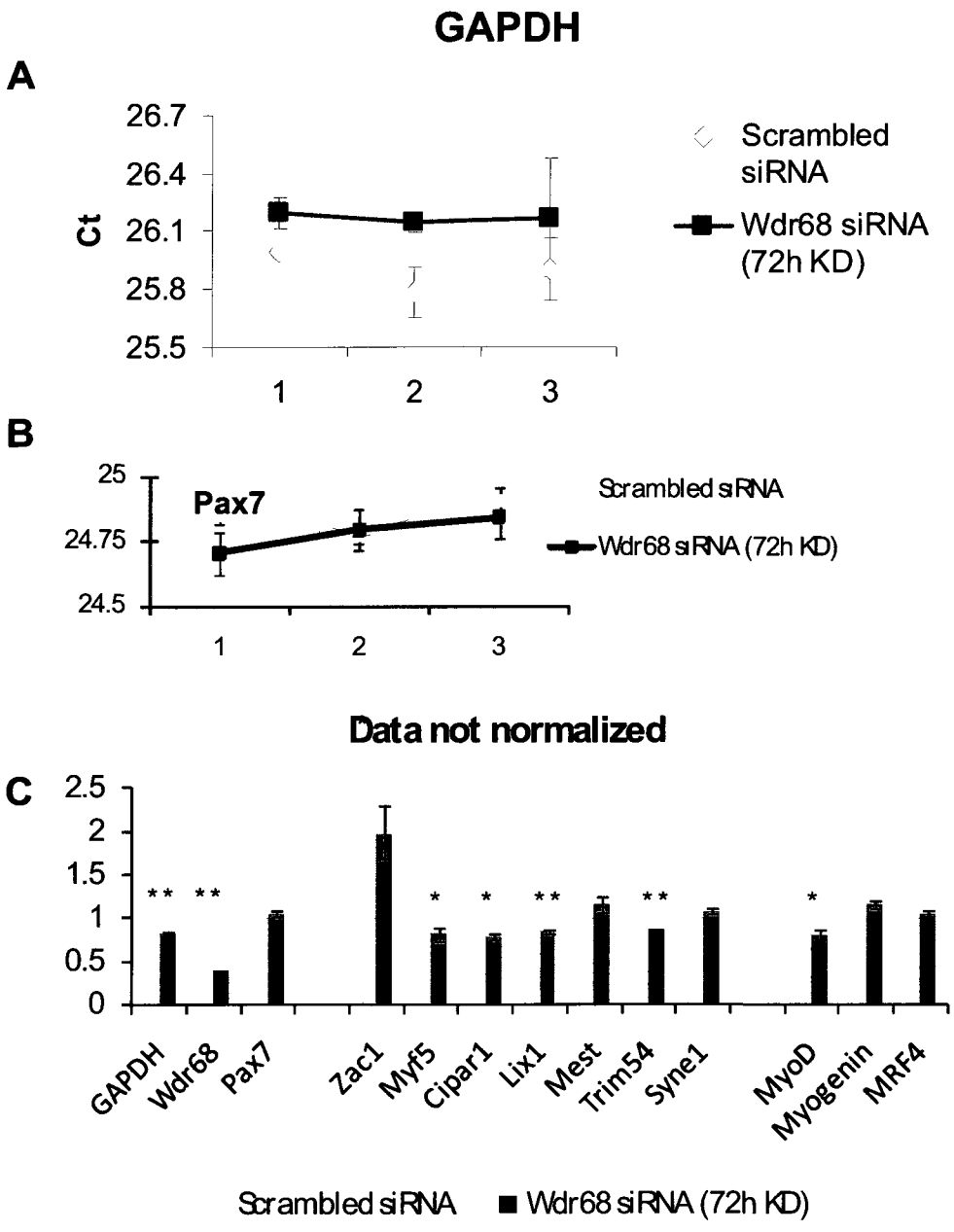

Figure S2.2: Pax7 expression is unaffected by Wdr68 knockdown (72h). Ct plot of the average values of three technical replicates for three biological replicates of (A) GAPDH, and (B) Pax7. (C) Non-normalized real-time PCR data. Error bars are SEM; *=p<0.05; **=p<0.01; n=3.

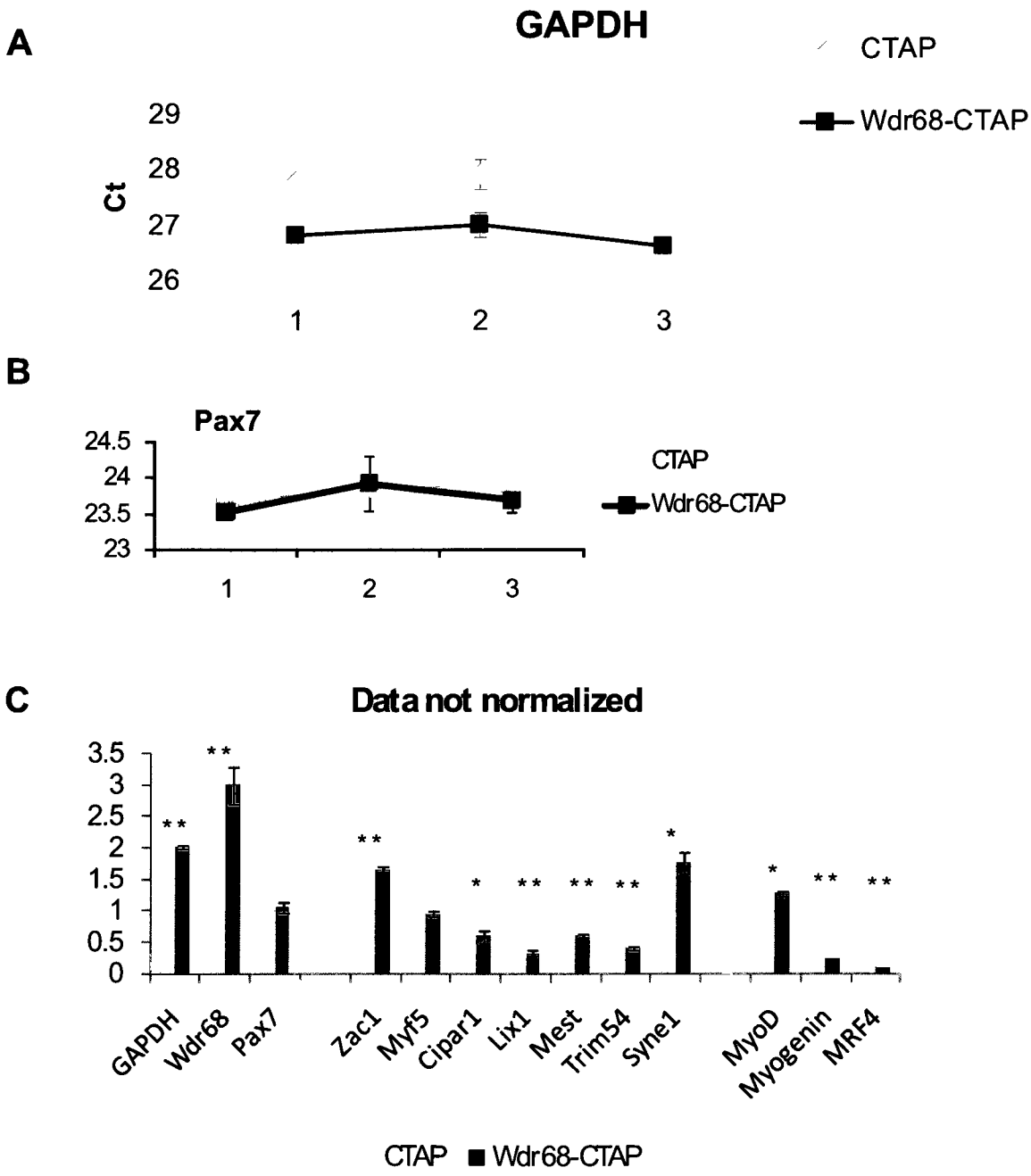

Figure S2.3: Pax7 expression is unaffected by Wdr68-CTAP over-expression. Ct plot of the average values of three technical replicates for three biological replicates of (A) GAPDH, and (B) Pax7. (C) Non-normalized real-time PCR data. Error bars are SEM; *=p<0.05; **=p<0.01; n=3.

APPENDIX III

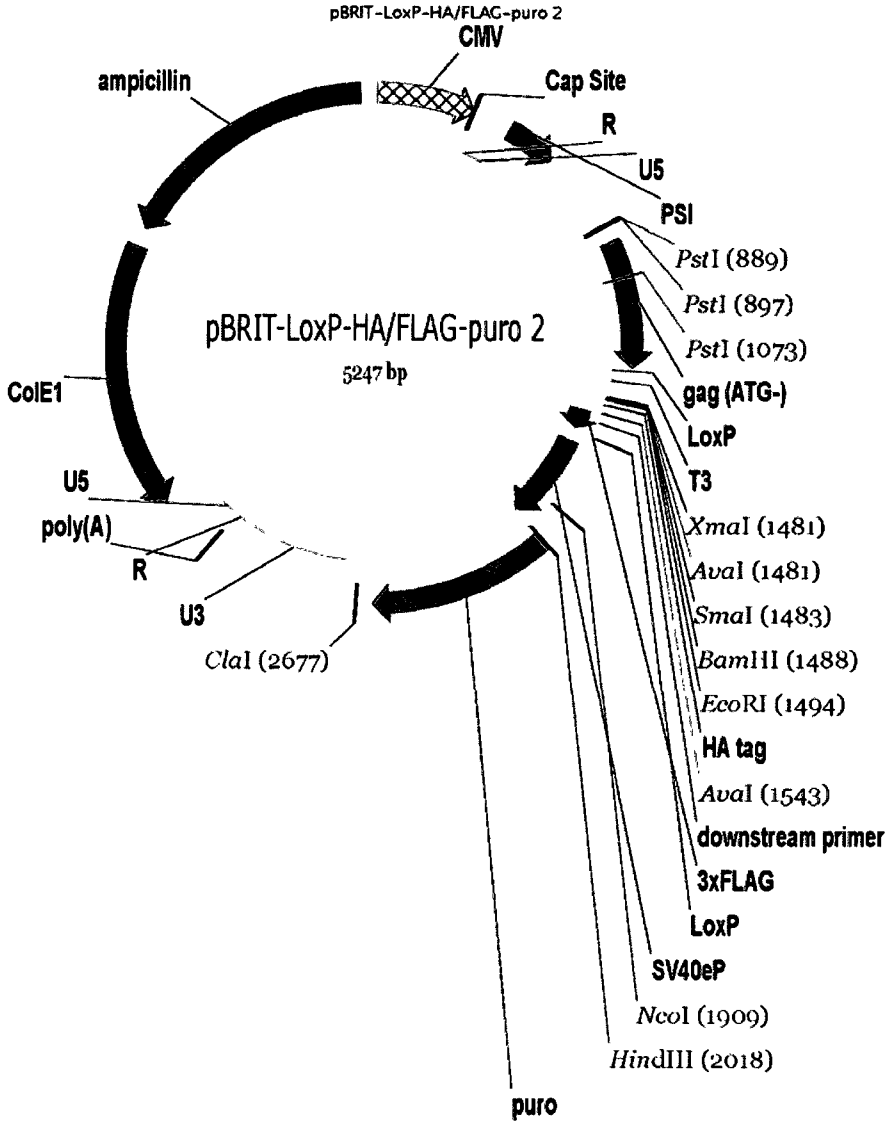

Figure S3.1: pBRIT plasmid backbone.